INFERRING EXPOSURE TO HARMFUL *PSEUDO-NITZSCHIA* BLOOMS FROM OCEAN-TO-ESTUARY GRADIENTS IN DOMOIC ACID CONCENTRATIONS IN HUMBOLDT BAY BIVALVES

By

Natasha Hope Ficzycz Winnacott

A Thesis Presented to

The Faculty of California State Polytechnic University, Humboldt

In Partial Fulfillment of the Requirements for the Degree

Master of Science in Natural Resources: Fisheries

Committee Membership

Dr. Eric Bjorkstedt, Committee Chair

Dr. Amy Sprowles, Committee Member

Dr. Andre Buchheister, Committee Member

Dr. Mark Henderson, Committee Member

Dr. Andrew Stubblefield, Program Graduate Coordinator

May 2023

ABSTRACT

INFERRING EXPOSURE TO HARMFUL PSEUDO-NITZSCHIA BLOOMS FROM OCEAN-TO-ESTUARY GRADIENTS IN DOMOIC ACID CONCENTRATIONS IN HUMBOLDT BAY BIVALVES

Natasha Hope Ficzycz Winnacott

Harmful algal blooms (HABs) result from outbreaks of any of several different species of toxin-producing phytoplankton and that can have major detrimental effects on marine ecosystems and pose severe health and economic threats to human communities. Of particular concern along the United States West Coast are HABs of pennate diatom genus *Pseudo-nitzschia* that produce the potent neurotoxin domoic acid (DA). The coastal ocean between Cape Mendocino, CA, and Cape Blanco, OR is a hotspot for *Pseudo-nitzschia* spp. HABs. Such blooms impact coastal fisheries and pose a potential threat to aquaculture operations in Humboldt Bay, California's second largest estuary and largest producer of oysters. Yet, despite evidence that tidal exchanges carry *Pseudo-nitzschia* spp. from the ocean into the Bay, regular assays rarely detect high uptake of domoic acid in cultured oysters and sentinel mussels in upper reaches of the Bay. This study examined the gradient to which ocean-origin DA and *Pseudo-nitzschia* spp. enter Humboldt Bay using naturally occurring bivalves as an integrated measure of exposure. Bivalves were collected along ocean to upper estuary transects and processed for DA concentrations in their soft tissues. These samples were augmented with water samples collected to characterize the concentrations of *Pseudo-nitzschia* spp. and DA in the water

column and to relate to DA concentrations in bivalves. Results demonstrate that DA concentrations in bivalves decline with increased distance from the mouth of the Bay in a manner that varies over time, and that this variability is linked to the variability and intensity of DA concentrations in the environment. These results provide strong support for the hypothesis that bivalves in the upper regions of the Bay experience less exposure to ocean-origin *Pseudo-nitzschia* spp. HABs. This study lays the foundation for understanding the dynamics and distribution of HABs in Humboldt Bay and warrants the development of future studies to map this risk in greater detail to support hypotheses regarding mechanisms that control HAB distributions and exposure.

ACKNOWLEDGEMENTS

I would like to thank my advisor, Dr. Eric Bjorkstedt for taking the chance and accepting me as a graduate student. Thank you for believing in me throughout my degree, even when I didn't believe in myself. I am also thankful for the support of my committee members, Dr. Andre Buchheister, Dr. Mark Henderson, and Dr. Amy Sprowles for their continued guidance and support throughout my degree. I would like to provide a special thanks to Dr. Amy Sprowles for providing invaluable support and training in how to use ELISA. I would like to thank James Ray from the California Department of Fish and Wildlife for providing help with planning and design of sample collection used for this project, and Lucas Sawyer from Hog Island and Todd Van Herpe from Humboldt Bay Oyster Company for site access and collection. I would like to thank Blair Winnacott, Eric Leblanc, Connor Stewart, Sarah Moreau, Braden Herman, and Eric Bjorkstedt for help collecting and processing bivalve samples. I would also like to thank the Kudela lab, and especially Kendra Hayashi, at UC Santa Cruz for processing water samples.

Funding for this project came from several sources and is appreciated greatly. These include, the Malcolm Oliphant Scholarship in Marine Science, the Marin Rod and Gun Club Award, and the Humboldt State University International Student Award. I also appreciate the opportunity to pursue this research while being supported as a member of the Trinidad Head Line Ocean Observing Program, which is supported by NOAA's Southwest Fisheries Science Center via the Cooperative Institute of Marine Earth and Atmospheric Sciences (CIMEAS).

Finally, I would like to thank my friends and family, all of whom have provided some form of support throughout my degree that I am forever grateful for. I thank my parents, Peter Ficzycz and Fairleth McCuaig, for always encouraging me to dream big. I also would like to thank my mother and father-in-law, Marguerite and Neal Winnacott, who have treated me as their own since the very beginning. Lastly, I would like to thank my husband, Blair Winnacott, whom I met during my first semester of graduate school and has been a pillar of support ever since.

TABLE OF CONTENTS

LIST OF TABLES

LIST OF FIGURES

LIST OF APPENDICES

INTRODUCTION

Harmful algal blooms (HABs) result from outbreaks of any of several different species of toxin-producing phytoplankton that can have major detrimental effects on marine ecosystems and pose severe health and economic threats to human communities (Gobler et al. 2017; Townhill et al. 2018; Gobler 2020; Brown et al. 2020). Of particular concern along the United States (US) West Coast are HABs of pennate diatom genus *Pseudo-nitzschia* that produce the potent neurotoxin domoic acid (DA) (Lelong et al. 2012; Trainer et al. 2012; Bates et al. 2018). Filter feeding organisms exposed to toxic *Pseudo-nitzschia* spp. (*Pseudo-nitzschia* hereafter) accumulate DA and pass it on to their predators, with potentially deleterious effects (e.g., enhanced disease in sea otters, *Enhydra lutris* [Miller et al. 2021]) and, at high enough concentrations DA can be potentially fatal and cause a condition called Amnesic Shellfish Poisoning in humans (Bates et al. 1989). DA can also accumulate through the pelagic food web and has caused the death of seabirds and marine mammals (McCabe et al. 2016). *Pseudo-nitzschia* HABs have occurred along the US West Coast since at least 1991 (Lewitus et al. 2012). In 2015, a massive *Pseudo-nitzschia* HAB occurred along the whole US West Coast, resulting in persistently elevated concentrations of DA in several major fisheries resources, extended closures of those fisheries, and increased mortality of marine mammals and seabirds (McCabe et al. 2016; McClatchie et al. 2016; Wells et al. 2017).

To mitigate risks to human consumers, monitoring programs regularly assay concentrations of DA (and other algal toxins, such as saxitoxins produced by

Alexandrium spp. [Costa et al. 2021]) in key species using quantitative assays (e.g., enzyme linked immunosorbent assay [ELISA; Litaker et al. 2008] or high-performance liquid chromatography [Quilliam et al. 1989]). When DA concentrations exceed the regulatory limit of 20 parts per million (ppm), fisheries harvests or mariculture sales are shut down to mitigate risks to human health. Such monitoring programs can lead to temporary (though sometimes extensive) harvest advisories for shellfish fisheries (e.g., razor clams (*Siliqua patula*) and Dungeness crab (*Metacarcinus magister*)), and result in substantial economic losses (e.g., McCabe et al. 2016; Ritzman et al. 2018; Moore et al. 2020).

Evidence suggests that tidal exchanges between the coastal ocean and Humboldt Bay carry *Pseudo-nitzschia* into the Bay (O'Connell 2013), which presents a substantial risk to the extensive aquaculture operations in the northern-most reaches of the Bay and to recreational harvesters. Despite this potential for toxic *Pseudo-nitzschia* to enter Humboldt Bay, elevated levels of DA are rarely detected in cultured oysters and sentinel mussels at aquaculture operations in the upper reaches of Humboldt Bay (Anderson and Kudela, unpublished data). The mechanisms that shield the upper estuary from intense HABs are poorly understood, as are patterns of exposure in the lower reaches of the Bay, where recreational harvest is more common. In this thesis, I analyze gradients in DA concentrations in naturally occurring bivalves, from which I infer spatial patterns in the exposure of benthic habitats in Humboldt Bay to HABs.

Pseudo-nitzschia HABs

The density and toxicity of phytoplankton cells varies substantially among species of *Pseudo-nitzschia* (Bates et al. 1989), and not all species produce DA. As a result, high densities of *Pseudo-nitzschia* may not always be correlated to increases in DA concentrations (e.g., Rowland-Pilgrim et al. 2019). Identifying *Pseudo-nitzschia* species with light microscopy is difficult, so *Pseudo-nitzschia* are instead placed into two groups: specimen that have a cell width greater than 3μm are put in the "seriata" size class, while those with a cell width less than 3μm are put in the "delicatissima" size class (Hasle and Syvertsen 1997). Species in the *Pseudo-nitzschia* size class *P. seriata* have been associated with intense HABs, such as *P. australis*, which was the cause of the massive 2015 HAB (McCabe et al. 2016). Species in the *P. delicatissima* size class are not often associated with severe HABs (Fehling et al. 2006; Rowland-Pilgrim et al. 2019).

Toxicity varies over the course of a *Pseudo-nitzschia* bloom, with evidence suggesting that DA production elevates during the stable or declining stages of a bloom (McCabe et al. 2016). Though the exact conditions that control DA production are poorly understood, it is likely that several factors may concurrently influence DA production synergistically (Lelong et al. 2012; Bates et al. 2018; Kelly et al. 2021). Studies indicate that DA production by *Pseudo-nitzschia* may depend on or be affected by a series of factors, including macro- and micronutrient supply. Macronutrients (e.g., nitrogen input and form; Thessen et al. 2009; Auro and Cochlan 2013; Radan and Cochlan 2018; and phosphate or silicate limitation; Parsons et al. 2002; Thorel et al. 2017) and

micronutrients (e.g., trace metals in the form of iron limitation or high concentrations of copper; Maldonado et al. 2002; Wells et al. 2005) have been shown to promote DA production. Abiotic conditions including increased temperature (e.g., McCabe et al. 2016; McKibben et al. 2017), and changes in pH (Trimborn et al. 2008; Sun et al. 2011; Wingert and Cochlan 2021; Ayache et al. 2021), and salinity (Doucette et al. 2008) have also been observed to increase DA concentrations, though these effects are more variable. Metabolites released by copepods and possibly by bivalves have also been shown to stimulate DA production, which suggests that toxin production may be an inducible response (Lundholm et al. 2018; Sauvey et al. 2021).

Regional Oceanography and *Pseudo-nitzschia* Hot Spots

The coastal waters that lie offshore of and connect to Humboldt Bay are part of the California Current System (CCS). During the spring and summer, upwelling brings cool, nutrient rich bottom waters from depth as surface waters are pushed offshore (Checkley & Barth 2009). Such enrichment supports the development and productivity of phytoplankton blooms, including blooms of *Pseudo-nitzschia* (Kudela et al. 2005; Kudela et al. 2010; Trainer et al. 2010; Pitcher et al. 2017). During periods of relaxation in upwelling, winds reverse, water temperature increases, and surface waters are transported closer to shore (Send and Beardsley 1987). Along the coast, water circulation is interrupted by coastal headlands and bathymetric features that can result in mesoscale features, some of which include eddies (Largier et al. 1993, Barth et al. 2000) and can act as retentive zones for *Pseudo-nitzschia* (e.g., Trainer et al. 2009).

Pseudo-nitzschia "hot spots" have been documented in retentive zones of the CCS, such as the Juan De Fuca eddy, Monterey Bay, and the coastal ocean between Cape Mendocino CA, and Cape Blanco, OR (Trainer et al. 2002; Trainer et al. 2020; Sandoval-Belmar et al. 2023). The last of these poses a major risk to aquaculture operations inside Humboldt Bay, given the Bay's proximity to this hot spot (Trainer et al. 2020). In these regions, *Pseudo-nitzschia* have been observed to occur at higher densities (Trainer et al. 2009; Pitcher et al. 2010; Sekula-Wood et al. 2011; Trainer et al. 2020) and evidence suggests that *Pseudo-nitzschia* in retentive zones occur at an increased frequency (Sekula-Wood et al. 2011; Trainer et al. 2020). Toxic *Pseudo-nitzschia* cells may sink to depths and become sequestered in sediment (Schnetzer et al. 2007; Sekula-Wood et al. 2009; Sekula-Wood et al. 2011), where they may accumulate in benthic infauna (Sekula-Wood et al. 2011; Smith et al. 2021). It has also been hypothesized that *Pseudo-nitzschia* in sediment or at depth can become resuspended by the onset of upwelling or turbulent mixing and form subsequent blooms in surface waters (Trainer et al. 2000; Wetz et al. 2004; Hubbard et al. 2014; Trainer et al. 2020).

Humboldt Bay: Structure and Connection to Coastal Ocean

Humboldt Bay is a large coastal lagoon located 50 km north of Cape Mendocino in Northern California and is connected to coastal waters spanned by a recently identified *Pseudo-nitzschia* HAB hot spot (Trainer et al. 2020). The Bay is formed by two long spits that separate it from the coastal ocean and consists of a deep entrance channel that leads to two large shallow bays, North Bay and South Bay, both of which consist of

extensive mudflats during low tide. South Bay is connected directly to the entrance channel, while North Bay is connected via a long, narrow channel (Barnhart et al. 1992; Costa and Glatzel 2002). Freshwater input to Humboldt Bay is dominated by influxes from the Eel River plume (mainly during winter storm events; Barnhart et al. 1992), with lesser contributions from smaller coastal watersheds that feed into the Bay (Freshwater Creek, Jacoby Creek, Salmon Creek, and the Elk River; Barnhart et al. 1992).

The primary drivers of circulation in the Bay are tidal exchange and wave action, both of which drive strong vertical mixing and tend to disrupt stratification, especially in the shallow regions of the Bay. During the spring and summer, coastal waters derived from upwelling are mixed into the waters that are advected into the Bay with each incoming tide. Under typical conditions, water that reaches the extensive mud flats of the Bay is heated by solar radiation and by contact with warmed sediments. As a result, temperature increases, whereas nutrients and chlorophyll generally decrease with increased distance from the mouth of the Bay (Pequegnat & Butler, 1981; Barnhart et al. 1992; Anderson 2010; Anderson 2019). Water masses of different characteristics (oceanic and estuarine) are separated by a nearly vertical frontal structure which presents a potential constraint to rapid mixing of ocean and estuarine water masses (Largier 1992). These distinct water masses shift with the tidal cycle, exposing extensive mudflats and habitat in North and South Bay during low tide (CeNCOOS, 2023). Strong tidal forcing generates the resuspension of sediment in Bay, driving increased turbidity, which likely affects the level of light that is available for phytoplankton to grow in the Bay (e.g., Monbet 1992; Trainer et al. 1998; Tas & Lundholm 2017). The degree of tidal forcing

also limits the time that oceanic waters spend in the estuary (which limits the exposure time of habitats in upper reaches of the Bay to oceanic phytoplankton, e.g., Álvarez-Salgado et al. 2008; Yñiguez et al. 2018; Qin and Shen 2019). This is clearly reflected in sharp shifts in phytoplankton communities driven by the tides, which are dominated by marine taxa at high tide or resuspended benthic diatoms at low tide (O'Connell 2013). As a result, HABs present in Humboldt Bay are likely from ocean origin (rather than in-situ development), and the distribution is closely tied to the reach of ocean waters into the Bay.

Processes and Considerations of Toxin Loading in Bivalves

Toxin loading in bivalves in Humboldt Bay is determined by their exposure as well as their species-specific feeding and elimination rates. The first element of risk of bivalve exposure to toxic *Pseudo-nitzschia* is dependent on the development of an ocean (or estuarine) HAB, and how effectively ocean to estuary exchange processes transport (or retain) HABs into the Bay. HABs in the Bay are affected by processes that govern retention and distribution of HABs within the Bay. DA in the environment can be retained in cells as particulate DA (pDA) or as dissolved DA (dDA) that is excreted by cells or released during “sloppy” feeding by copepods (e.g., Teegarden et al. 2003). DA in the particulate form is the dominant, perhaps sole, form of DA taken up by bivalves (see e.g., Novaczek et al. 1991). As a result, the risk of DA contamination in bivalves is determined by the concentration, and toxicity of *Pseudo-nitzschia* cells (both absolute and relative to the rest of the phytoplankton community), and the net effect of a species-

specific uptake rate (including selective rejection of *Pseudo-nitzschia*), and the depuration rate (i.e., the rate at which toxins are eliminated from the gut and tissues of a bivalve; Figure 1).

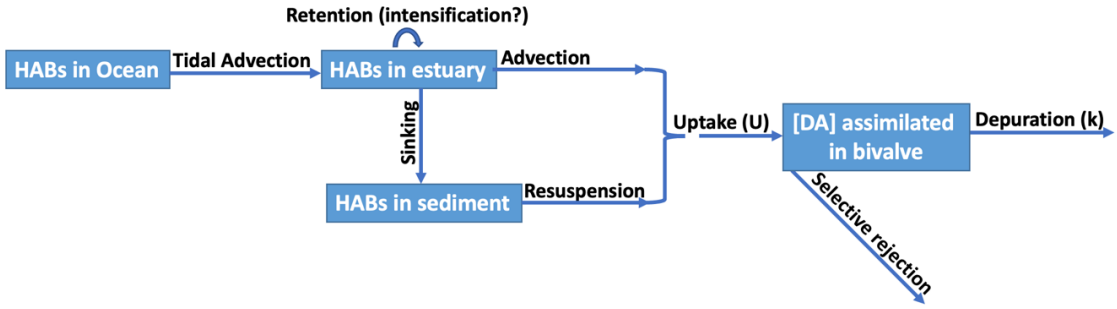

Figure 1. Conceptual model of factors governing exposure of bivalves to HABs within an estuary.

The dynamics governing the time dependent toxin loading in a bivalve can be summarized by the following equation outlined in Silvert & Subba Roa (1992):

$$dC_M/dt = F \cdot A \cdot C_A - D \cdot C_M$$

where F is a bivalves filtering rate, A is the concentration of *Pseudo-nitzschia* (cells/L), C_A is the concentration of DA in *Pseudo-nitzschia*, D is the depuration rate, and C_M is the concentration of DA in the bivalve. This model summarizes the conceptual basis for understanding how to relate the variability of environmental DA to toxin loading in a bivalve. This model is a simplified expression of the relevant dynamics under constant conditions, in which uptake is a constant linear process and depuration represents a constant proportional loss over time, however these processes are affected by a series of environmental and biological factors.

Uptake of DA depends on the presence and concentration of DA in *Pseudo-nitzschia* in the surrounding environment (Sauvey et al. 2021). This is countered by the

rate at which bivalves remove toxins from their body, often referred to as depuration, through egestion, excretion (Bricelj & Shumway 1998) or possibly chemical degradation (Stewart et al. 1998). Both uptake and depuration generally differ among species and are possibly size and temperature dependent. In general uptake (e.g., Saucedo et al. 2004; Rollwagen-Bollens et al. 2021) and depuration (Novaczek et al. 1992; Blanco 2006) increase with increasing temperature. Uptake occurs per allometric relationships between gill area and length or weight (reviewed by Cranford et al. 2011). The effect of weight on depuration is not well understood, as some studies have shown that smaller individuals depurate DA faster than larger ones (Novaczek et al. 1992), and others have found that body weight has no significant effect on depuration (Blanco et al. 2002; Mafra et al. 2010a).

Ecological controls on filtration include foraging behavior, ingestion versus deflection to pseudo-feces and physical and competitive influences. Phytoplankton exceeding some minimum threshold may be required to trigger active feeding (e.g., Riisgård et al. 2003), and the number of cells ingested can saturate at high concentrations (Foster-Smith 1975). Bivalves have been observed to reduce filtration when exposed to *Pseudo-nitzschia* in a monoculture, regardless of toxicity (Mafra et al. 2009a; Mafra et al. 2009b; Thessen et al. 2010; Sauvey et al. 2021), and this is consistent with observations that ingestion of *Pseudo-nitzschia* and consequent uptake of DA is countered by selective rejection of *Pseudo-nitzschia* as pseudo feces (Mafra et al. 2009a, Mafra et al. 2009b; Mafra et al. 2010b; Thessen et al. 2010; Jennings et al. 2020; Sauvey et al. 2021). The accessibility of phytoplankton to benthic filter feeders depends on how much of the water

column is effectively connected to the benthic boundary layer through vertical mixing (Cloern et al. 1985; Cloern 1991) and competition among bivalves as they deplete phytoplankton stocks (Cloern 1982; Kimmerer and Thompson 2014; Lucas et al. 2016).

Different rates of depuration among species might reflect differences in metabolism, the presence (or absence) of bacteria in bivalves that can degrade DA (Stewart et al. 1998), or how DA is distributed among tissues (Novaczek et al. 1992; Silvert and Cembella 1995; Blanco et al. 2002; Álvarez et al. 2020). Depuration rates can also be sensitive to toxin concentrations (high toxin loads suppress depuration; Silvert & Subba Rao 1992). Simple one-compartment models assume that DA accumulates in a single compartment within a bivalve's body and that depuration from this pool occurs at a constant rate (Novaczek et al. 1992; Blanco et al. 2002). Multiple-compartment models treat DA as being sequestered in different tissues, subject to different rates of enrichment and loss (i.e., as has been shown for razor clams; Horner et al. 1993). Mussels depurate DA in a matter of hours to days due to their relatively fast depuration rates (1.4-1.6 day^{-1}; Mafra et al. 2010a), and as a result a single-compartment model appears to be best at describing depuration over relatively short timescales (up to a few weeks), though there is evidence that they can retain very low amounts of DA for longer periods (Mafra et al. 2010a; Novaczek et al. 1991). A multi compartment model is best at describing depuration in razor clams (*Siliqua patula*) which can take months to depurate DA from their tissues (Wekell et al. 1994).

Research Objectives and Hypotheses

The goal of this study was to take the first step towards elucidating the spatial and temporal variability of *Pseudo-nitzschia* HABs in Humboldt Bay, which has important implications for understanding present and future risk of exposure faced by commercial aquaculture operations and recreational fisheries in the Bay. I sought to (1) quantify the spatial pattern of toxin loading in naturally occurring bivalve species along ocean-to-estuary transects in Humboldt Bay, and (2) correlate toxin loading in bivalves to HAB intensity measured in Bay waters through time. My hypotheses were:

1. Bivalves near the mouth of the Bay would have DA concentrations similar to bivalves on the open coast.
2. Bivalves in North and South Bay would be synchronous in their response to HABs in the water column.
3. DA concentrations in bivalves would decrease with increased distance from the mouth of the Bay; and
4. Temporal patterns in DA concentrations in bivalves would reflect trends of toxic *Pseudo-nitzschia* blooms in the water column.

To evaluate these hypotheses, I collected three types of samples from the system. First, native bivalves were collected at eleven sites along ocean to upper estuary transects in Humboldt Bay and at one site on the open coast over several sampling occasions, and these samples were assayed to measure concentrations of DA in their soft tissues. Second, I collected water samples from two locations (Trinidad Wharf on the open coast

and Hog Island Wharf in Humboldt Bay) and assayed them to assess HAB presence and intensity. Lastly, I collected environmental data assembled from several sources to provide broader context for the observed variability in HABs and toxin loading. Based on the environmental data and analysis of water samples, I also explored an ancillary hypothesis that water characteristics and phytoplankton concentrations in Humboldt Bay at high tide would be like those observed in the coastal ocean.

MATERIALS AND METHODS

Bivalve Collection

Sampling for this study was conducted from May to October 2020 and May to September 2021, which generally spans the months of anticipated HAB exposure during a given year. Bivalves were collected at low tide from seven sites in 2020 and expanded to eleven sites in 2021. During the 2020 sampling season, mussels were collected from the lower reaches of North Bay at two sites at the entrance (North and South Jetty) and off the side of a dock at one site on the main channel (Hog Island Wharf; Figure 2). Butter clams were collected from the South Bay at a site near the entrance of the Bay (South Entrance), a site deeper in the Bay (Above the Marine Protected Area), and a site across the channel from the entrance to the Bay (Fields Landing). These same sites were sampled during the 2021 sampling season, with the addition of three new mussel sampling locations inside the North Bay (Samoa Campground on the main channel in the lower Bay, Woodley Island off the main channel in the upper Bay, and Mad River Slough in the northernmost reaches of the Bay where aquaculture production occurs) and one site on the open coast (Trinidad State Beach; Figure 2). Mussels were collected off rocks at Samoa Campground and Trinidad State Beach, and off the side of docks at Woodley Island and Mad River Slough. Other species were collected for this study (*Tresus nuttallii* and *Clinocardium nuttallii* from Chevron Docks in North Bay, *Clinocardium nuttallii*

from the North Entrance, and *Mya arenaria* from the Above the Marine Protected Area site) but were not analyzed due to resource limitations and lack of replicate sites.

Bivalves were collected in a manner consistent with legal methods and bag limits allowed under a recreational fishing license, under the auspices of James Ray, California Department of Fish and Wildlife's Senior Environmental Scientist, during the period spanning my field sampling. Bivalves were collected at the lowest tide on a two-week interval using clam guns, rakes, or by hand, as appropriate per recreational fishery regulation. During each sampling occasion, the goal was to collect at least six bivalves from each site, though on occasion a minimum number of four were collected. Shortly after collection, bivalves were rinsed with fresh water, placed in separate Ziploc bags, and stored at -20^{0}C prior to processing.

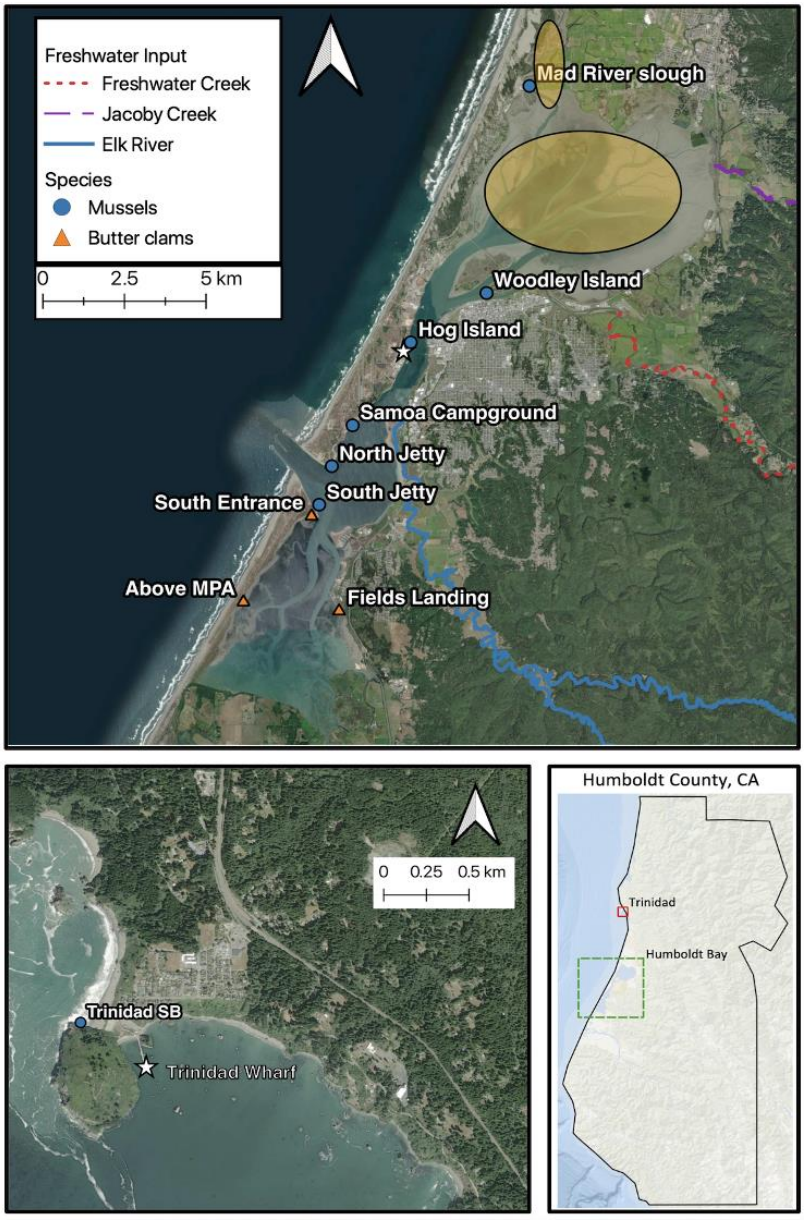

Figure 2. Map of sampling locations of mussels (blue circles) and butter clams (orange triangles) along ocean to upper estuary transects in Humboldt Bay (top panel). Bottom left panel shows the sampling location of mussels from Trinidad State Beach (Trinidad SB). Bottom right panel indicates location of Humboldt Bay, CA (green dashed box) and Trinidad, CA (red solid box). Stars represent water sampling locations at Trinidad Wharf and Hog Island Wharf. Yellow shaded ellipses represent the broad location of aquaculture operations in north Humboldt Bay.

DA assay

In the lab, each bivalve was thawed, measured (length and width), shucked, and weighed. All tissue and liquid recovered from the shell, including any liquid released during thawing and retained in the Ziploc bag, was combined, and homogenized in a commercial blender. If a bivalve was too small to process with a blender, a knife was used to finely mince tissues to a consistency similar to that produced by the blender. All tools were rinsed with fresh water and soap between specimens. To extract DA from the homogenized tissue, I combined an aliquot of homogenate with 50:50 methanol:deionized water at a 1 g: 9 ml ratio in a 50mL Falcon Tube, and immediately vortexed the mixture to generate a homogenous, well-mixed suspension. The suspension was centrifuged at 3500 RPM for 10 minutes to settle the clam tissue out of suspension, and the supernatant was carefully transferred using a sterile pipette to a 5mL centrifuge tube and stored at -80^{o}C pending subsequent analysis.

In the lab, supernatants were thawed and DA in each bivalve was assayed with ELISA kits (Mercury Science Test Kits, Jericho Sciences) following methods outlined in Litaker et al. (2008). Briefly, a DA antibody solution was added to each well which binds to DA at the bottom of the well. Each kit uses a 96 well plate (12x8) and can analyze 36 samples in duplicate, with the first two wells of every column being used for a control. After the control and samples were added, the plate was then shaken for 30 minutes, after which a DA tracer solution was added, and shaken for another 30 minutes. The DA tracer competes with DA in the samples to bind with the DA antibody at the bottom of each well. Each well was then washed, and a substrate solution added, which forms a color

that is negatively related to the amount of DA in each well (more color means less DA). A stop solution was then added that stops this reaction from occurring, and the plate was analyzed with a microplate reader at 450nm.

Spectrophotometric readings were generated with a SpectraMax i3x Multi-Mode Microplate Reader (Molecular Devices, San Jose CA). These readings are converted to estimates of DA as parts per million (ppm) based on a dose-response curve developed by Litaker et al (2008). This curve is a relation between: B_O, the observed signal (light transmission) for DA-free controls, B, the signal of the unknown sample, the slope of data that has been logistically transformed, and ED_{50}, the DA concentration in the middle of the curve. ED_{50} and the slope are defined constants, so all that is needed to calculate DA concentration is B_O and B using the following equation:

$$[DA] = ED_{50}[(B_O/B)\text{-}1]^{-slope}$$

B_O/B is used as a diagnostic for data quality, as the assay is most accurate when the ratio of B_O/B is equal to 0.5, which is the middle of the linear portion of the sigmoidal response curve. In practice, an acceptable range for B_O/B is 0.4-0.6 over which the response is very close to linear with DA concentration.

Preliminary assays were conducted on composite samples of all individuals per species by site and sampling occasion. I then used each composite sample to make a dilution series to identify or estimate the dilution that is the closest to 0.5 B_O/B (the middle of the range 0.4-0.6). Individual samples included in each composite sample were then assayed using the groups estimated best dilution. Samples that individually fell

outside B_O/B = [0.4,0.6] were re-assayed after adjusting the dilution based on comparison to the original site- and occasion-specific dilution curve.

Environmental Data: Abiotic Conditions and potential HAB Indicators

Water samples were collected at high tide inside Humboldt Bay at Hog Island Wharf and on the open coast at Trinidad Wharf (Figure 2). These samples were collected to compare the composition of the phytoplankton community (with emphasis on quantifying *Pseudo-nitzschia*), as well as DA concentrations (both particulate and total fractions) in Humboldt Bay to conditions nominally representative of ocean source waters to the Bay. Sampling occurred weekly from July to October 2020 and July to September 2021. Samples were collected with a 15-liter bucket from which several aliquots were collected and processed as follows.

Total DA and particulate DA

Aliquots of 60 ml were collected from water samples, and frozen at -20^{0}C for subsequent assay of total DA (tDA). Concurrently collected 250 ml aliquots from water samples were filtered onto 25mm diameter Whatman GF/F filters with a pore size of 0.7µm. Filter disks were placed in 12x75mm disposable glass test tubes and stored at -20^{0}C for subsequent assay of particulate DA, which is the fraction of tDA that is in the particulate form. Assays for tDA and pDA were conducted by collaborators at the University of California Santa Cruz using Liquid chromatography-mass spectrometry (LC-MS) with Select Ion Monitoring on an Agilent 6130 system following Wang et al., (2007) (R. Kudela, pers. comm., 2019).

Phytoplankton community structure and *Pseudo-nitzschia* density assay

The phytoplankton community was sampled by filtering 5-15 L of sampled seawater through a 20µm mesh sieve and preserving the retained particles in 1% Lugols' solution in 100 ml of filter seawater (sand filtered, obtained from HSU Marine Lab). In the lab, each sample was thoroughly resuspended by shaking the bottle. A 1mL subsample of each phytoplankton sample was counted under magnification using a Sedgewick-Rafter counting slide. All phytoplankton cells were counted in the first 30 fields, or until 300 total cells were reached. Phytoplankton were identified to the lowest practicable taxonomic level.

To improve density estimates, *Pseudo-nitzschia* cells were counted in additional fields until a minimum number of 10 cells were counted. All *Pseudo-nitzschia* cells were measured to differentiate the *P. seriata* (cell width > 3µm) and *P. delicatissima* (cell width < 3µm) size groups (Hasle and Syvertsen 1997).

Information on the fraction of the sample assessed for both phytoplankton community abundance and more specific counts of *Pseudo-nitzschia* was used to convert total counts to estimates of the numbers of cells per liter (cells/L) as an index of abundance.

Environmental data

High resolution time series of the following variables were obtained: temperature, salinity, chlorophyll α (a proxy for phytoplankton biomass) and sea water pressure (a proxy for tidal height). These time series were obtained from two CeNCOOS observation

sites in Humboldt Bay (Humboldt Bay shore stations at Chevron Docks and Hog Island) and one on the open coast (Trinidad Wharf shore station; CeNCOOS, 2023).

Statistical Analysis

All data analysis was developed in the statistical software language R (Version 4.1.0, R Core Team 2021), and all figures were created using the R package "ggplot2" (Wickham 2016).

Environmental patterns: Humboldt Bay-ocean connections

To test the ancillary hypothesis that water samples inside Humboldt Bay at high tide resembles that of the coastal ocean, I assessed whether phytoplankton community composition differed between coastal (Trinidad Wharf) and Humboldt Bay (Hog Island Wharf) sampling sites over the study period. I applied non-metric multidimensional scaling analysis (nMDS; 'metaMDS' in the 'vegan' package; Oksanen 2020) to a water sample-by-species matrix. The number of dimensions (axes) was minimized to maintain stress ≤ 0.20, indicative of a reasonable representation of the data that supports parsimonious interpretation (Clarke and Warick 2001). Only species that occurred in at least 5% of samples were used in this analysis. NMDS values from Trinidad Wharf and Hog Island Wharf were extracted and plotted by sampling date to assess similarities (or differences) in phytoplankton community composition during each sampling event. Trends in NMDS between Trinidad Wharf and Hog Island Wharf were then assessed using a Pearson correlation coefficient with significance tested at $\alpha=0.05$.

Bivalve analysis

Data structure. Constraints on the number of available assays for processing bivalves for DA concentrations required prioritization of samples that could be analyzed. Therefore, analysis focused on mussels and butter clams because they were well distributed between each basin. Further, a subset of sampling occasions was chosen to span the range of high and low HAB exposure based on observed HAB indices (HAB indices from water samples described below).

Two sample *t*-test. A two-sample *t*-test was used to test Hypothesis 1 that mean DA concentrations in mussels located near the mouth of Humboldt Bay were the same as mussels located on the open coast. DA concentrations in mussels were $\log_{10}$-transformed to achieve a normal distribution and meet model assumptions. Assumptions for this analysis (i.e., normality and homogeneity of variance) were assessed visually. Mean $\log_{10}$-transformed DA concentrations in mussels located at North Jetty and South Jetty (at the mouth of Humboldt Bay) were compared to mussels located at Trinidad State Beach (on the open coast). The statistical significance level for this analysis was set at $\alpha=0.05$.

Pairwise correlation. To test Hypothesis 2, that bivalves in North and South Bay will be synchronous in their response to HABs in the water column, I compared mean DA in mussels and butter clams using pairwise correlation analysis. Mean DA was calculated across all sites for each sampling occasions for both mussels and butter clams. The statistical significance level for this analysis was set at $\alpha=0.05$.

Spatial pattern and environmental drivers of DA loading

Measures of distance. I consider two measures of distance as the basis for evaluating spatial gradients in bivalve DA concentrations. Linear distance (i.e., as a crow flies) was calculated as the distance between the mouth of the Bay and each sampling site (km). The second distance measure was based on using 'age of water' extracted from a circulation model of Humboldt Bay as a proxy for the level of exposure to waters coming in from the ocean extracted for the years 2015-2018 (J. Anderson, pers. comm., 2022). Age of water is a measure of the time water has spent at a given region of the Bay since it entered the boundary of the system (i.e., the coastal ocean outside the Bay; Camacho et al. 2015). This was calculated by fitting a generalized additive model (R package "mgcv"; Wood 2011) relating age of water to day of year using a cyclic cubic spline to ensure continuity across the December - January transition (Table 1; see Appendix A for plots). This measure accounted for quasi-climatological, seasonal variability in age of water across sites (Figure 3). For convenience, the estimates for age of water taken from the generalized additive model are assumed to be very precise approximations in subsequent modeling (i.e., any uncertainty in these estimates is not accounted for in subsequent modeling).

Table 1. Measures of distance as linear distance (km) and the range of age of water (days) spanning the months during which bivalves were collected (May through October) at all mussel and butter clam sampling locations in the North and South Bay. Age of water measures were obtained from years 2015-2018 from a circulation model of Humboldt Bay and was calculated by fitting a generalized additive model to the source data, relating age of water to day of year using a cubic spline. For each species, sites are listed in order of closest to the mouth of the Bay and increase in distance away.

Species	*Site*	*Distance (km)*	*Range of Age of Water (days)*
Mussels	South Jetty	0	13 - 18
	North Jetty	0.1	12 - 17
	Samoa Campground	1.5	14 - 19
	Hog Island Wharf	4.6	18 - 26
	Woodley Island	7.2	25 - 40
	Mad River Slough	14.0	44 - 65
Butter clams	South Entrance	0.4	12 - 17
	Fields Landing	3.2	18 - 24
	Above the MPA	3.9	20 - 27

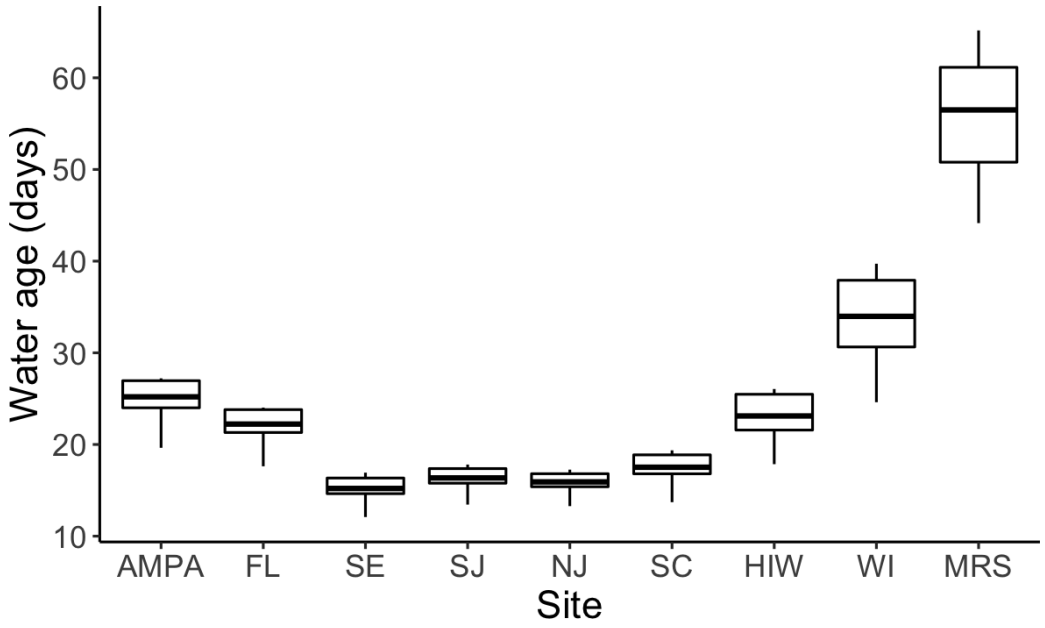

Figure 3. Boxplot of age of water (y-axis) in butter clams and mussels at each sampling site (x-axis) across the months during which samples were collected (May through October). Sites are listed from most southern to northern in Humboldt Bay and abbreviated as Above the MPA (AMPA), Fields Landing (FL) , South Entrance (SE), South Jetty (SJ), North Jetty (NJ), Samoa Campground (SC), Hog Island Wharf (HI), Woodley Island (WI), and Mad River Slough (MRS). Note that butter clams were only collected from AMPA, FL and SE and mussels were only collected from SJ, NJ, SC, HI, WI, and MRS. Boxes capture the interquartile range and horizontal solid black lines indicate the median value.

Environmental drivers. Preliminary efforts to develop predictive models linking pDA to environmental drivers were not successful (Appendix B). Therefore, I used linear interpolation to generate a time series of estimated daily pDA concentrations from observations collected at a roughly weekly interval at Hog Island Wharf. I then used this time series to iteratively calculate an index of DA concentration in a bivalve (DA_B^*) at time *t* as:

$$DA_B^*(t) = \alpha\, DA_E(t) + DA_B^*(t-1)e^{-k}$$

where α is the clearance rate (i.e., the volume of water a bivalve filters per unit time), $DA_E(t)$ is the linearly interpolated pDA concentration from Hog Island Wharf at time *t*., and *k* is the depuration rate. I used clearance rates of 40L day^{-1} for mussels (Silvert & Subba Rao 1992) and 48L day^{-1} for butter clams (Jennings 2012). In combination, $\alpha\, DA_E(t)$ is an index of the net uptake of DA from the environment. Depuration rates, which set the fraction of DA already in the bivalve that is removed per unit time, were set at 1.5 day^{-1} for mussels (Mafra et al. 2010a) and 0.84 day^{-1} for butter clams (Jennings 2012).

This simple model does not include potential effects of size or environment on DA_B^*, and thus represents a bivalve of average size experiencing constant uptake and depuration rates regardless of temperature, and DA_B^* is best understood as an index of HAB toxin in a bivalve rather than an explicit DA concentration. Therefore, DA_B^* is an integrated measure of pDA concentrations from Hog Island Wharf.

HAB index spatial models. Generalized linear mixed effects models (GLMMs) were used to test Hypothesis 3, that DA concentrations in bivalves will decrease with

increased distance from the mouth of the Bay, and Hypothesis 4, that temporal patterns in DA concentrations in bivalves reflect trends of DA and *Pseudo-nitzschia* blooms in the water column. Models were designed to test how DA concentrations in bivalves were related to covariates of distance (linear distance [km] and age of water [days]) and integrated pDA (i.e., DA_B^*) from Hog Island Wharf. Preliminary analysis indicated that the two measures of distance (linear and age of water) were colinear for mussels (r = 0.97; $p << 0.001$) and butter clams (r = 0.99; $p << 0.001$), so these distances were fit separately in all spatial models fit.

Model fitting was conducted following protocols outlined in Zuur (2009). First, different random effects structures for the GLMM were evaluated using Akaike information criterion, corrected for small sample size (AICc) by maintaining all fixed effects (distance, integrated pDA, and the interaction between distance and integrated pDA) in the model (R package "lme4"; Bates et al. 2015). The best random structure was a random intercept for sampling occasion to account for the lack of independence within a sampling occasion, and this performed better than models that also included random slopes for either distance or integrated pDA. The model

$$\log(DA_B) \sim Distance + pDA + Distance{:}pDA + (1|Occasion)$$

relates $\log_{10}$-transfromed DA concentrations in a bivalve at a given location (DA_B) to the distance from the ocean (either linear or age of water), integrated pDA from Hog Island Wharf, an interaction between distance and integrated pDA, and a random intercept for sampling occasion that accounts for variability in DA_B at the mouth of Humboldt Bay (maximum ocean exposure). The "dredge" function (R package "MuMin"; Barton &

Barton 2015) was then applied to the mixed effect model to find the optimal fixed effect structure using AICc. Model assumptions (homogeneity of variance and normally distributed residuals) were visually assessed using residuals vs. fitted, residuals vs. covariates, and histogram of residuals. Results were plotted using model predictions with 95% confidence intervals estimated using bootstrapping (function "bootMer", R package "lme4"; Bates et al. 2015). Mussel and butter clam DA concentrations were modeled separately. Preliminary analysis identified a significant species:distance interaction, but lack of overlap in species distributions meant that this could not be cleanly interpreted as a function of species or major basin in the Bay (i.e., North Bay v. South Bay). Weight was excluded from the model because experimental literature suggests weight does not affect DA concentrations in mussels (Mafra et al. 2010a) and there was no indication of a $\log_{10}$(DA)-weight relationship at the site level (but see Appendix C).

Spatial models. To further test Hypothesis 3, that DA concentrations in bivalves decrease with increased distance from the mouth of the Bay, I examined if a pattern could be resolved without including information on environmental HABs. To do so, I created descriptive spatial models that related DA concentrations in bivalves to each measure of distance (linear distance and age of water), without including integrated pDA from Hog Island Wharf as a covariate. This GLMM

$$\log\left(DA_B\right) \sim Distance + (1 + Distance|Occasion)$$

relates $\log_{10}$-transformed DA concentrations in a bivalve at a given location (DA_B) to distance from the ocean, and sampling occasion with a random intercept intended to account for variability in DA_B at the mouth of Humboldt Bay (maximum ocean exposure)

and a random slope to account for the variability among sites depending on sampling occasion. The model was fit with R package “lme4” (Bates et al. 2015). This random effect structure was deemed superior to alternative random effects structures based on AICc (differing from the previous set of models that included the integrated pDA covariate), following protocols outlined in Zuur et al 2009. Model assumptions (homogeneity of variance and normally distributed residuals) were visually assessed using graphs of residuals vs. fitted values, residuals vs. covariate values, and histograms of residuals. Results were plotted using model predictions with 95% confidence intervals estimated using bootstrapping (function “bootMer”, R package “lme4”; Bates et al. 2015).

Post-hoc analysis: Exploring the sensitivity of spatial patterns to sites

GLMMs were initially fit to the entire data set (i.e., using all sites) for each species. For butter clams, this approach posed no obvious challenges, but prompted post-hoc analysis of how changes in DA concentrations in butter clams might differ between the gradient along the western shoreline of Humboldt Bay (South Entrance to Above MPA) and a gradient that crossed the Bay (South Entrance to Fields Landing).

For mussels, models fit to data from all sites were found to suffer from problematic spatial patterns in the residuals, and patterns in the results that could not be readily interpreted as being real or being artifacts of the imbalanced sampling design (due to substantially lower sample sizes in the northernmost sites through time). Therefore, GLMMs for mussels exclude the Mad River Slough and Woodley Island sites and only

included observations collected at a core set of sites in the lower portion of the North Bay (i.e., South Jetty, North Jetty, Samoa Campground, and Hog Island Wharf), all of which are situated on the western shore of the Bay. I then used these models to predict DA concentrations for the relevant sampling occasions at Woodley Island and Mad River Slough and compared these predictions to observations as a test of whether dynamics in the lower Bay are useful indicators of what DA concentrations are in bivalves further from the ocean, and to identify the characteristics of any departures from this hypothesized pattern.

RESULTS

Environmental Patterns: Humboldt Bay-Ocean Connections

Oceanographic observations

Throughout this study, waters inside Humboldt Bay were generally warmer than coastal waters observed at Trinidad Wharf, and sites inside Humboldt Bay located further from the mouth were generally warmer than those located near the mouth (Figure 4). Despite differences between monitoring sites, temperature observations inside Humboldt Bay are positively correlated to temperature observations on the coast at high tide during 2020 ($r = 0.76$; $p << 0.001$) and 2021 ($r = 0.63$; $p << 0.001$) (Figure 5). Observations of both chlorophyll and salinity inside Humboldt Bay followed similar trends to observations on the coast from Trinidad Wharf. Chlorophyll inside Humboldt Bay was positively correlated to chlorophyll at Trinidad Wharf at high tide during 2020 ($r = 0.24$; $p = 0.001$) and 2021 ($r = 0.46$; $p << 0.001$) (Figure 5). Salinity observations were deemed less reliable: COVID-19 lockdowns in 2020 precluded necessary calibrations which undermined the quality of these observations (Gavin Zirkel, pers. comm., 2022).

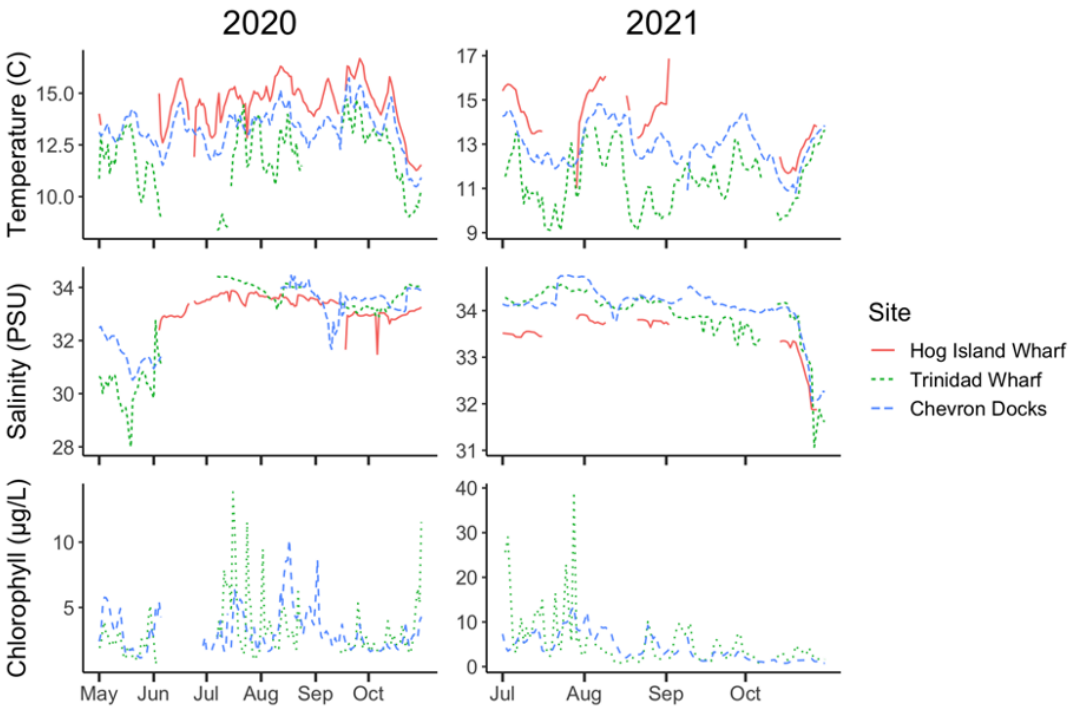

Figure 4. Temporal trends in daily average values of temperature (C), salinity (PSU), and chlorophyll (ug/L) from 2020 (left pots; May through October) and 2021 (right plots; July through October) at Hog Island Wharf (solid red line), Chevron Docks (dotted green line) and Trinidad Wharf (dashed blue line). Breaks in lines represent missing data. Note that no chlorophyll data was available at Hog Island Wharf in 2020 and 2021.

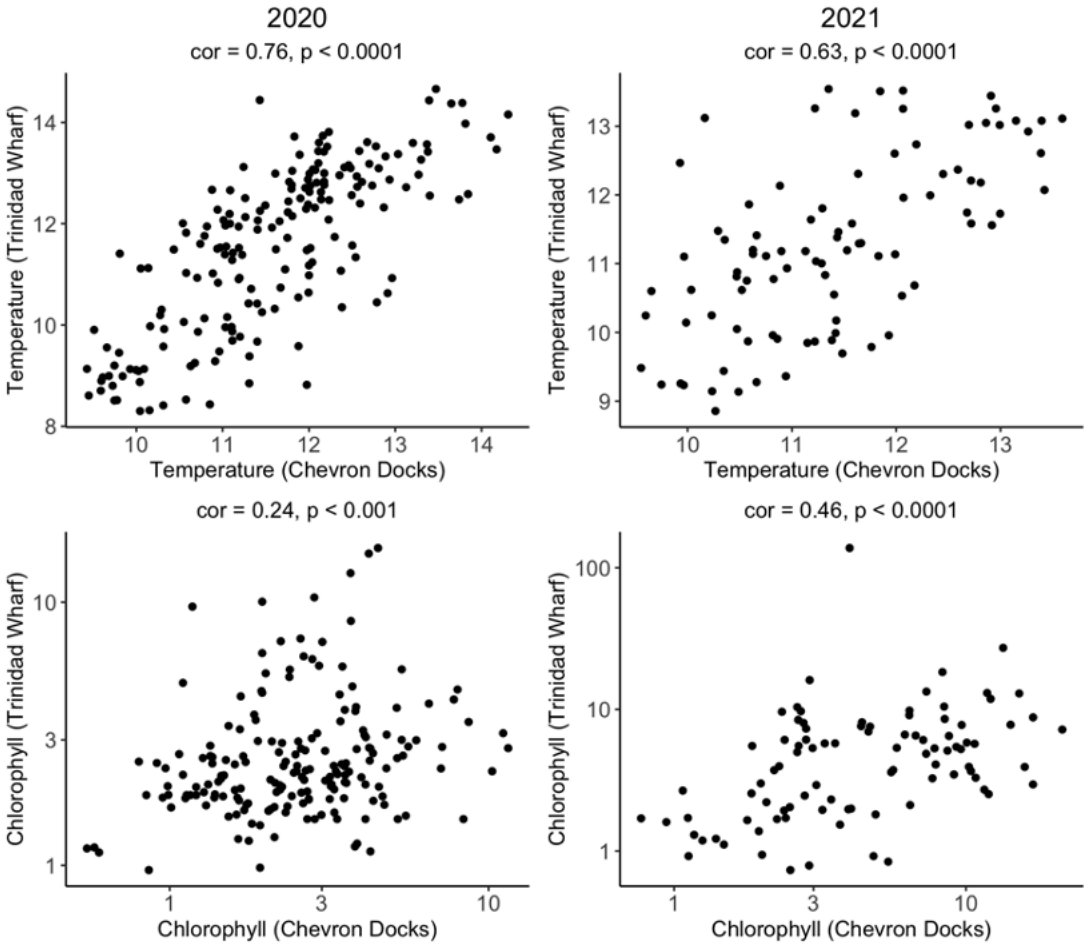

Figure 5. Pairwise scatter plots comparing daily high tide values of temperature and chlorophyll between Chevron Docks (inside Humboldt Bay) and Trinidad Wharf (coastal ocean) from 2020 (left pots; May through October) and 2021 (right plots; July through October). The Pearson correlation coefficient and p-value for each relationship is indicated above each plot. Note chlorophyll concentration is on a $\log_{10}$-transformed scale.

Water sampling observations: DA, *Pseudo-nitzschia*, and total phytoplankton

Analysis of concentrations of total DA (tDA), particulate DA (pDA), *Pseudo-nitzschia*, and total phytoplankton is based on 31 water samples collected from Hog Island Wharf and Trinidad Wharf. Due to the timing of tides, no samples for *Pseudo-nitzschia* and total phytoplankton concentrations were collected on the August 28th, 2020 sampling occasion.

Total DA (tDA). During the 2020 sampling season, concentrations of tDA inside Humboldt Bay resembled those observed in coastal waters at Trinidad Wharf (Figure 6). Despite these similarities, a sharp increase in tDA at Trinidad Wharf in the end of September 2020 strongly differed from low tDA observed at Hog Island Wharf. There was a weak positive correlation between these two sites when unusually high tDA in late September 2020 was included ($r = 0.09$; $p = 0.82$), and a strong positive correlation when that single point was removed ($r = 0.77$; $p = 0.04$). During the 2021 sampling season, concentrations of tDA were below detection limits on all sampling occasions at both sites.

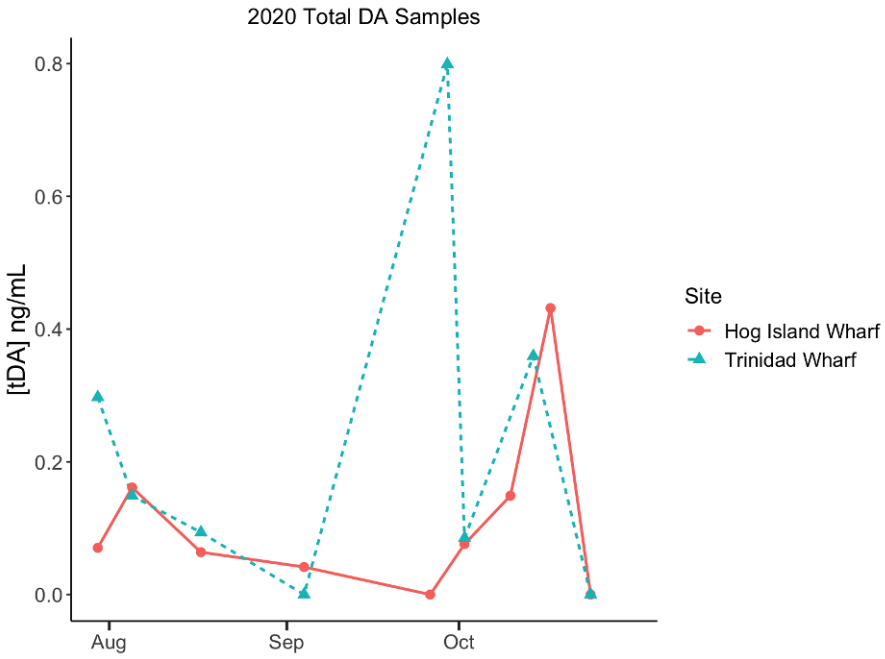

Figure 6. Temporal variability in tDA collected at high tide from Hog Island Wharf (solid red line and circles) inside Humboldt Bay and Trinidad Wharf (dashed blue line and triangles) on the coastal ocean from July 30th through October 24th 2020.

Particulate DA (pDA). Throughout both the 2020 and 2021 sampling season, pDA was detected at relatively low concentrations (Figure 7). In general, there was a significant positive correlation in pDA between Hog Island Wharf and Trinidad Wharf (r = 0.38; p = 0.02). This positive relationship weakened when assessing data from only 2020 (r = 0.14; p = 0.68) but increased when assessing data from only 2021 (r = 0.44; p = 0.08). The lack of strong correlations, particularly in 2020, is likely due to sharp increases in pDA at Trinidad Wharf (late September 2020 and early August 2021) during declines in pDA at Hog Island Wharf (Figure 7).

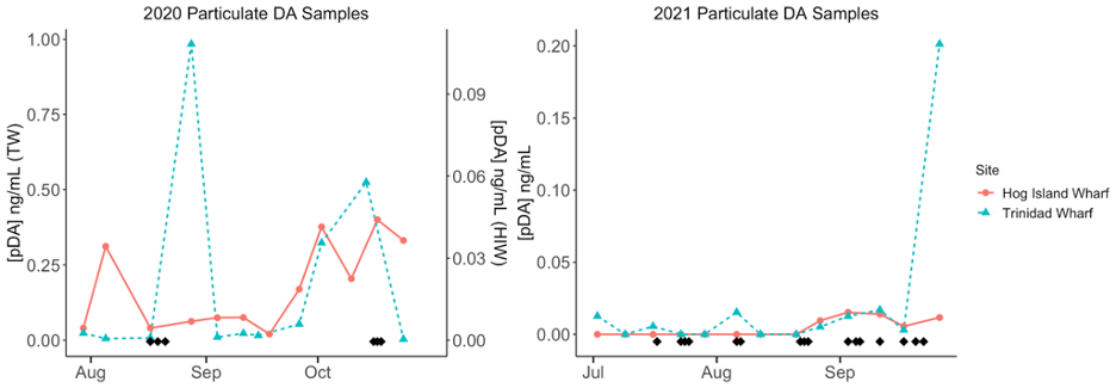

Figure 7. Temporal variability in pDA collected at high tide from Hog Island Wharf (solid red line and circles) inside Humboldt Bay and Trinidad Wharf (dashed blue line and triangles) on the coastal ocean. Panels from left to right: pDA samples collected in 2020 (July 30th through October 24th) and 2021 (July 2nd through September 26th). Black diamonds represent dates when bivalves were sampled and retained for analysis. Note the double y-axis for data collected in 2020.

Pseudo-nitzschia concentrations. Of the *Pseudo-nitzschia* types sampled during this study, *P. delicatissima* was observed at low frequencies and concentrations compared to the frequently occurring and abundant *P. seriata*. Analysis for this study focuses on *P. seriata*. Throughout both years of the study, *P. seriata* concentrations (cells/L) inside Humboldt Bay generally resembled those observed in coastal waters at Trinidad Wharf (Figure 8). Strong similarities in trends of *P. seriata* concentrations between Trinidad Wharf and Hog Island Wharf reflect a strong positive correlation ($r = 0.90$; $p << 0.001$). This strong positive relationship between coastal and Humboldt Bay sites weakened substantially when assessing data from 2020 only ($r = 0.05$; $p = 0.88$) and remained strong when assessing data from 2021 only ($r = 0.89$; $p << 0.001$). Differences in the strength of the correlation is likely due to a sharp increase in *P. seriata* concentrations in 2020 (mid-August) at Hog Island Wharf, when concentrations declined slightly at Trinidad Wharf (Figure 8).

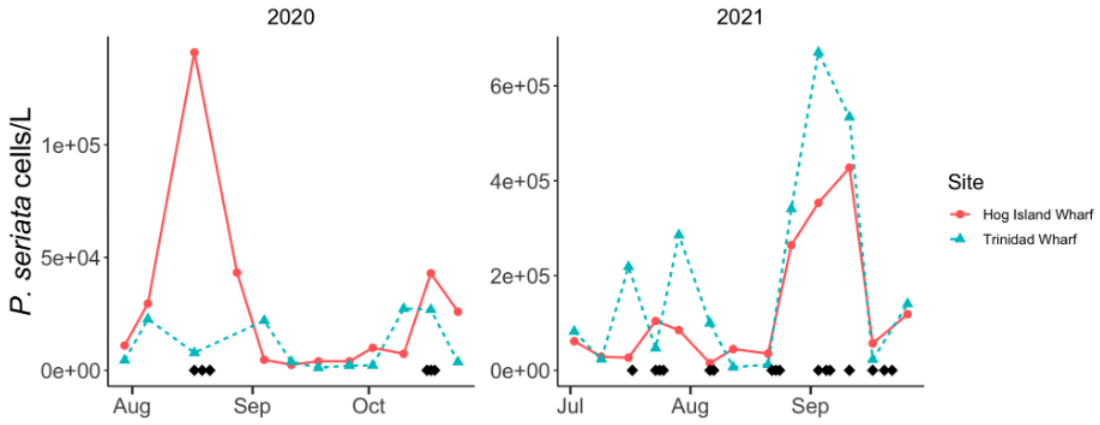

Figure 8. Temporal variability in *P. seriata* concentrations (cells/L) at high tide from Hog Island Wharf (solid red line and circles) inside Humboldt Bay and Trinidad Wharf (dashed blue line and triangles) on the coastal ocean. Panels from left to right: *P. seriata* collected in 2020 (July 30th through October 24th) and 2021 (July 2nd through September 26th). Black diamonds represent dates when bivalves were sampled and retained for analysis.

Phytoplankton community. NMDS on four dimensions (stress=0.15) yielded interpretable patterns in the phytoplankton community (n = 43 out of 94 species that occurred in at least 5% of the samples) at high tide between Trinidad Wharf and Hog Island Wharf. Phytoplankton composition, indexed by NMDS, at Trinidad Wharf and Hog Island Wharf followed almost identical trends over both the 2020 and 2021 sampling periods. Phytoplankton composition at Hog Island Wharf is generally strongly correlated with phytoplankton composition at Trinidad Wharf at high tide as captured by correlation analysis of each of the axes in NMDS (Figure 9).

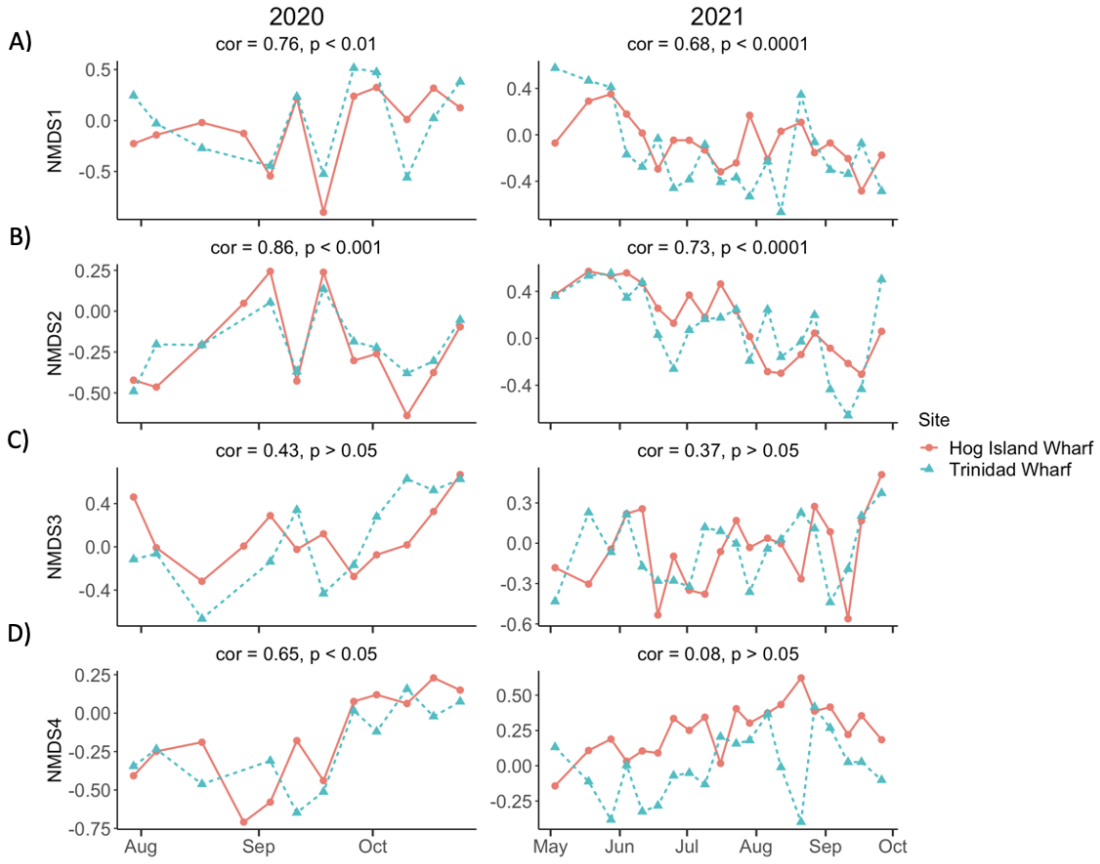

Figure 9. Time series of nonmetric multidimensional (NMDS) scaling ordination scores at Hog Island Wharf and Trinidad Wharf along axis 1 (A), 2 (B), 3 (C) and 4 (D) during the 2020 (left plots) and 2021(right plots) sampling seasons. Color, symbol, and line type corresponds to Hog Island Wharf (red circles and solid red lines) or Trinidad Wharf (blue triangles and dashed blue lines) water sampling sites. The Pearson correlation coefficient (*r*) and its significance, used to assess the strength of the correlation of trends in phytoplankton composition between Hog Island Wharf and Trinidad Wharf, is indicated above each plot.

General DA Patterns in Bivalves

Based on the samples that were collected, my analysis focused on 210 mussels (*Mytilus* spp) and 119 butter clams (*Saxidomus nuttalli*) collected during seven sampling occasions likely to be affected by HABs (8-10 May 2020, 17-18 August 2020, 16-18 October 2020, 6-7 August 2021, 22-24 August 2021, 3-6 September 2021, and 17-22 September 2021) and one sampling occasion likely to have low exposure (21-25 July 2021; Table 2). In Humboldt Bay, mussels were collected from sites in the lower reaches of the Bay at the entrance and on the main channel (South Jetty, North Jetty, Samoa Campground, and Hog Island Wharf), a site off the main channel to the east of Duluwat Island (Woodley Island), and a site in the northernmost reaches of the Bay (Mad River Slough). Mussels were also collected at Trinidad State Beach as a representative example for mussels along the open coast. Mad River Slough and Woodley Island were included to see if patterns observed in the lower reaches of the Bay held here, and the Trinidad State Beach site was included as an open ocean comparison. Butter clams were collected from three sites in South Humboldt Bay designated as South Entrance, Fields Landing and Above the Marine Protected Area. No mussels were collected during the first sampling event in May 2020 and no butter clams were collected during the last sampling event in late September 2021. Due to tides and timing, I was unable to collect butter clams from Fields Landing in August 2020 and mussels from South Jetty in late September 2021.

Table 2. Numbers of mussels collected from South Jetty (SJ), North Jetty (NJ), Samoa Campground (SC), Hog Island Wharf (HIW), Woodley Island (WI), Mad River Slough (MRS) in North Bay and Trinidad State Beach (TSB) from August 2020 to the end of September 2021 and butter clams collected from South Entrance (SE), Fields Landing (FL) and Above the MPA (AMPA) in South Bay from May 2020 to the beginning of September 2021. For each species, sites are listed in order of sites closest to the mouth of the Bay to sites located farthest away from the mouth. Spaces left blank indicate that no mussels or butter clams were collected on this date from a given site.

Species	*Site*	*8-10 May '20*	*17-18 Aug '20*	*16-18 Oct '20*	*21-25 Jul '21*	*6-7 Aug '21*	*22-24 Aug '21*	*3-6 Sept '21*	*17-22 Sept '21*
Mussel	SJ		6	5	6	6	6	6	
	NJ		5	6	6	6	6	6	6
	SC				6	6	6	6	6
	HIW		6	4	6	6	6	5	6
	WI				6	6	6	6	6
	MRS							6	5
	TSB				6		6	6	6
Butter clam	SE	6	6	6	6	6	6	6	
	FL	5		6	6	6	6	6	
	AMPA	6	6	6	6	6	6	6	

Throughout the study period, DA concentrations in bivalves remained well below the public health thresholds of 20ppm. The range of variation in DA concentrations in individuals at each site was often high, with a greater range of variability at sites located closer to the mouth compared to those located further away. For mussels, mean DA concentration across all sites and sampling occasions was 0.182 (± 0.148) ppm. In general, DA concentration in mussels decreased with increased distance from the mouth

of Humboldt Bay, with mean DA concentrations dropping from 0.251 (± 0.245) ppm at the North Jetty to 0.079 (± 0.041) ppm at Mad River Slough (Figure 10 and Figure 11). In butter clams, mean DA concentration across all sites and sampling occasions was 0.111 (± 0.073) ppm. Across all sampling occasions, DA concentrations in butter clams consistently decreased with increased distance from the mouth of the Bay, with mean DA concentrations at South Entrance being 0.150 (± 0.086) ppm to 0.074 (± 0.023) ppm Above the Marine Protected Area (Figure 10 and Figure 12). Across both species, DA concentrations varied depending on the sampling occasion, but were generally higher in October 2020 and September 2021 (Figure 11 and Figure 12).

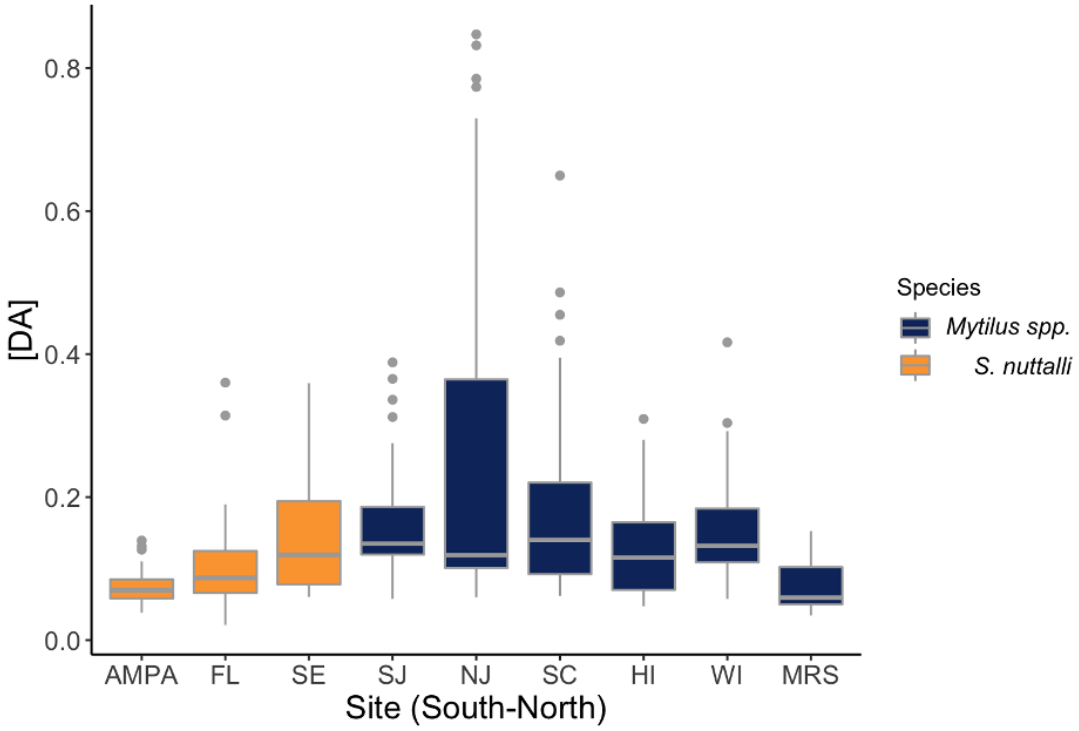

Figure 10. Boxplot of DA concentrations (y-axis) in butter clams and mussels at each sampling site (x-axis) across all sampling occasions. Sites are listed from most southern to northern in Humboldt Bay and abbreviated as Above the MPA (AMPA), Fields Landing (FL) , South Entrance (SE), South Jetty (SJ), North Jetty (NJ), Samoa Campground (SC), Hog Island Wharf (HI), Woodley Island (WI), and Mad River Slough (MRS). Note that butter clams were only collected from AMPA, FL and SE and mussels were only collected from SJ, NJ, SC, HI, WI, and MRS. Boxes capture the interquartile range, horizontal solid gray lines indicate the median value, and gray dots indicate outliers.

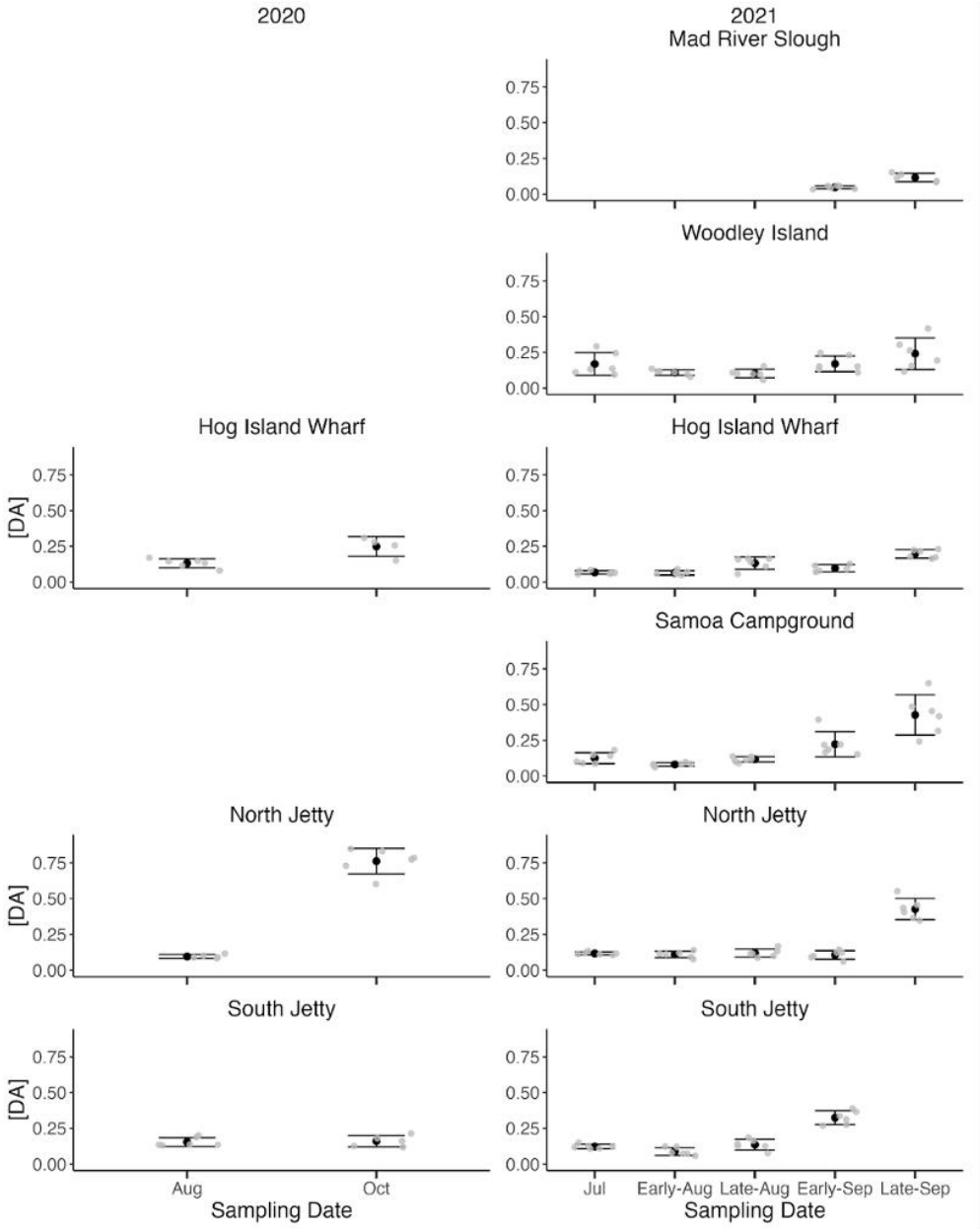

Figure 11. Interval plots showing mean concentration of DA ± SE (y-axis) in mussels during each sampling date (x-axis) in 2020 (left panels) and 2021 (right panels). Panels from top to bottom are listed from furthest from the mouth of Humboldt Bay (Mad River Slough) to closest (North Jetty and South Jetty). Black points indicate the mean, gray points indicate observed values, and vertical black lines above and below the mean represent ± SE.

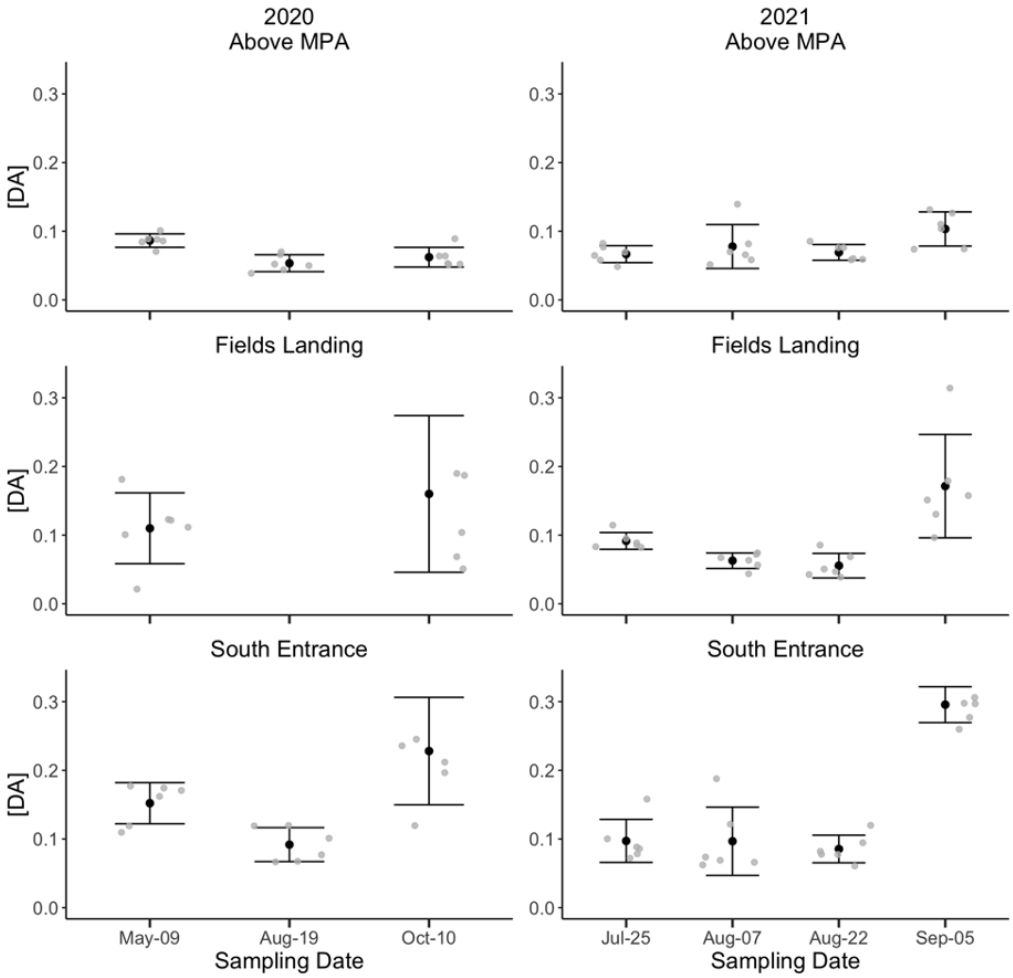

Figure 12. Interval plots showing mean concentration of DA ± SE (y-axis) in butter clams during each sampling date (x-axis) in 2020 (left panels) and 2021 (right panels). Panels from top to bottom are listed from furthest from the mouth of Humboldt Bay (Above MPA) to closest (South Entrance). Black points indicate the mean, gray points indicate observed values, and vertical black lines above and below the mean represent ± SE.

DA Concentrations in Mussels from Humboldt Bay Entrance and Open Coast

Two-sample *t*-tests of mean $\log_{10}$-tranformed DA concentration in bivalves between coastal sites (Trinidad State Beach) and sites located at the entrance of Humboldt Bay (North Jetty and South Jetty) generally support the hypothesis that DA concentrations in bivalves are similar between entrance and coastal sites. (Figure 13). This analysis was conducted for each of the four-sampling occasions where mussels were collected at Trinidad State Beach. During the late September 2021 sampling occasion, no mussels were collected from South Jetty due to the timing of tides, thus the *t*-tests were only conducted between North Jetty and Trinidad State Beach. DA concentrations at Trinidad State Beach were often similar to concentrations observed at North Jetty and South Jetty during each occasion Trinidad State Beach was sampled. For three out of the four sampling occasions, there was no significant difference ($p > 0.05$) in mean DA concentration between Trinidad State Beach and either site near the entrance to Humboldt Bay. The only occasion for which DA concentrations differed between Trinidad State Beach and locations inside Humboldt Bay was in early September 2021. During this occasion, DA concentrations were significantly higher at Trinidad State Beach compared to North Jetty ($p = 0.004$), and at South Jetty compared to Trinidad State Beach ($p = 0.003$).

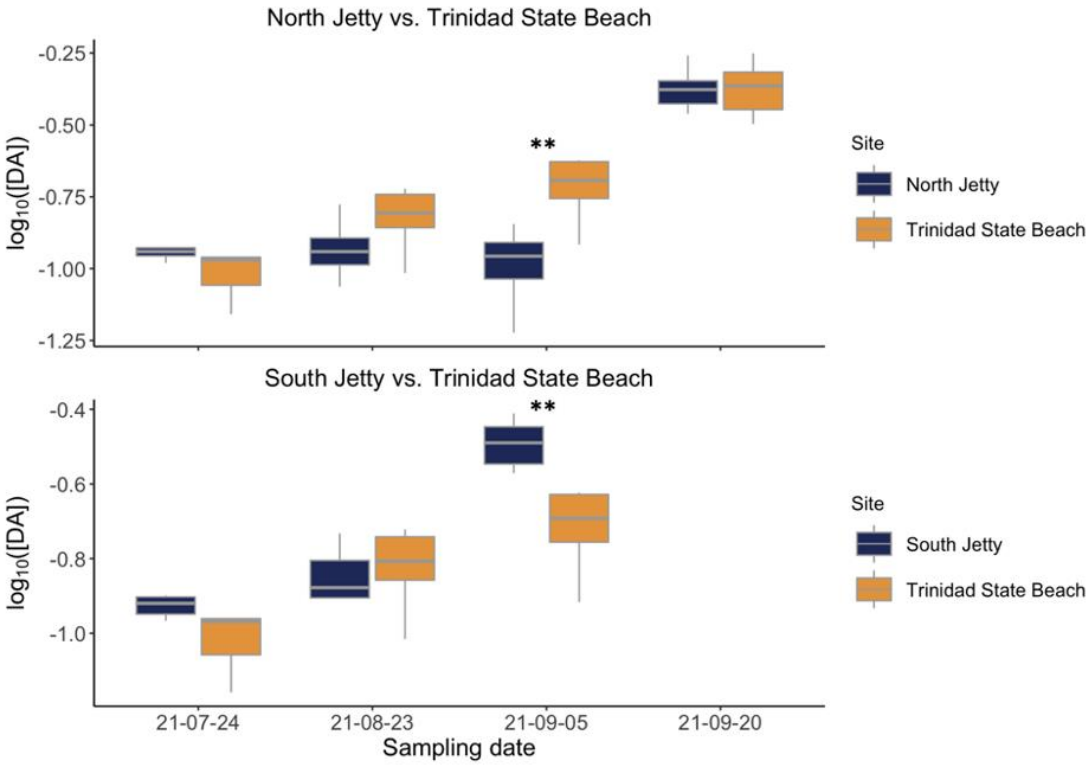

Figure 13. Boxplots comparing mean DA concentration (y-axis) in mussels at Trinidad State Beach and North Jetty (top panel) and South Jetty (bottom panel) by sampling date (x-axis). Significant differences ($p < 0.05$) were tested using a paired- samples t test. The significance level is set at: * = $p < 0.05$ and ** = $p < 0.01$. The y-axis indicates DA concentration on a $\log_{10}$-transformed scale. Boxes capture the interquartile range and horizontal solid gray lines indicate the median value. No mussels were collected at South Jetty in late September 2021.

Similarities in DA concentrations in bivalves from North and South Bay

Pairwise correlation analysis of mean DA concentrations in mussels and butter clams generally supports the hypothesis that bivalves in North and South Bay are synchronous in their response to HABs in the water column, though this relationship was not significant (r = 0.55; p = 0.26; Figure 14).

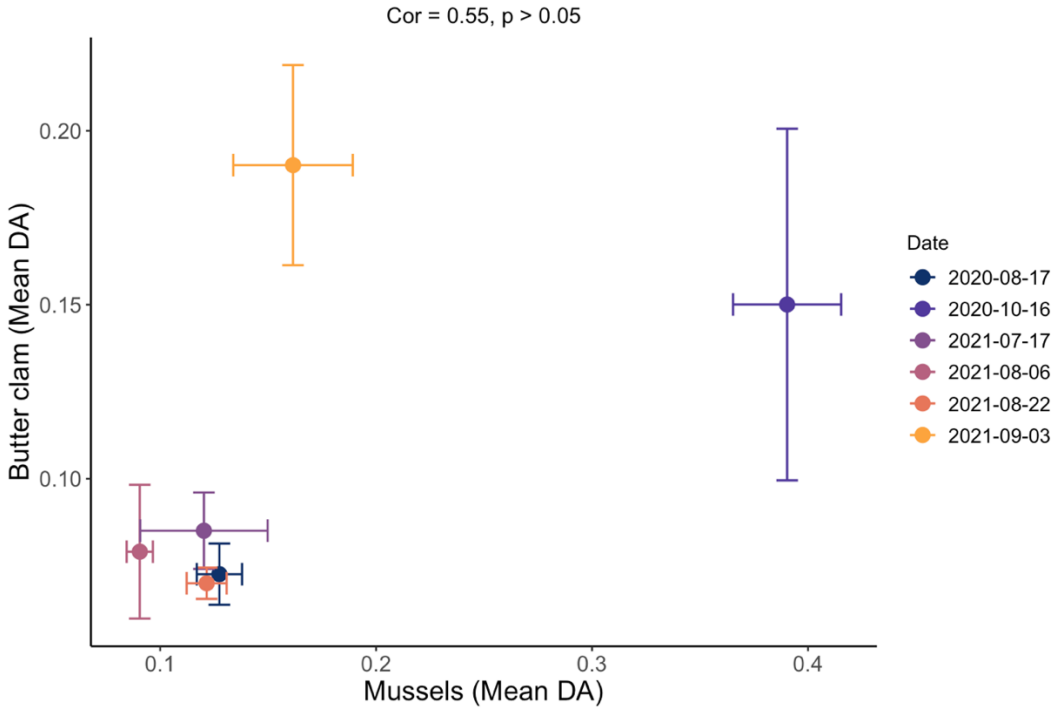

Figure 14. X-y plots showing mean concentration of DA ± SD (y-axis) in butter clams (y-axis) versus mussels (x-axis). Colored points indicate the mean DA concentrations for a given sampling occasion across all butter clams and mussel sites, and vertical and horizontal lines above and below and on either side of the mean represent ± SD. Colors represent the different sampling occasions when bivalves were collected. The Pearson correlation coefficient (r) and its significance, used to assess the strength of the correlation of mean DA concentrations between mussels and butter clams, is indicated above plot.

HAB Index Spatial Models: Mussels

Linear distance (km)

The best model for mussels using linear measures of distance (km) includes distance and integrated pDA from Hog Island Wharf as covariates and a random intercept for date (sampling occasion) (Figure 15). This model had a significant decline in (log_{10}-transformed) DA concentrations in mussels with increasing (linear) distance from the ocean (fixed effects slope: -0.0358 ± 0.0075; $p << 0.001$), and a significant increase in (log_{10}-transformed) DA concentrations with increasing integrated pDA (fixed effects slope: 0.2747 ± 0.0974; $p = 0.025$). Variability in the slope for sampling occasion explained less than half of the total variance in the data (r^2_{total} = 0.62, of which r^2_{fixed}= 0.35). There was an outlier of high log_{10}-transformed DA concentrations in mussels at a moderate value of integrated pDA (Figure 15). Available data also offered modest support (dAICc = 1.63) for a model that included a random intercept for date (sampling occasion) and a negative interaction between distance and integrated pDA but the interaction term was non-significant (fixed effects slope: -0.0101 ± 0.0137; $p = 0.4619$). No other plausible models were identified (Appendix D).

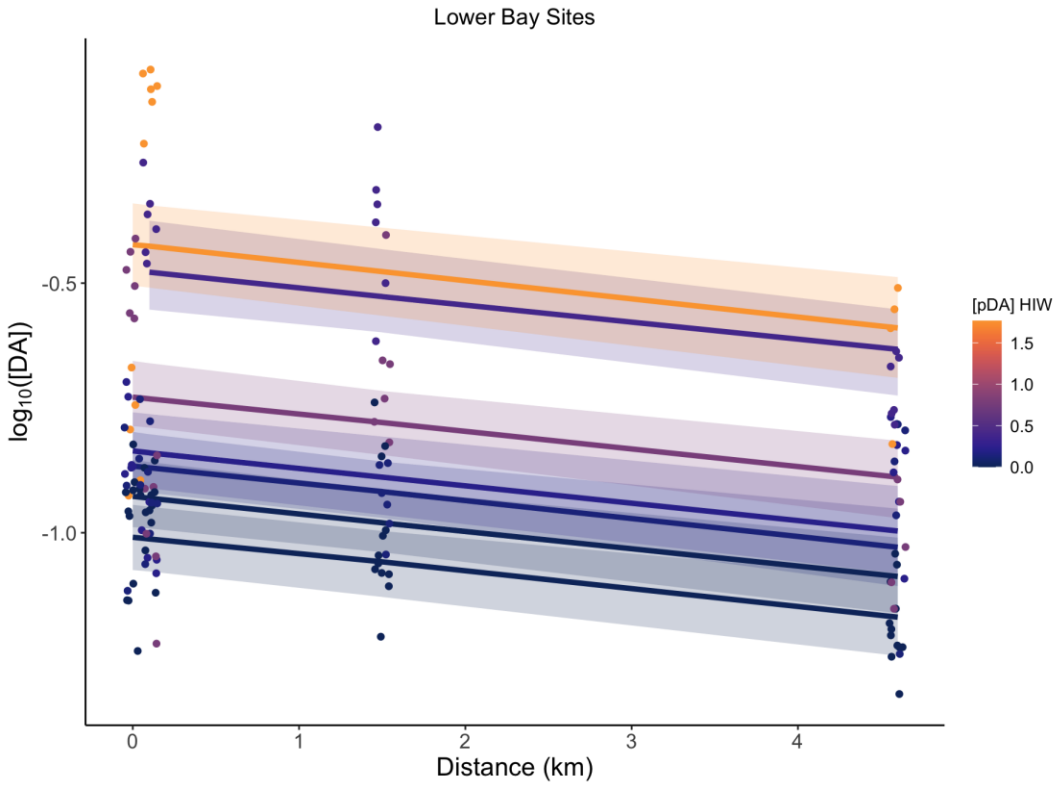

Figure 15. Generalized linear mixed model results from the effect of distance (km; x-axis) and integrated pDA concentrations from Hog Island Wharf on DA concentrations in mussels (y-axis) across all sampling occasions. Fitted regression lines of DA concentrations as a function of distance and integrated pDA with a random intercept for date. Colored lines correspond to integrated pDA concentrations during a given sampling occasion (date). Shaded regions are the 95% confidence intervals which were estimated using bootstrapping. Each point represents mean DA across replicate assays for an individual mussel. The y-axis indicates DA concentration in mussels on a $\log_{10}$-transformed scale.

Age of water (days)

The best model for mussels using age of water (days) included age of water and integrated pDA from Hog Island Wharf as covariates and a random intercept for date (sampling occasion) (Figure 16). This model had a significant decline in (log_{10}-transformed) DA concentrations in mussels with increasing age of water (fixed effects slope: -0.0218 ± 0.0044; $p << 0.001$), and a significant increase in (log_{10}-transformed) DA concentrations with increasing integrated pDA (fixed effects slope: 0.2923 ± 0.1027; $p = 0.025$). Variability in the slope for sampling occasion explained less than half of the total variance in the data (r^2_{total} = 0.64, of which r^2_{fixed} = 0.34). There was an outlier of high log_{10}-transformed DA concentrations in mussels at a moderate value of integrated pDA (Figure 16). Available data also offered modest support (dAICc = 1.37) for a model that included a random intercept for date (sampling occasion) and a negative interaction between age of water and integrated pDA but the interaction term was non-significant (fixed effects slope: -0.0067 ± 0.0075; $p = 0.3709$). No other plausible models were identified (Appendix D).

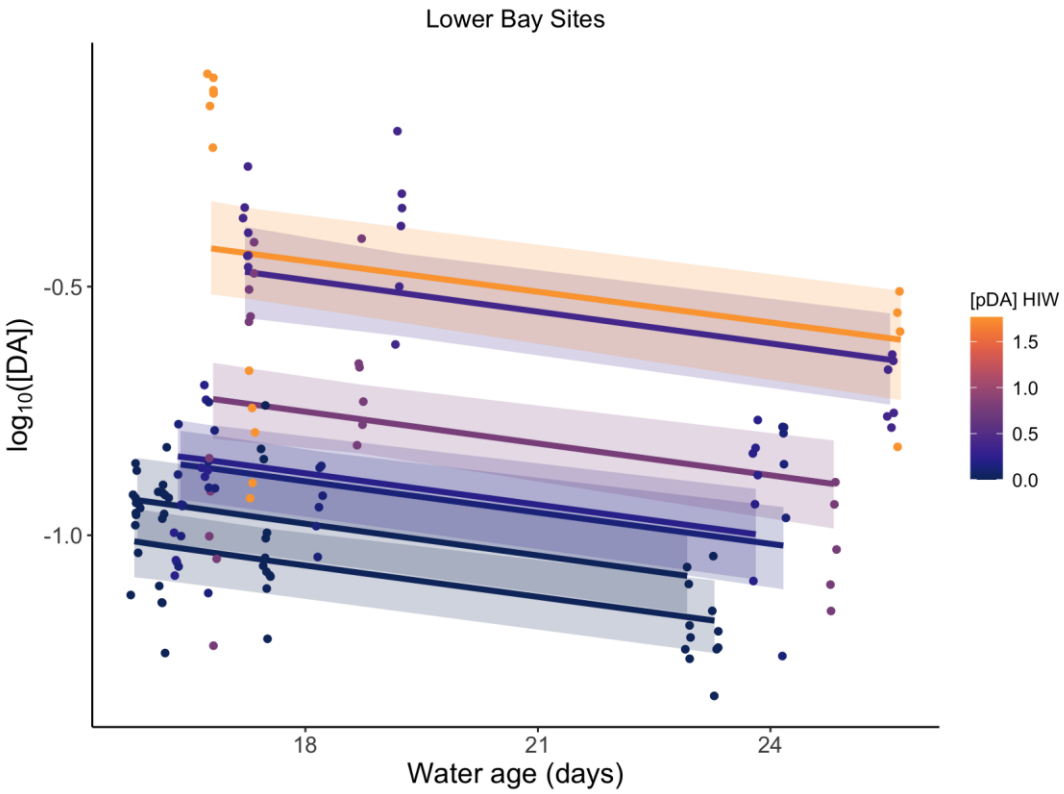

Figure 16. Generalized linear mixed model results from the effect of age of water (days; x-axis) and integrated pDA concentrations from Hog Island Wharf on DA concentrations in mussels (y-axis) across all sampling occasions. Fitted regression lines of DA concentrations as a function of age of water and integrated pDA with a random intercept for date. Colored lines correspond to integrated pDA concentrations during a given sampling occasion (date). Shaded regions are the 95% confidence intervals which were estimated using bootstrapping. Each point represents mean DA across replicate assays for an individual mussel. The y-axis indicates DA concentration in mussels on a $\log_{10}$-transformed scale.

Spatial Models: Mussels

Linear distance (km)

The best model for mussels using linear measures of distance (km) include a significant decline in (log_{10}-transformed) DA concentrations in mussels with increasing (linear) distance from the ocean (fixed effects slope: -0.0379 ± 0.0119; p = 0.0187; Figure 17). Variability in the intercept and slope of this trend associated with sampling occasion explained a substantial fraction of the total variance in the data (r^2_{total} = 0.70, of which r^2_{fixed} = 0.06). Random intercepts and slopes were strongly negatively correlated (r = -0.66).

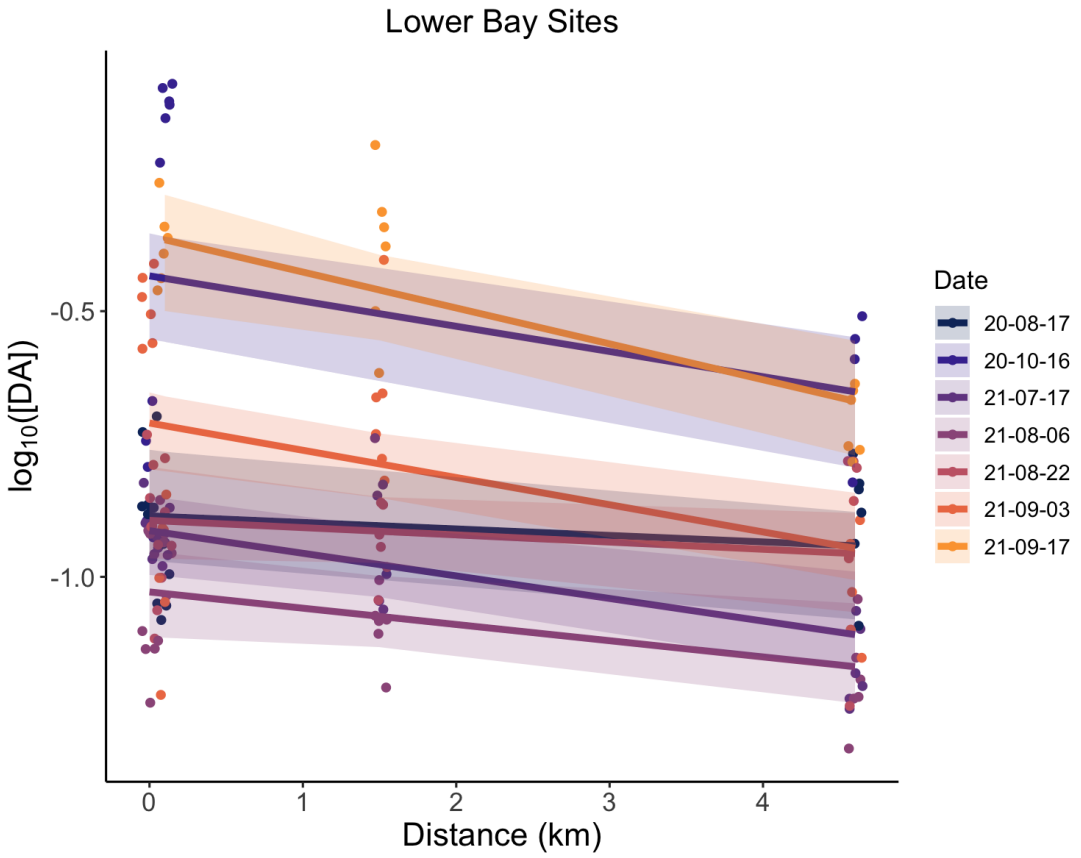

Figure 17. Generalized linear mixed model results from the effect of distance (km; x-axis) on DA concentrations in mussels (y-axis) across all sampling occasions. Fitted regression lines of DA concentrations as a function of distance and sampling occasion are displayed as colored lines. Shaded regions are the 95% confidence intervals which were estimated using bootstrapping. Each point represents mean DA across replicate assays for an individual mussel. The y-axis indicates DA concentration in mussels on a $\log_{10}$-transformed scale.

Age of water (days)

The best model included a random intercept for sampling occasion, and no random slope for the age of water. This model includes a significant decline in (log_{10}-transformed) DA concentrations in mussels with increasing age of water (fixed effects slope: -0.0220 ± 0.0044; $p << 0.001$; Figure 18) and indicated that variability in the intercept of this trend associated with sampling occasion explained a substantial fraction of the total variance in the data (r^2_{total} = 0.70, r^2_{fixed} = 0.06).

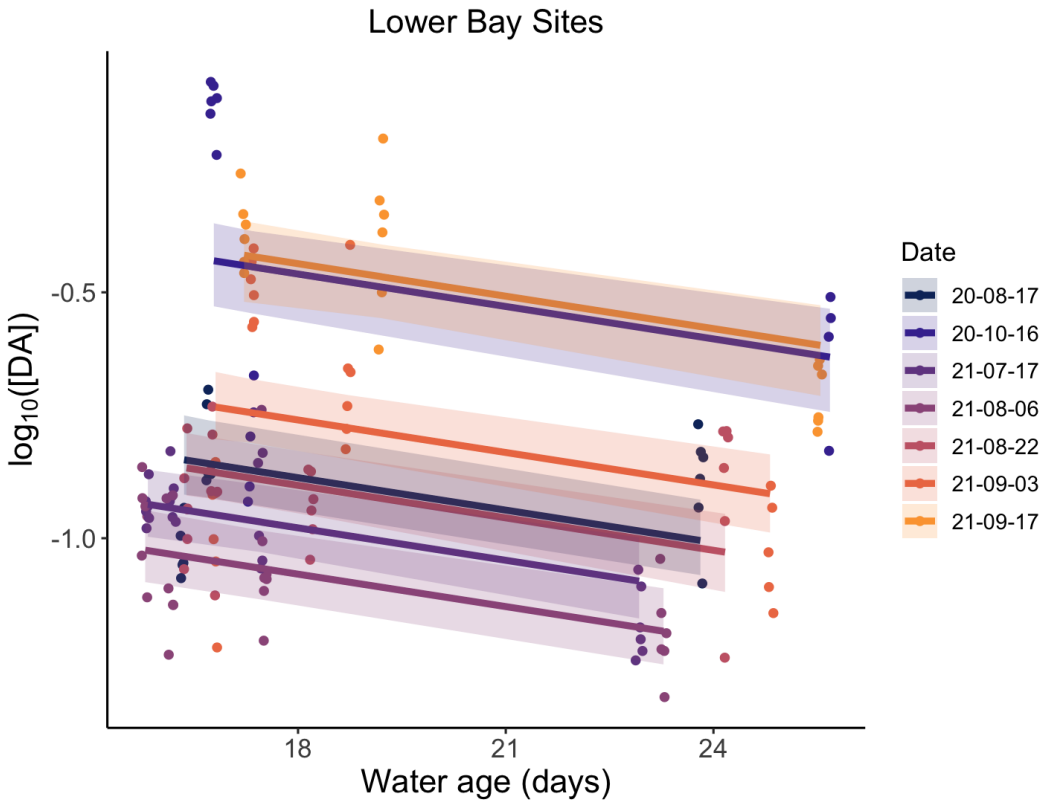

Figure 18. Generalized linear mixed model results from the effect of age of water (days; x-axis) in Humboldt Bay on DA concentrations in mussels (y-axis) across all sampling occasions. Fitted regression lines of DA concentrations as a function of age of water and sampling occasion are displayed as colored lines. Shaded regions are the 95% confidence intervals which were estimated using bootstrapping. Each point represents mean DA across replicate assays for an individual mussel. The y-axis indicates DA concentration in mussels on a $\log_{10}$-transformed scale.

Predicting DA at Mad River Slough and Woodley Island

The HAB index spatial GLMMs and spatial GLMMs that were fit to sites in lower reaches of the Bay (South Jetty, North Jetty, Samoa Campground and Hog Island Wharf) as a function of alternate measures of distance (linear distance (km) and age of water (days)) generally predict what (log_{10}-transformed) DA concentrations would be at Woodley Island (Figure 19) and Mad River Slough (Figure 20), but the range is lower than the observed values in most cases.

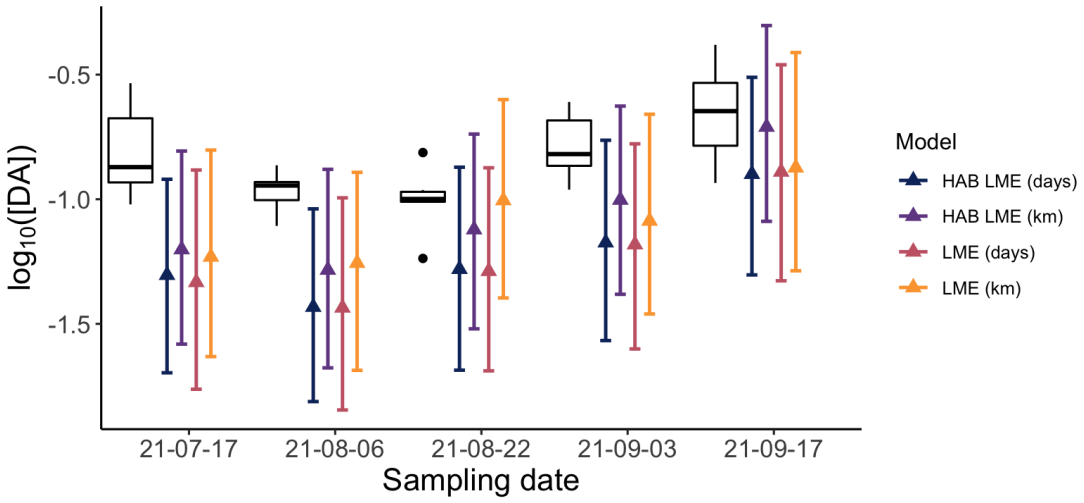

Figure 19. Predicted DA concentrations at Woodley Island from models fit to mussels at sites in the lower reaches of the Bay (South Jetty, North Jetty, Samoa Campground and Hog Island Wharf). Linear mixed effects models (LME) relate log_{10}-transformed DA concentrations in mussels to a measure of distance, with a random intercept for date and slope for distance, though the LME with the age of water only has a random intercept. HAB index linear mixed effects models (HAB LME) relate log_{10}-transformed DA concentrations in mussels to alternate measures of distance including linear distance (km) and the age of water (days) and integrated pDA concentrations from Hog Island Wharf, with a random intercept for date. Boxes capture the interquartile range of observed mean DA concentrations in mussels and horizontal solid black lines indicate the median value.

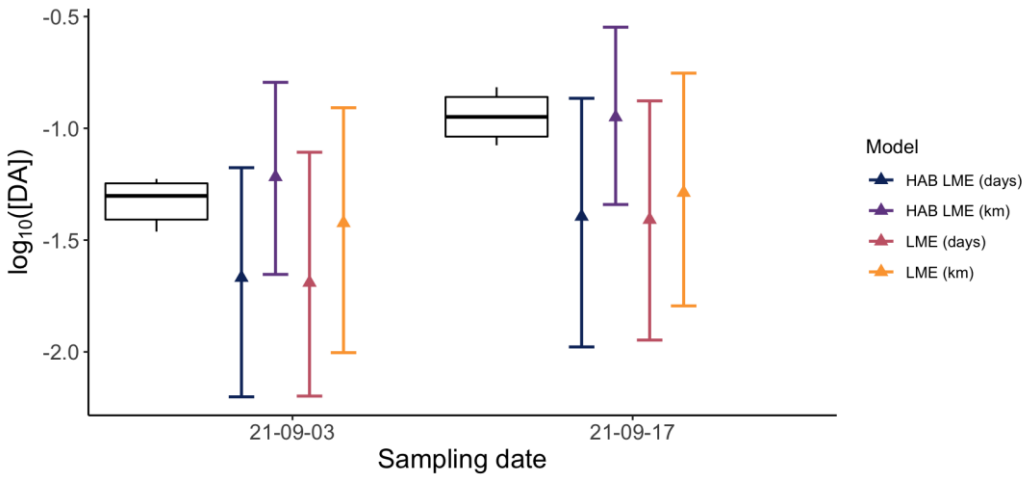

Figure 20. Predicted DA concentrations at Mad River Slough from models fit to mussels at sites in the lower reaches of the Bay (South Jetty, North Jetty, Samoa Campground and Hog Island Wharf). Linear mixed effects models (LME) relate $\log_{10}$-transformed DA concentrations in mussels to a measure of distance, with a random intercept for date and slope for distance, though the LME with the age of water only has a random intercept. HAB index linear mixed effects models (HAB LME) relate $\log_{10}$-transformed DA concentrations in mussels to alternate measures of distance including linear distance (km) and the age of water (days) and integrated pDA concentrations from Hog Island Wharf, with a random intercept for date. Boxes capture the interquartile range of observed mean DA concentrations in mussels and horizontal solid black lines indicate the median value.

HAB Index Spatial Models: Butter Clams

Linear distance (km)

The best model for butter clams using linear measures of distance (km) included a significant negative interaction between distance and integrated pDA from Hog Island Wharf (fixed effects slope: -0.0390 ± 0.0092; $p << 0.001$) and a random intercept for date (sampling occasion) (Figure 21). Variability in the slope for sampling occasion explained less than half of the total variance in the data (r^2_{total} = 0.64, of which r^2_{fixed} = 0.45). There was an outlier of high $\log_{10}$-transformed DA concentrations in butter clams at a moderate value of integrated pDA (Figure 21). No other plausible models were identified (Appendix E).

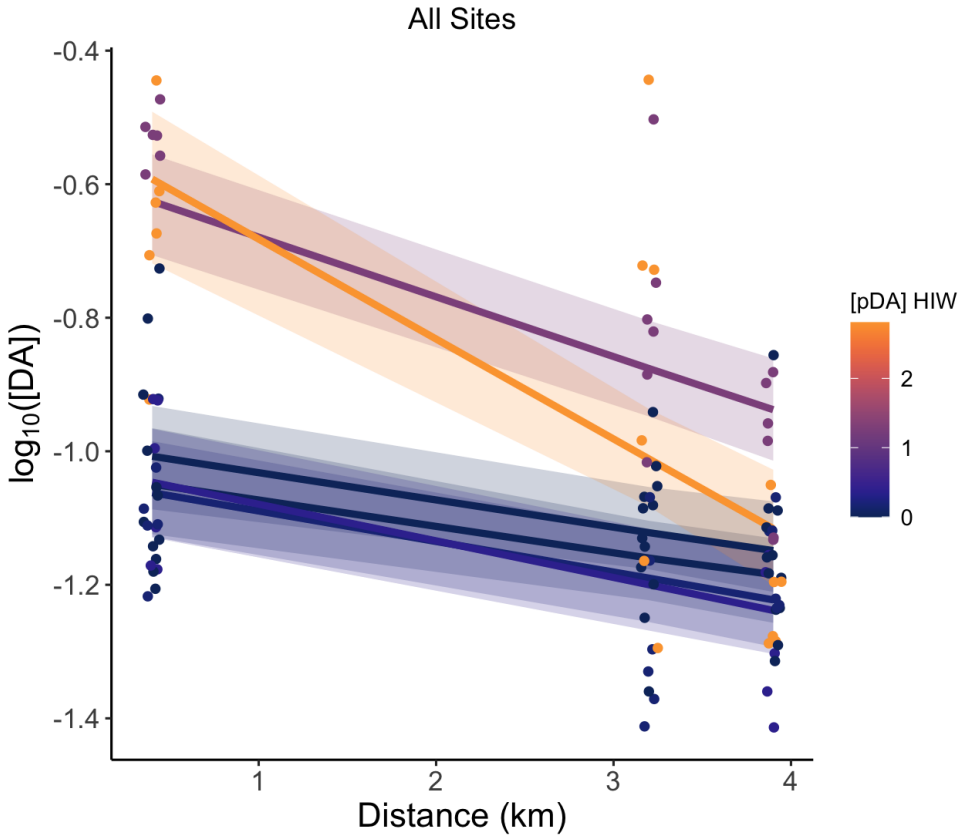

Figure 21. Generalized linear mixed model results from the effect of distance (km; x-axis) and integrated pDA concentrations from Hog Island Wharf on DA concentrations in butter clams (y-axis) across all sampling occasions. Fitted regression lines of DA concentrations as a function of distance and integrated pDA with a random intercept for date. Colored lines correspond to integrated pDA concentrations during a given sampling occasion (date). Shaded regions are the 95% confidence intervals which were estimated using bootstrapping. Each point represents mean DA across replicate assays for an individual butter clam. The y-axis indicates DA concentration in butter clams on a $\log_{10}$-transformed scale.

Age of water (days)

The best model for butter clams using age of water (days) included a significant negative interaction between age of water and integrated pDA from Hog Island Wharf (fixed effects slope: -0.0136 ± 0.0030; $p << 0.001$) and a random intercept for date (sampling occasion) (Figure 22). Variability in the slope for sampling occasion explained less than half of the total variance in the data (r^2_{total} = 0.65, of which r^2_{fixed} = 0.47). There was an outlier of high $\log_{10}$-transformed DA concentrations in butter clams at a moderate value of integrated pDA (Figure 22). No other plausible models were identified (Appendix E).

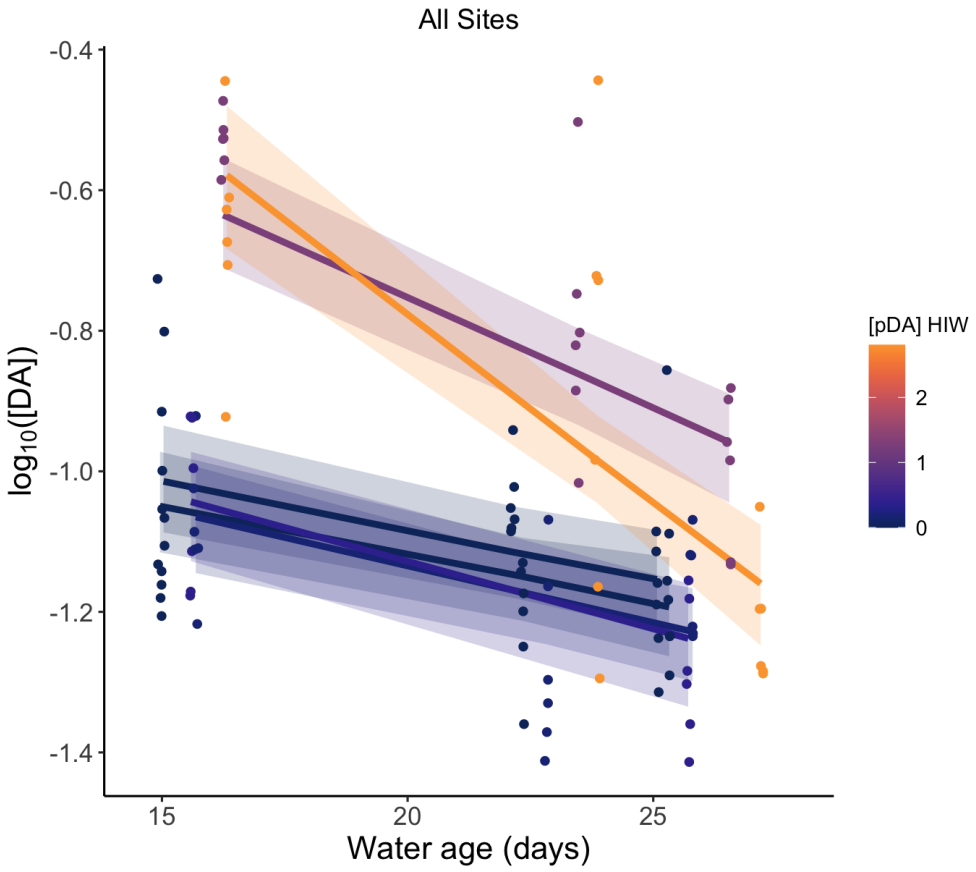

Figure 22. Generalized linear mixed model results from the effect of age of water (days; x-axis) and integrated pDA concentrations from Hog Island Wharf on DA concentrations in butter clams (y-axis) across all sampling occasions. Fitted regression lines of DA concentrations as a function of age of water and integrated pDA with a random intercept for date. Colored lines correspond to integrated pDA concentrations during a given sampling occasion (date). Shaded regions are the 95% confidence intervals which were estimated using bootstrapping. Each point represents mean DA across replicate assays for an individual butter clam. The y-axis indicates DA concentration in butter clams on a $\log_{10}$-transformed scale.

Spatial Models: Butter Clams

Linear distance (km)

The best model for (log_{10}-transformed) DA concentrations in butter clams includes a significant decline with increasing (linear) distance from the ocean (fixed effects slope: -0.0688 ± 0.0163; p = 0.0054), and indicates that variability in the intercept and slope of this trend associated with sampling occasion explained a substantial fraction of the total variance in the data (r^2_{total} = 0.65, r^2_{fixed} = 0.20) (Figure 23). Random intercepts and slopes were strongly negatively correlated (r = -0.97).

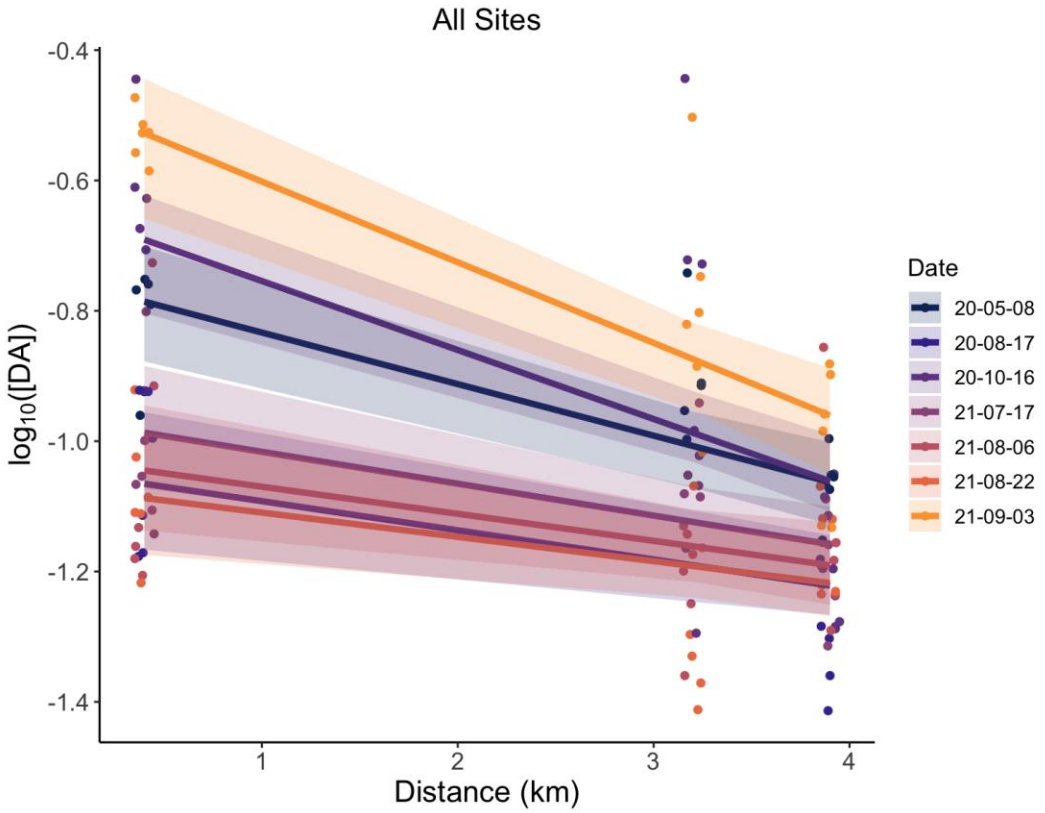

Figure 23. Generalized linear mixed model results from the effect of distance (km; x-axis) on DA concentrations in butter clams (y-axis). Fitted regression lines of DA concentrations as a function of distance and sampling occasion are displayed as colored lines. Shaded regions are the 95% confidence intervals which were estimated using bootstrapping. Each point represents mean DA across replicate assays for an individual butter clam. The y-axis indicates DA concentration in butter clams on a $\log_{10}$-transformed scale.

Age of water (days)

The best model included a random intercept for sampling occasion, and no random slope for the age of water. This model includes a significant decline in (log_{10}-transformed) DA concentrations in butter clams with increasing age of water (fixed effects slope: -0.0253 ± 0.0032; $p << 0.001$) (Figure 24) and indicated that variability in the intercept of this trend associated with sampling occasion explained slightly over half of the total variance in the data (r^2_{total} = 0.63, r^2_{fixed} = 0.23).

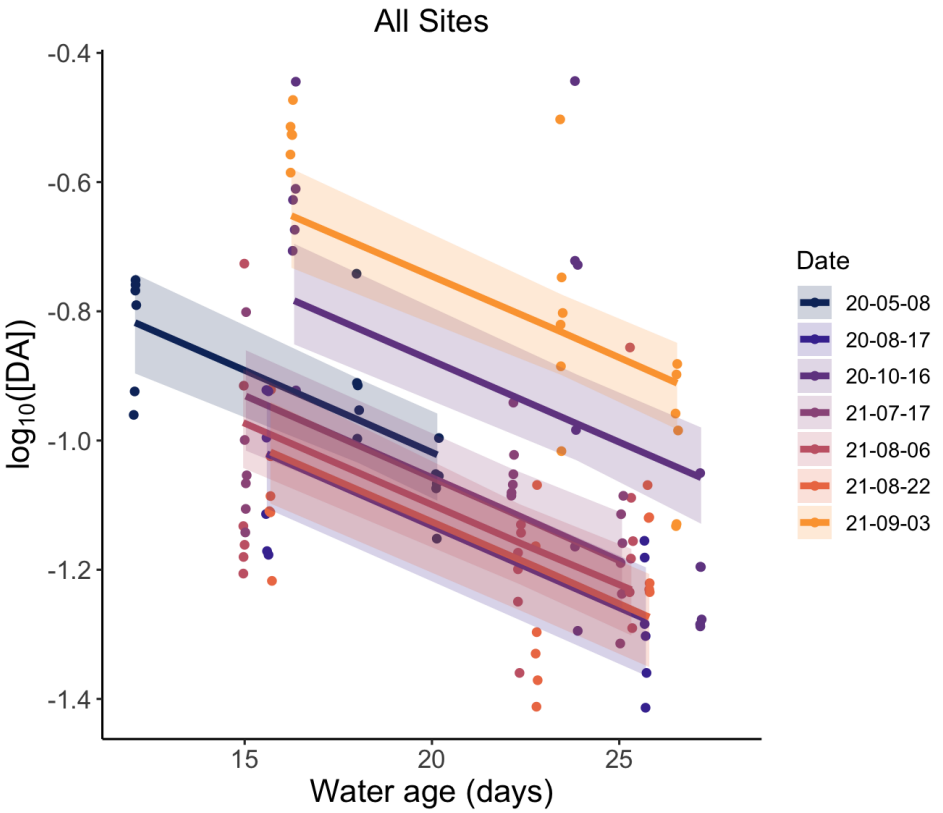

Figure 24. Generalized linear mixed model results from the effect of age of water (days; x-axis) in Humboldt Bay on DA concentrations in butter clams (y-axis). Fitted regression lines of DA concentrations as a function of age of water and sampling occasion are displayed as colored lines. Shaded regions are the 95% confidence intervals which were estimated using bootstrapping. Each point represents mean DA across replicate assays for an individual butter clam. The y-axis indicates DA concentration in butter clams on a $\log_{10}$-transformed scale.

Sensitivity to Endpoints

Post-hoc analysis was conducted using HAB index GLMMs and spatial GLMMs for butter clams to explore sensitivity to sampling transect design (i.e., analysis that excluded observations from either Fields Landing or Above the MPA).

Results from HAB index spatial GLMMs revealed that models fit without Above the MPA site included distance and integrated pDA from Hog Island Wharf as covariates and a random intercept for date (sampling occasion). This model had a significant decline in (log_{10}-transformed) DA concentrations in butter clams with increasing distance (fixed effects slope: -0.0597 ± 0.0140; $p << 0.001$), and a significant increase in (log_{10}-transformed) DA concentrations with increasing integrated pDA (fixed effects slope: 0.1479 ± 0.0510; $p = 0.0278$) (Figure 25). Variability in the slope for sampling occasion explained less than half of the total variance in the data (r^2_{total} = 0.65, of which r^2_{fixed} = 0.45). Models fit without the Fields Landing site had a significant negative interaction between distance and integrated pDA concentrations (fixed effects slope: -0.0481 ± 0.0079; $p << 0.001$) (Figure 25). Variability in the slope for sampling occasion explained less than half of the total variance in the data (r^2_{total} = 0.76, of which r^2_{fixed} = 0.57).

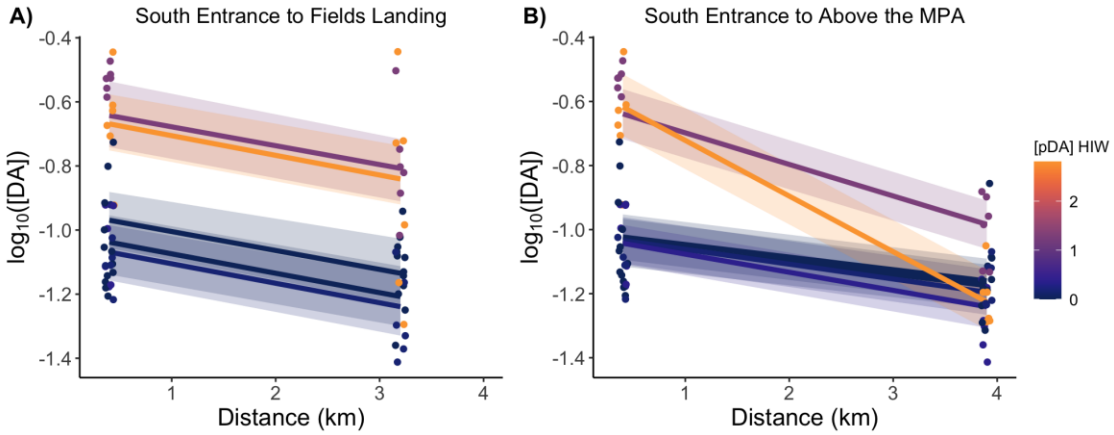

Figure 25. Generalized linear mixed model results from the effect of distance (km; x-axis) and integrated pDA concentrations from Hog Island on DA concentrations in butter clams (y-axis). Panels from left to right: models without the Above the MPA site (A) and without the Fields Landing site (B). Fitted regression lines of DA concentrations as a function of distance and integrated pDA with a random intercept for date. Colored lines correspond to integrated pDA concentrations during a given sampling occasion (date). Shaded regions are the 95% confidence intervals which were estimated using bootstrapping. Each point represents mean DA across replicate assays for an individual butter clam. The y-axis indicates DA concentration in butter clams on a $\log_{10}$-transformed scale.

Results from spatial GLMMs revealed that models fit without the Above the MPA site included only a random intercept for date (sampling occasion) and no random slope for distance. The variability in the intercept in this model explained a large fraction of the variance in the data (r^2_{total} = 0.70, r^2_{fixed} = 0.09). Models fit without the Fields Landing site had a similar structure to the model with all sites. The variability in the intercept and slope in this model explained a large fraction of the variance in the data (r^2_{total} = 0.77, r^2_{fixed} = 0.30). The observed decline in ($\log_{10}$-transformed) DA concentration in butter clams over distance was stronger along a transect between South Entrance and Above the MPA (slope = -0.0740 ± 0.0198; p = 0.0096) than for a transect between South Entrance and Fields Landing (slope = -0.0552 ± 0.0125; $p << 0.001$) (Figure 26).

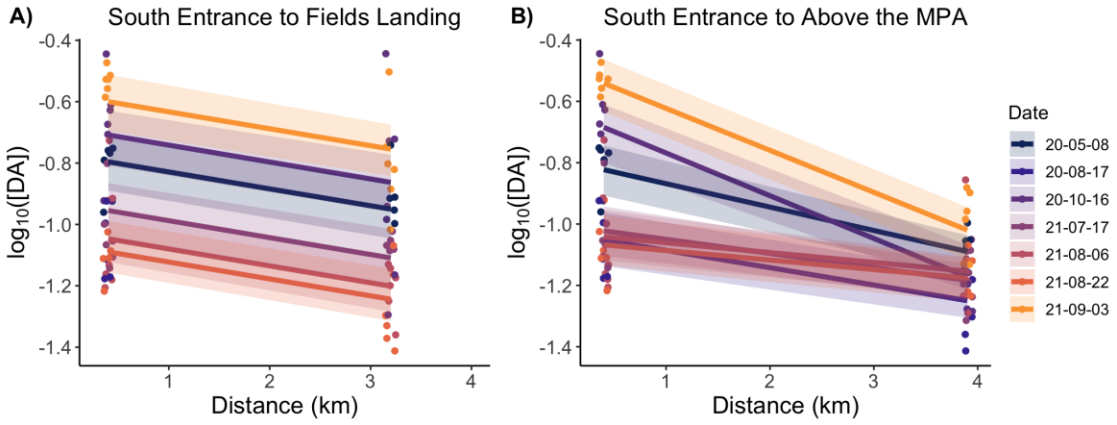

Figure 26. Generalized linear mixed model results from the effect of distance (km; x-axis) on DA concentrations in butter clams (y-axis). Panels from left to right: models without the Above the MPA site (A) and without the Fields Landing site (B). Fitted regression lines of DA concentrations as a function of distance and sampling occasion are displayed as colored lines. Shaded regions are the 95% confidence intervals which were estimated using bootstrapping. Each point represents mean DA across replicate assays for an individual butter clam. The y-axis indicates DA concentration in butter clams on a $\log_{10}$-transformed scale.

Comparing Trends in Bivalve DA Concentrations Between Spatial GLMMs

To further assess the hypothesis that bivalves in north and south Humboldt Bay respond synchronously to HAB's in the water column, random intercepts and slopes from the best mussel and butter clam spatial GLMMs fit to linear distance (km) were extracted and plotted over time (Figure 27). Random intercepts appear to follow similar temporal patterns and showed a positive correlation during each sampling occasion, though this correlation is not significant ($r = 0.75$; $p = 0.09$). The random slopes also appear to follow similar temporal patterns and showed a positive correlation during each sampling occasion and this correlation was slightly significant ($r = 0.79$, $p = 0.06$).

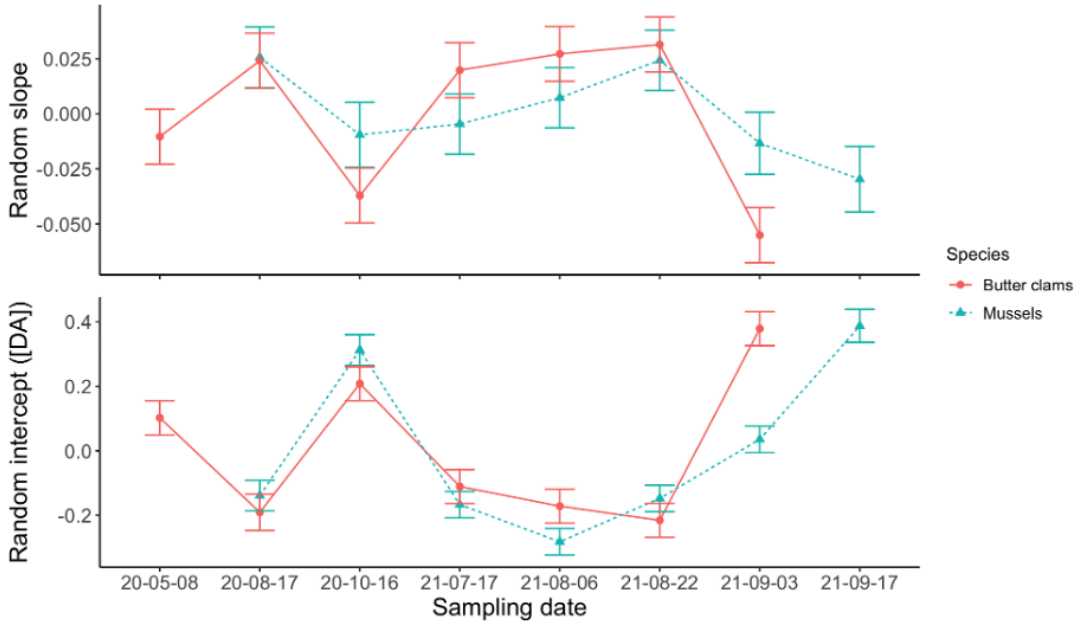

Figure 27. Plot of random slopes (top panel) and random intercepts (bottom panel) extracted from mussel (dashed line) and butter clam (solid line) spatial mixed effects models that relate log10[DA] in bivalves to distance from the mouth of Humboldt Bay (km) with a random intercept for sampling occasion and slope for distance. Intercepts represent maximum exposure in mussels and butter clams at the mouth of Humboldt Bay. Slopes represent the variability in DA concentrations by distance during each sampling occasion. Error bars represent ± 1 standard deviation.

Comparing Measures of Distance to Explain DA Concentration in Bivalves

HAB index spatial models

Based on AICc comparisons of HAB index spatial GLMMs relating (log_{10}-transformed) DA concentration in bivalves to alternate measures of distance (linear [km] and age of water [days]) and integrated pDA concentrations from Hog Island Wharf, age of water (days) is the best at describing DA concentrations in both mussels and butter clams (Table 3).

Table 3. Model selection table for HAB index spatial generalized linear mixed effects models relating log_{10}-transformed DA concentration in bivalves as a function of integrated pDA sampled from Hog Island Wharf, alternate measures of distance, and an interaction between the two (if it was included in the model). The alternate measures of distance were distance (km) and the age of water (days). The first three models were fit to mussel data with sites in the main channel (South Jetty, North Jetty, Samoa Campground and Hog Island Wharf), and the second set of three models were fit to butter clam data with all sites retained. The best models have a delta AICc of zero.

Spp.	*Measure of Distance*	$R^2_{multiple}$	$R^2_{adjusted}$	*AICc*	*Detal AICc*
Mussels	Distance (km)	0.62	0.35	-68.8	1.3
	Age of Water (days)	0.64	0.34	-70.1	0
Butter clams	Distance (km)	0.64	0.45	-77.8	3.8
	Age of Water (days)	0.65	0.47	-81.6	0

Spatial models

Based on AICc comparisons of spatial GLMMs relating (log_{10}-transformed) DA concentration in bivalves to alternate measures of distance (linear [km] and age of water [days]), linear distance (km) is the best at describing DA concentrations in mussels, though this was only slightly better than the age of water (Table 4). Linear distance (km) was determined to be the best at describing DA concentrations in butter clams in models fit to all sites (Table 4).

Table 4. Model selection table for spatial generalized linear mixed models relating log_{10}-transformed DA concentration in bivalves as a function of alternate measures of distance (distance (km), and the age of water (days)). The first three models were fit to mussel data with sites in the main channel (South Jetty, North Jetty, Samoa Campground and Hog Island Wharf), and the second set of three models were fit to butter clam data with all sites retained. The best models have a delta AICc of zero.

Spp.	*Measure of Distance*	R^2_{full}	R^2_{fixed}	*AICc*	*Delta AICc*
Mussels	Distance (km)	0.70	0.06	-55.0	0
	Age of Water (days)	0.70	0.06	-54.9	0.1
Butter clams	Distance (km)	0.65	0.20	-82.5	0
	Age of Water (days)	0.63	0.23	-74.6	7.8

DISCUSSION

This study provides the first empirical assessment of the spatial pattern in DA loading of bivalves in Humboldt Bay, and how this pattern changes over time and in response to measures of HAB intensity. Despite observations not spanning a period affected by a major *Pseudo-nitzschia* HAB, results from generalized linear mixed effects models indicate that DA concentrations in mussels in the lower reaches of North Bay and butter clams in South Bay generally decrease with increased distance from the mouth of the Bay, but this pattern varies depending on the date that samples were collected. Generalized linear mixed effect models with information on HABs in the environment indicate that part of the variability in this pattern is driven by the intensity of the *Pseudo-nitzschia* HAB in the water. DA concentrations in upper reaches of the Bay appear to be connected to dynamics affecting the lower Bay. This indicates that such extrapolation from observations in the lower Bay have some skill in predicting conditions in the upper Bay. This study contributes to work that is currently being done to understand the degree of risk that HABs pose to commercial aquaculture and recreational fisheries (Ding et al. 2022; Free et al. 2022; Zheng et al. 2022; Cuellar-Martinez et al. 2023) and lays the foundation for understanding the dynamics and distribution of HABs in Humboldt Bay. Further, results from this study support the development of hypotheses related to patterns and mechanisms that control HAB distributions and exposure.

Ocean-Estuary Exchange

The hypotheses I examined were fundamentally grounded in the assumption that the dynamics of Humboldt Bay are dominated by tidal exchange with the coastal ocean. Analysis of abiotic conditions, phytoplankton concentrations and community structure, and DA concentrations were similar between Humboldt Bay and Trinidad Wharf at high tide, and this was manifested in a strong coherence in the DA concentrations in bivalves on the open coast and near the mouth of Humboldt Bay (Figure 13). This is consistent with previous observations that Humboldt Bay is well connected to the coastal ocean at high tide (O'Connell 2013) and is consistent with observations of ocean-estuary exchange dynamics reported in other estuaries along the U.S. West Coast (Roegner & Shanks 2001; Hickey et al. 2002; Hickey & Banas 2003; Roegner et al. 2011; Shanks et al. 2014). In addition, DA concentrations in bivalves at the entrance of North and South Bay appeared to vary coherently (Figure 27), suggesting similar delivery of ocean water to the entrance of each subbasin of Humboldt Bay.

Spatial Pattern and Environmental Drivers of HAB Loading

The hypothesis that DA concentrations in bivalves decrease with increased distance from the mouth of the Bay was generally supported by observations across all spatial models fit to mussels in lower reaches of North Bay and butter clams in South Bay. This pattern generally varied depending on the sampling occasion. All patterns observed were generally consistent across alternate measures of distance, each of which

is a proxy for the exposure to oceanic water experienced by each site. These results demonstrate that in South Bay and the lower regions of North Bay, exposure to toxic *Pseudo-nitzschia* is a result of HABs entering the Bay with each tide and attenuating with increased distance from the mouth, as opposed to being maintained inside these regions of the estuary (e.g., Clark et al. 2019; Ajani et al. 2020). Bivalves near the mouth of the Bay have higher DA concentrations because they experience higher exposure to ocean-origin waters, and presumably the ocean-origin HABs that they carry (Cziesla 1998; Banas et al. 2007; Sutula et al. 2017; Tas and Lundholm 2017).

The results from HAB index spatial generalized linear mixed effects models indicate that DA concentrations in bivalves decline with increased distance from the mouth of the Bay and that the nature of this decline depends on the intensity of HAB exposure in the environment (Adams et al. 2006; Blanco et al. 2021; Ji et al. 2022). Further, these results confirm that most of the variability in the random effects that were identified in spatial generalized linear mixed effects models are explained by the variability of the HAB in the environment (e.g., Sauvey et al. 2021). For both species, these models identified elevated DA concentrations in bivalves at a moderate level of integrated pDA in the environment (e.g., Figure 15 and Figure 21). This suggests that the weekly collection of water samples missed a peak in pDA concentrations, and a result this peak was missed in the linearly interpolated data. This finding highlights the need to collect water samples at a higher frequency to ensure that fluctuations in pDA concentrations are not missed.

During the summer months, Humboldt Bay experiences little direct freshwater input, and as a result tidal exchange is the primary driver of circulation within the Bay (Barnhart et al. 1992). Results from this study demonstrate that ocean origin DA and *Pseudo-nitzschia* HABs are higher near the mouth of the Bay, and that the gradient in this pattern is tied to the extent that oceanic water enters the Bay. This similar pattern of higher concentrations of *Pseudo-nitzschia* near the entrance has been observed in other estuaries on the US West Coast that experience strong tidal forcing and little freshwater input during the summer months such as Coos Bay in Oregon and Willapa Bay in Washington (Cziesla 1998; Newton & Horner 2003). In contrast, estuaries that experience higher retention of water within the Bay have resulted in increased HABs as longer retention times appear to promote toxicity within a Bay (Álvarez-Salgado et al. 2008; Yñiguez et al. 2018; Qin and Shen 2019). On the US West coast, this is apparent in the northern region of Monterey Bay, where typical circulation patterns lead to high water retention (Graham & Largier 1997), which is considered one of the conditions that promote *Pseudo-nitzschia* HABs in the Bay (Ryan et al. 2014). As a result, Monterey Bay is considered a hot spot for *Pseudo-nitzschia* HABs (Sandoval-Belmar et al. 2023).

Alternate Measures of Distance

In this study, I was able to demonstrate the utility of using the age of water as an alternate measure of distance. The age of water obtained from a circulation model of Humboldt Bay (Anderson 2010; Anderson 2019) is a measure of the time water has spent at a given region of the Bay since it entered the boundary of the system (i.e., the coastal

ocean outside the Bay; Camacho et al. 2015). These results suggest that measures of connectivity derived from circulation models have the potential to be useful for understanding and predicting bivalve exposure to ocean origin HABs. Circulation models are useful tools as they can quantify the actual path that water flows while integrating the effects of mixing and accounting for retention and exchange rates of water that is already in the Bay (Bilgili et al. 2005; Murawski et al. 2021). Water masses in the upper reaches of the Bay are typically substantially warmer than ocean waters (Anderson 2010; Anderson 2019) which can result in a nearly vertical front that can limit mixing between estuarine and oceanic water masses (Largier 1992). This leads to higher retention of estuarine water in upper reaches of the Bay and an increased age of water that a simple linear measure of distance does not necessarily capture (Lucas et al. 1999; Cira et al. 2021). These patterns were apparent in the different structures of the models fit with either Fields Landing or Above the MPA as an endpoint (Figure 25 and Figure 26). Fields Landing is across the Bay from South Entrance and Above the MPA, in a deeper region of the estuary where water flows at a fast rate (Figure 2). Being in a shallower region of the Bay, water is retained for longer periods at the Above the MPA site (Anderson 2010; Anderson 2019), which likely drives differences in exposure compared to Fields Landing (Roegner 1998; Geyer et al. 2018).

Mussels in Upper Humboldt Bay

Predictions for what DA concentrations would be at Woodley Island and Mad River Slough based on generalized linear mixed effects models fit to mussels in the lower

reaches of the Bay were generally accurate, though the range was lower than the observed values in most cases (Figure 19 and Figure 20). Mussels may retain DA for long periods of time at low concentrations (Mafra et al. 2010a; Novaczek et al. 1991), so this may be a driving factor in this observed pattern since DA concentrations remained extremely low throughout this study. It is also possible that there is retention of *Pseudo-nitzschia* in these regions of the Bay (Peierls et al. 2012; Hall et al. 2013; Geyer et al. 2018). Though mixing of estuarine and oceanic water may be limited in these regions (Largier 1992), it is possible that *Pseudo-nitzschia* can be deposited and sequestered in sediment in these retentive regions (i.e., high age of water; Anderson 2010; Anderson 2019) where they can accumulate in benthic infauna or possibly become resuspended when supplied with turbulent mixing (Trainer et al. 2000; Hubbard et al. 2014). *Pseudo-nitzschia* maintained in these regions of the Bay may have increased DA production from trace metals supplied through turbulent mixing of sediments (Ryan et al. 2014) or from nutrients supplied from the small freshwater inputs in the upper regions of the Bay (Figure 2). The latter point has been observed in other estuaries on the US West coast, where DA production has increased after periods of intense river discharge (Trainer et al. 1998; Trainer et al. 2007; Phlips et al. 2011).

Bivalve Feeding

This study used an uptake-depuration function that considers species specific feeding rates of bivalves to obtain an integrated measure of exposure to HABs in the environment. Such functions have been used in other studies (Silvert & Subba Rao 1992;

Mafra et al. 2010a; Jennings 2012) and are useful as they consider what bivalves have accumulated in the past and are still expelling (depuration), and what they continue to accumulate in the present (Sauvey et al. 2021). Integrated pDA from Hog Island Wharf was useful as an input to this function, which is supported by other studies which show that DA concentrations in bivalves track the concentrations and intensity of pDA in the surrounding environment (Anderson et al. 2016; Rourke et al. 2021). While the function used in this study is useful for integrating rapid uptake and depuration dynamics of species like mussels and butter clams, explicitly accounting for uptake and depuration dynamics would be more essential for modelling organisms with slow depuration rates (e.g., razor clams; Wekell et al. 1994) and for bivalves that are collected closer in time to one another, as DA concentrations in the organisms during each sampling occasion would likely not be independent on the temporal scale.

Sampling Biases and Statistical Considerations

Several sources of potential bias bear consideration for understanding the current study and future efforts. The first considers the fact that no major *Pseudo-nitzschia* HAB occurred over the course of this study. The following two involve how measures of distance from the mouth of the Bay and the HAB indices that were defined. The remaining two consider sampling of bivalves (weight and submersion).

Patterns in DA concentrations in bivalves observed in this study were based on conditions when no major *Pseudo-nitzschia* HAB occurred, and DA concentrations in bivalves across all sampling occasions were well below the public health threshold of

20ppm. As a result, insights on the spatial pattern of toxin loading in bivalves must be taken with caution. However, during the massive 2015 *Pseudo-nitzschia* HAB (McCabe et al. 2016), DA concentrations at aquaculture operations in the upper reaches of the Bay remained well below this threshold (Anderson and Kudela, unpublished data). In all the models fit for this study, there was a pattern of decreasing DA concentrations in bivalves with increased distance from the mouth of the Bay. This is likely a result of the higher exposure to oceanic waters that bivalves near the mouth of the Bay experience (Newton & Horner 2003). Given this, and the fact that DA concentrations in the upper reaches of the Bay remained relatively low during the 2015 HAB (i.e., did not exceed thresholds, despite elevated DA concentrations observed in coastal ocean systems; McCabe et al. 2016), it is possible that this pattern would hold during an intense HAB. Future studies will be required to test this conjecture.

Evidence for location-specific divergence from simple linear relationships with distance suggests that there is a need to resolve spatial patterns in two dimensions to account for variability in transport paths, retention, and mixing in the Bay. Preliminary efforts to develop such a model confirm the potential for such approaches to resolve richer structure in the pattern of exposure (Appendix F), and specifically in this case to capture the tendency for higher DA concentrations in bivalves located at sites on the east side of the Bay (e.g., Woodley Island and Fields Landing). Fields Landing is in a deep section of South Bay, while Woodley Island is in the shallower upper reaches of North Bay (Figure 2). These differences in bathymetry might be linked to variability in oceanographic flow patterns that cause differences in biotic and abiotic conditions in

those locations (Beecraft and Wetz 2022; Geyer et al. 2022; Tominack and Wetz 2022). For this study, regardless of the measure of distance that was used, the patterns of DA concentrations in bivalves were robust among all models.

Water samples were collected from Hog Island Wharf in North Bay and Trinidad Wharf on the coastal ocean on a weekly basis, and linearly interpolated to obtain daily values of pDA concentrations from each site. *Pseudo-nitzschia* and DA concentrations can be highly variable depending on a suite of environmental conditions (Lelong et al. 2012; Trainer et al. 2012; Bates et al. 2018), thus using linear interpolation is a crude estimate. It is possible that trends in pDA concentrations were missed, introducing uncertainty or potential bias in my estimates of HAB indices. This was apparent in the HAB index generalized linear mixed effects models fit to butter clams and mussels, which show that DA concentrations in bivalves were elevated at a moderate level of integrated pDA. This suggests that a peak in pDA concentrations might have been missed, or that linear interpolation among sparse water samples was a poor approximation for the actual exposure experienced by bivalves at that time. Further, no water samples were collected from the South Bay, so bivalves located here could only be related to integrated pDA concentrations from North Bay. Despite observations of strong relationships between DA concentrations in bivalves from both North and South Bay integrated pDA concentrations from Hog Island Wharf, future studies may be more robust if water samples were collected on a more frequent basis and from more locations throughout the Bay.

The potential effect of weight on DA concentrations in mussels was considered but yielded a global positive pattern that was not reflected at the site level (see Appendix C). This global pattern is contradictory to reports in the experimental literature, where the relationships between weight and DA concentrations are relatively non-existent (e.g., Mafra et al. 2010a). To my knowledge, there has been no examination of the effect of weight on DA concentrations in butter clams. More importantly, the current study is motivated by the effect of distance on DA concentrations in bivalves. I expect exposure to DA concentrations in the water column to be higher in bivalves that are located closer to the mouth of the Bay, regardless of the effect of weight on DA concentrations in bivalves. Future studies may be more robust if size-distributions of sampled organisms were similar across all sites, however this may prove difficult given the availability of organisms in the Bay and might require the deployment of "sentinel" bivalves rather than sampling from natural populations.

Exposure time to oceanic water differed between mussels collected for this study. Mussels from South Jetty, North Jetty and Samoa Campground were exposed at low tide, while mussels from Hog Island Wharf, Woodley Island and Mad River Slough were collected off the side of docks that were constantly submerged in water. Evidence suggests that bivalves that are constantly submerged do not respond to tidal cycles, and rather feed continuously if phytoplankton concentrations are above a minimum threshold (Thompson and Bayne 1972; Winter 1978). Evidence in Humboldt Bay suggests that the phytoplankton community differs between high and low tide (O'Connell 2013), so it is

unlikely that mussels that were constantly submerged were exposed to *Pseudo-nitzschia* HABs of ocean origin differently than mussels that were exposure during low tide.

Future Research

Results from this study provide a strong foundation for developing hypotheses that further explore the spatial distribution of DA concentrations in Humboldt Bay bivalves. Some specific questions that arise from this study include: how do the patterns observed in the Bay change over the course of a HAB, and are there places where simple linear relationships with distance tend to break down? This study used a relatively simple uptake-depuration function, how would it improve model fits if more variables were included that possibly affect bivalve feeding? And finally, given that the results from this study demonstrate that the age of water derived from circulation models is useful for describing the patterns of DA concentrations in Humboldt Bay bivalves, would hours of exposure provide a better model fit? Ideas on how to address these questions in future research projects are outlined below.

Sites used in my study were largely aligned along the two spits that form the western edge of Humboldt Bay; however, there were two sites located on the east side of the Bay (Woodley Island and Fields Landing), and one site in the northernmost reaches of the Bay (Mad River Slough). On occasion, mussels in the lower reaches of the Bay underpredicted what DA concentrations would be at Woodley Island and Mad River Slough (Figure 19 and Figure 20). To map the spatial pattern of exposure more completely in Humboldt Bay, future studies should monitor sentinel mussels of similar

size at sites that are more spatially explicit at resolving gradients in more than one dimension to identify where breaks in the gradient occur. Ideally, such surveys would be conducted over a range of *Pseudo-nitzschia* HAB intensities to quantify how this pattern develops over the course of a HAB. Such sampling would support the further development of spatial models regarding toxin loading in Humboldt Bay bivalves (Appendix F).

This study indicates that naturally occurring bivalves in Humboldt Bay can serve as useful measures of what DA concentrations are in the water column (Sauvey et al. 2021; Kvrgić et al. 2022). Therefore, including collections of naturally occurring bivalves from select locations throughout the Bay concurrently with a sentinel mussel survey could be used to assess whether DA concentrations are similar between the two groups, and as a basis for mapping risk to the recreational harvest of bivalves in the Bay. To model this, such a study could use the generalized linear mixed effect models that were used in this study, though it would have to include a correlation structure that accounts for the fact that DA concentrations in samples will not be independent from one another on the temporal scale.

The uptake-depuration function used in this study was relatively simple and did not consider factors that plausibly influence bivalve uptake and depuration rates, including allometric relationships between gill surface area or weight and feeding (reviewed by Cranford et al. 2011), temperature (Blanco 2006; Rollwagons-Bollens et al. 2021), and non-constant, adaptive feeding behaviors (Riisgård et al. 2003; Foster-Smith 1975). Temperature is particularly important, because bivalves located in the upper

reaches of the Bay are exposed to increased temperatures during summer (Anderson 2010; Anderson 2019). Future studies should further develop the uptake-depuration function used here by taking these into account to obtain a more robust measure of integrated HAB exposure. These studies could also obtain a more dynamic indicator of potential HABs in the form of high-resolution *Pseudo-nitzschia* concentrations, such as those that can be obtained with newly developed technologies like the Imaging FlowCytobot (IFCB; Olson and Sosik 2007; Sosik and Olson 2007). Lastly, future studies should collect water samples at more locations in the Bay, more frequently to obtain measures of pDA in the surrounding water and to not miss possible peaks in pDA concentrations.

Results from this study have demonstrated the utility of using alternate measures of exposure to toxins. Temperature transitions sharply across the tidal cycle in the Bay, meaning that there are distinct water masses and each site in the Bay has a fraction of time under Bay or oceanic water, which affects their exposure to ocean-origin HABs (Largier 1992; Newton & Horner 2003). Future studies would be more robust if they had a measure of tidal exposure to use as an input to the models described above. To do this, studies will benefit from continued development of water circulation models for Humboldt Bay to obtain more accurate estimates of how long each site is exposed to oceanic water and rates of mixing affecting the intensity of this exposure. This would help to inform the differences in tidal exposure between sites, which could then be used as inputs in models to help better map the distribution of DA concentrations in Humboldt Bay bivalves.

CONCLUSIONS

Understanding the spatial distribution of DA concentrations in Humboldt Bay bivalves has important implications for the management of commercial and recreational fisheries here. Results from this study show that in general, there is a pattern of decreasing DA concentrations in bivalves with increased distance from the mouth of the Bay, and that these patterns are tied to what *Pseudo-nitzschia* HAB concentrations are in the surrounding water column. Spatial generalized linear mixed effects models demonstrate that this pattern can be resolved without information on the HAB intensity in the water. This is particularly useful for aquaculture management that may not have access to what DA concentrations are in the water column, though this should be used with caution as no major HAB occurred over the course of my study.

This study lays the foundation for understanding the spatial pattern of DA concentrations in Humboldt Bay bivalves and makes a strong case that future studies to resolve these patterns and their evolution in greater detail are likely to be successful. Further developing the uptake-depuration function and circulation model used in this study will provide more accurate measures of exposure to help fully resolve this spatial structure in exposure and uptake of HABs. The patterns observed in this research suggest that such a study would be informative as it would help to fully develop a map of the distribution of DA loading in bivalves in Humboldt Bay to inform aquaculture management on where it is safe to expand operations, and when and where it is safe to harvest bivalves in recreational or traditional fisheries. This would also provide a

blueprint of how to conduct similar studies in other tidally driven estuaries at risk of HAB impacts along the US West Coast (e.g., Newton & Horner 2003; Kudela et al. 2020).

LITERATURE CITED

Adams, N. G., A. MacFadyen, B. M. Hickey, and V. L. Trainer. 2006. The nearshore advection of a toxigenic Pseudo-nitzschia bloom and subsequent domoic acid contamination of intertidal bivalves. African Journal of Marine Science, 28(2), 271-276.

Ajani, P. A., M. E. Larsson, S. Woodcock, A. Rubio, H. Farrell, S. Brett, and S. A. Murray. 2020. Fifteen years of Pseudo-nitzschia in an Australian estuary, including the first potentially toxic P. delicatissima bloom in the southern hemisphere. Estuarine, Coastal and Shelf Science, 236, 106651.

Álvarez-Salgado, X.A., U. Labarta, M. J. Fernández-Reiriz, F. G. Figueiras, G. Rosón, S. Piedracoba, R. Filgueira, and J. M. Cabanas. 2008. Renewal time and the impact of harmful algal blooms on the extensive mussel raft culture of the Iberian coastal upwelling system (SW Europe). Harmful Algae 7(6):849-855.

Álvarez, G., J. Rengel, M. Araya, F. Álvarez, R. Pino, E. Uribe, R. Pino, P. Díaz, A. E. Rossignoli, A. López-Rivera, and J. Blanco. 2020. Rapid Domoic Acid Depuration in the Scallop Argopecten purpuratus and Its Transfer from the Digestive Gland to Other Organs. Toxins 12(11):698.

Anderson, C., R. Kudela, M. Kahru, Y. Chao, L. K. Rosenfeld, F. L. Bahr, D. M. Anderson, and T. A. Norris. 2016. Initial skill assessment of the California Harmful Algae Risk Mapping (C-HARM) system. Harmful Algae 59:1-18.

Anderson, J. 2010. A Three-Dimensional Hydrodynamic and Transport Model of Humboldt Bay. Poster Presentation. Eureka, CA.

Anderson, J. 2019. Three-Dimensional Modeling of Hydrodynamics, Salinity and Temperature in Humboldt Bay. Poster Presentation. Eureka, CA.

Auro, M. E., W. P. Cochlan. 2013. Nitrogen utilization and toxin production by two diatoms of the Pseudo-nitzschia pseudodelicatissima complex: P. cuspidata and P. fryxelliana. Journal of phycology 49(1):156-169.

Ayache, N., N. Lundholm, F. Gai, F. Herve, Z. Amzil, and A Caruana. 2021. Impacts of ocean acidification on growth and toxin content of the marine diatoms Pseudo-nitzschia australis and P. fraudulenta. Marine Environmental Research 169:105380.

Banas, N. S., B. M. Hickey, J. A. Newton, and J. L. Ruesink. 2007. Tidal exchange, bivalve grazing, and patterns of primary production in Willapa Bay, Washington, USA. Marine Ecology Progress Series, 341, 123-139.

Barnhart, R.A., M.J. Boyd and J.E. Pequegnat. 1992. The ecology of Humboldt Bay, California: An estuarine profile. U.S. Department of the Interior, Fish and Wildlife Service, Washington D.C., USA 1-121.

Barth, J. A., S. D. Pierce and R. L. Smith. 2000. A separating coastal upwelling jet at Cape Blanco, Oregon, and its connection to the California Current System, Deep Sea Res., Part II, 47, 783 – 810.

Barton, K, and K. M. Barton. 2015. Package 'mumin'. Version 1.18: 439.

Bates, D. M., Mächler, B. Bolker, S. Walker. 2015. Fitting Linear Mixed-Effects Models Using lme4. Journal of Statistical Software. 67(1), 1-48.

Bates, S. S., C. J. Bird, A. D. Freitas, R. Foxall, M. Gilgan, L. A. Hanic, G. R. Johnson, A. W. McCulloch, P. Odense, R. Pocklington and M. A. Quilliam. 1989. Pennate diatom Nitzschia pungens as the primary source of domoic acid, a toxin in shellfish from eastern Prince Edward Island, Canada. Canadian Journal of Fisheries and Aquatic Sciences 46.7: 1203-1215.

Bates, S. S., K. A. Hubbard, N. Lundholm, M. Montresor and C. P. Leaw. 2018. Pseudo-nitzschia, Nitzschia, and domoic acid: new research since 2011. Harmful Algae 79:3-43.

Beecraft, L., and M. S. Wetz. 2022. Temporal Variability in Water Quality and Phytoplankton Biomass in a Low-Inflow Estuary (Baffin Bay, TX). Estuaries and Coasts, 1-12.

Bilgili, A., J. A. Proehl, D. R. Lynch, K. W. Smith, and M. R. Swift. 2005. Estuary/ocean exchange and tidal mixing in a Gulf of Maine Estuary: A Lagrangian modeling study. Estuarine, Coastal and Shelf Science, 65(4), 607-624.

Blanco, J., M. B. de la Puente, F. Arevalo, C. Salgado and A. Morono. 2002. Depuration of mussels (Mytilus galloprovincialis) contaminated with domoic acid. Aquatic Living Resources 15(1):53-60.

Blanco, J., C. P. Acosta, C. Mariño, S. Muñiz, H. Martín, Á. Moroño, J. Correa, F. Arévalo, and C. Salgado. 2006. Depuration of domoic acid from different body compartments of the king scallop Pecten maximus grown in raft culture and natural bed. Aquatic Living Resources. 19, no. 3: 257-265.

Blanco, J., Á. Moroño, F. Arévalo, J. Correa, C. Salgado, A. E. Rossignoli, and J. P. Lamas. 2021. Twenty-Five Years of Domoic Acid Monitoring in Galicia (NW Spain): Spatial, Temporal and Interspecific Variations. Toxins, 13(11), 756.

Bresnan, E., R. J. Fryer, S. Fraser, N. Smith, L. Stobo, N. Brown, and E. Turrell. 2017. The relationship between Pseudo-nitzschia (Peragallo) and domoic acid in Scottish shellfish. Harmful Algae, 63, 193-202.

Bricelj, V. M., and S. E. Shumway. 1998. Paralytic shellfish toxins in bivalve molluscs: occurrence, transfer kinetics, and biotransformation. Reviews in Fisheries Science 6.4: 315-383.

Brown, A. R., M. Lilley, J. Shutler, C. Lowe, Y. Artioli, R. Torres, E. Berdalet and C. R.Tyler. 2020. Assessing risks and mitigating impacts of harmful algal blooms on mariculture and marine fisheries. Reviews in Aquaculture 12(3):1663-1688.

Camacho, R. A., Martin J. L., B. Watson, M. J. Paul, L. Zheng, and J. B. Stribling. 2015. Modeling the factors controlling phytoplankton in the St. Louis Bay Estuary, Mississippi and evaluating estuarine responses to nutrient load modifications. Journal of Environmental Engineering. 141(3):04014067.

CeNCOOS. Humboldt Bay. https://www.cencoos.org/data-by-location/humboldt-bay/. Accessed 18 Mar. 2023.

Cira, E. K., T. A. Palmer, and M. S. Wetz. 2021. Phytoplankton dynamics in a low-inflow estuary (Baffin Bay, TX) during drought and high-rainfall conditions associated with an El Niño event. Estuaries and Coasts, 1-13.

Checkley Jr, D. M., and J. A. Barth. 2009. Patterns and processes in the California Current System. Progress in Oceanography 83.1-4: 49-64.

Clark, S., K. A. Hubbard, D. M. Anderson, D. J. McGillicuddy Jr, D. K. Ralston, and D. W. Townsend. 2019. Pseudo-nitzschia bloom dynamics in the Gulf of Maine: 2012–2016. Harmful algae 88: 101656.

Clarke, K.R. and R. M. Warwick. 2001. Change in marine communities: an approach to statistical analysis and interpretation. 2nd edn, PRIMER-E, Plymouth, UK.

Cloern, J. E. 1982. Does the benthos control phytoplankton biomass in south San Francisco Bay. Marine ecology progress series 9(2):191-202.

Cloern, J. E., B. E. Cole, R. L. Wong, and A. E. Alpine. 1985. Temporal dynamics of estuarine phytoplankton: a case study of San Francisco Bay. In Temporal dynamics of an estuary: San Francisco Bay 153-176. Springer, Dordrecht.

Cloern, J. E. 1991. Tidal stirring and phytoplankton bloom dynamics in an estuary. Journal of marine research 49(1):203-221.

Costa, A., V. Alio, S. Sciortino, L. Nicastro, M. Cangini, F. Pino, I. Servadei, A. La Vignera, G. Fortino, S. Monaco, and S. Dall'Ara. 2021. Algal blooms of Alexandrium spp. and Paralytic Shellfish Poisoning toxicity events in mussels farmed in Sicily. Italian Journal of Food Safety, 10(1).

Costa, S. L., and K. A. Glatzel. 2002. Humboldt Bay, California, Entrance Channel. US Army Corps of Engineers 29p.

Cranford, P. J., J. E. Ward, and S. E. Shumway. 2011. Bivalve filter feeding: variability and limits of the aquaculture biofilter. Shellfish aquaculture and the environment: 81-124.

Cuellar-Martínez, T., A. del Rocío Huanca Ochoa, S. Sánchez, A. Aguirre-Velarde, E. O. Martínez Ocas, A. M. Rodriguez Velasquez, R. I. Saavedra Querevalú, F. Colas, J. Tam, and D. Gutiérrez. 2023. Abundance and distribution of potentially toxic phytoplankton in aquaculture sites along the Peruvian coast. Journal of Marine *Systems*: 103865.

Cziesla, C. A. 1998. The transport and distribution of the toxic diatom Pseudo-nitzschia spp. in the Coos Bay estuary and the adjacent continental shelf. Diss. Thesis (MS)-University of Oregon.

Ding, W., C. Zhang, and S. Shang. 2022. The early assessment of harmful algal bloom risk in the east China sea. Marine Pollution Bulletin, *178*, 113567.

Doucette, G. J., K. L. King, A. E. Thessen, and Q. Dortch. 2008. The effect of salinity on domoic acid production by the diatom Pseudo-nitzschia multiseries. Nova Hedwigia 133:31-46.

Fehling, J., K. Davidson, C. Bolch, & P. Tett. 2006. Seasonality of Pseudo-nitzschia spp.(Bacillariophyceae) in western Scottish waters. Marine Ecology Progress Series, *323*, 91-105.

Foster-Smith, R. L. 1975. The effect of concentration of suspension on the filtration rates and pseudofaecal production for Mytilus edulis L., Cerastoderma edule (L.) and Venerupis pullastra (Montagu). Journal of Experimental Marine Biology and Ecology. 17(1), 1-22.

Fox, J., S. Weisberg, D. Adler, D. Bates, G. Baud-Bovy, S. Ellison, D. Firth, M. Friendly, G. Gorjanc, S. Graves, and R. Heiberger. 2012. Package 'car'. Vienna: R Foundation for Statistical Computing, 16.

Free, C. M., S. K. Moore, and V. L. Trainer. 2022. The value of monitoring in efficiently and adaptively managing biotoxin contamination in marine fisheries. Harmful Algae, 114, 102226.

Geyer, N. L., M. Huettel, and M. S. Wetz. 2018. Phytoplankton spatial variability in the river-dominated estuary, Apalachicola Bay, Florida. Estuaries and Coasts, 41, 2024-2038.

Geyer, N. L., D. Balwada, E. Simons, K. Speer, and M. Huettel. 2022. Drifter and dye tracks reveal dispersal processes that can affect phytoplankton distributions in shallow estuarine environments. Estuarine, Coastal and Shelf Science, 269, 107811.

Gobler, C. J., O. M. Doherty, T. K. Hattenrath-Lehmann, A. W. Griffith, Y. Kang, and R. W. Litaker. 2017. Ocean warming since 1982 has expanded the niche of toxic algal blooms in the North Atlantic and North Pacific oceans. Proceedings of the National Academy of Sciences 114(19):4975-4980.

Gobler, C. J. 2020. Climate change and harmful algal blooms: Insights and perspective. Harmful Algae 91:101731.

Graham, W. M., and J. L. Largier. 1997. Upwelling shadows as nearshore retention sites: the example of northern Monterey Bay. Continental Shelf Research. 17(5): 509-532.

Hall, N. S., H. W. Paerl, B. L. Peierls, A. C. Whipple, & K. L. Rossignol. 2013. Effects of climatic variability on phytoplankton community structure and bloom development in the eutrophic, microtidal, New River Estuary, North Carolina, USA. Estuarine, Coastal and Shelf Science, 117, 70-82.

Hasle, G. R., and E. E. Syvertsen. 1997. Marine diatoms. Identifying marine phytoplankton. Tomas, CR San Diego.

Hickey, B. M., X. Zhang, and N. Banas. 2002. Coupling between the California Current System and a coastal plain estuary in low riverflow conditions. Journal of Geophysical Research: Oceans, 107(C10), 30-1.

Hickey, B. M., & N. S. Banas. 2003. Oceanography of the US Pacific Northwest coastal ocean and estuaries with application to coastal ecology. Estuaries, 26, 1010-1031.

Horner, R. A., M. B. Kusske, B. P. Moynihan, R. N. Skinner, & J. C. Wekell. 1993. Retention of domoic acid by Pacific razor clams, Siliqua patula(Dixon, 1789): preliminary study. Journal of Shellfish Research, 12(2), 451-456.

Hubbard K.A., C.E. Olsen, and E.V. Armburst. 2014. Molecular characterization of Pseudo-nitzschia community structure and species ecology in a hydrographically complex estuarine system (Puget Sound, Washington USA). Marine ecology progress series, 507:39-55.

Jacox, M. G., C. A. Edwards, E. L. Hazen, and S. J. Bograd. 2018. Coastal upwelling revisited: Ekman, Bakun, and improved upwelling indices for the U.S. west coast, Journal of Geophysical Research 123(10):7332-7350 doi:10.1029/2018JC014187.

Jennings, E. D. 2012. Toxic or Not? Modeling Pseudo-nitzschia Consumption and Domoic Acid Cycling in Washington's Intertidal Bivalves. University of Washington.

Jennings, E. D., M. S. Parker and C. A. Simenstad. 2020. Domoic acid depuration by intertidal bivalves fed on toxin-producing Pseudo-nitzschia multiseries. Toxicon: X, 6, 100027.

Ji, Y., G. Yan, G. Wang, J. Liu, Z. Tang, Y. Yan, J. Qiu, L. Zhang, W. Pan, Y. Fu and T. Li. 2022. Prevalence and distribution of domoic acid and cyclic imines in bivalve mollusks from Beibu Gulf, China. Journal of Hazardous Materials, 423, p.127078.

Kelly, K.J., F. X. Fu, X. Jiang, H. Li, D. Xu, N. Yang, M. A. DeMers, J. D. Kling, K. Gao, N. Ye, and D. A. Hutchins. 2021. Interactions between ultraviolet B radiation, warming, and changing nitrogen source may reduce the accumulation of toxic Pseudo-nitzschia multiseries biomass in future coastal oceans. Frontiers in Marine Science 8:433.

Khangaonkar, T., W. Long, and W. Xu. 2017. Assessment of circulation and inter-basin transport in the Salish Sea including Johnstone Strait and Discovery Islands pathways. Ocean Modelling, 109, 11-32.

Kimmerer, W. J. and J. K. Thompson. 2014. Phytoplankton growth balanced by clam and zooplankton grazing and net transport into the low-salinity zone of the San Francisco Estuary. Estuaries and Coasts 37(5):1202-1218.

Kudela, R., G. Pitcher, T. Probyn, F. Figueiras, T. Moita and V. Trainer. 2005. Harmful algal blooms in coastal upwelling systems. Oceanography 18(2).

Kudela, R. M., S. Seeyave and W. P. Cochlan. 2010. The role of nutrients in regulation and promotion of harmful algal blooms in upwelling systems. Progress in Oceanography 85(1-2):122-135.

Kudela, R. M., K. Hayashi, and C. G. Caceres. 2020. Is San Francisco Bay resistant to Pseudo-nitzschia and domoic acid?. Harmful algae, 92, 101617.

Kvrgić, K., T. Lešić, N. Džafić, and J. Pleadin. 2022. Occurrence and Seasonal Monitoring of Domoic Acid in Three Shellfish Species from the Northern Adriatic Sea. Toxins, 14(1), 33.

Largier, J. L. 1992. Tidal intrusion fronts. Estuaries, 15, 26-39.

Largier, J. L., B. A. Magnell, and C. D. Winant. 1993. Subtidal circulation over the northern California shelf. Journal of Geophysical Research: Oceans 98(C10):18147-18179.

Lelong, A., H. Hegaret, P. Soudant and S. Bates. 2012. Pseudo-nitzschia (Bacillariophyceae) species, domoic acid and amnesic shellfish poisoning: revisiting previous paradigms. Phycologia 51.2: 168-216.

Lewitus, A.J., R. A. Horner, D. A. Caron, E. Garcia-Mendoza, B. M. Hickey, M. Hunter, D. D. Huppert, R. M. Kudela, G. W. Langlois, J. L. Largier, and E. J. Lessard. 2012. Harmful algal blooms along the North American west coast region: History, trends, causes, and impacts. Harmful algae, 19, pp.133-159.

Lindgren, F., H. Rue, and J. Lindström. 2011. An explicit link between Gaussian fields and Gaussian Markov random fields: the stochastic partial differential equation approach. Journal of the Royal Statistical Society: Series B (Statistical Methodology). 73(4), 423-498.

Litaker, R.W., T. N. Stewart, B. T. L. Eberhart, J. C. Wekell, V. Trainer, R. M. Kudela, P. E. Miller, A. Roberts, C. Hertz, T. A. Johnson and G. Frankfurter. 2008. Rapid enzyme-linked immunosorbent assay for detection of the algal toxin domoic acid. Journal of Shellfish Research 27.5: 1301-1310.

Lucas, L. V., J. R. Koseff, S. G. Monismith, J. E. Cloern, and J. K. Thompson. 1999. Processes governing phytoplankton blooms in estuaries. II: The role of horizontal transport. Marine Ecology Progress Series, *187*, 17-30.

Lucas, L. V., J. E. Cloern, J. K. Thompson, M. T. Stacey, and J. R. Koseff. 2016. Bivalve grazing can shape phytoplankton communities. Frontiers in Marine Science 3:14.

Lundholm, N., B. Krock, U. John, J. Skov, J. Cheng, M. Pančić, S. Wohlrab, K. Rigby, T. G. Nielsen, E. Selander, and S. Harðardóttir. 2018. Induction of domoic acid production in diatoms—Types of grazers and diatoms are important. Harmful Algae 79:64-73.

Mafra Jr, L. L., V. M. Bricelj, C. Ouellette, C. Léger, and S. S. Bates. 2009a. Mechanisms contributing to low domoic acid uptake by oysters feeding on

Pseudo-nitzschia cells. I. Filtration and pseudofeces production. Aquatic Biology 6:201-212.

Mafra Jr, L. L., V. M. Bricelj, and J. E. Ward. 2009b. Mechanisms contributing to low domoic acid uptake by oysters feeding on Pseudo-nitzschia cells. II. Selective rejection. Aquatic Biology 6:213-226.

Mafra Jr, L. L., V. M. Bricelj and K. Fennel. 2010a. Domoic acid uptake and elimination kinetics in oysters and mussels in relation to body size and anatomical distribution of toxin. Aquatic toxicology 100(1):17-29.

Mafra Jr, L. L. V. M. Bricelj, C. Ouellette, and S. S. Bates. 2010b. Feeding mechanics as the basis for differential uptake of the neurotoxin domoic acid by oysters, Crassostrea virginica, and mussels, Mytilus edulis. Aquatic Toxicology 97(2):160-171.

Maldonado, M. T., M. P. Hughes, E. L. Rue, and M. L. Wells. 2002. The effect of Fe and Cu on growth and domoic acid production by Pseudo-nitzschia multiseries and Pseudo-nitzschia australis. Limnology and Oceanography 47(2):515-526.

Martins, T. G., D. Simpson, F. Lindgren and H. Rue. 2013. Bayesian computing with INLA: new features. Computational Statistics & Data Analysis. 67, 68-83.

McCabe, R. M., B. M. Hickey, R. M. Kudela, K. A. Lefebvre, N. G. Adams, B. D. Bill, F. M. D. Gulland, R. E. Thomson, W. P. Cochlan, and V. Trainer. 2016. An unprecedented coastwide toxic algal bloom linked to anomalous ocean conditions. Geophysical Research Letters 43.19: 10-366.

McClatchie, S., Goericke, R., Leising, A., Auth, T.D., Bjorkstedt, E., Robertson, R.R., Brodeur, R.D., Du, X., Daly, E.A., Morgan, C.A., Chavez, F.P., Debich, A.J., Hildebrand, J., Field, J., Sakuma, K., Jacox, M.G., Kahru, M., Kudela, R., Andserson, C., Largier, J., Lavaniegos, B.E., Gomez-Valdes, J., Jimenez-Rosenberg, S.P.A., McCabe, R., Melin, S.R., Ohman, M.D., Sala, L.M., Peterson, B., Fisher, J., Shroeder, I.D., Bograd, S.J., Hazen, E.L., Schneider, S.R., Golightly, R.T., Suryan, R.M., Gladics, A.J., Loredo, S., Porquez, J.M., Thompson, A.R., Weber, E.D., Watson, W., Trainer, V., Warzybok, P., Bradley, R., Jahncke, J., 2016. State of the California Current 2015–16: Comparisons with the 1997–98 El Ni.o. Calif. Coop. Oceanic Fish. Invest. Rep. 57, 5–61.

McKibben, S. M., W. Peterson, A. M. Wood, V. Trainer, M. Hunter and A. E. White. 2017. Climatic regulation of the neurotoxin domoic acid. Proceedings of the National Academy of Sciences 114(2):239-244.

Miller M.A., M.E. Moriarty, P.J. Duignan, T.S. Zabka, E. Dodd, F.I. Batac, C. Young, A. Reed, M.D. Harris, K. Greenwalk, R.M. Kudela. 2021. Clinic signs and pathology associated with domoic acid toxicosis in southern sea otters (Enhydra lutris nereis). Frontiers in Marine Science. 8:585501.

Monbet, Y. 1992. Control of phytoplankton biomass in estuaries: a comparative analysis of microtidal and macrotidal estuaries. Estuaries *15*(4):563-571.

Moore, S. K., S. J. Dreyer, J. A. Ekstrom, K. Moore, K. Norman, T. Klinger, E. H. Allison, and S. L. Jardine. 2020. Harmful algal blooms and coastal communities: Socioeconomic impacts and actions taken to cope with the 2015 US West Coast domoic acid event. Harmful algae 96: 101799.

Moreno, A. R., C. Anderson, R. M. Kudela, M. Sutula, C. Edwards, and D. Bianchi. 2022. Development, calibration, and evaluation of a model of Pseudo-nitzschia and domoic acid production for regional ocean modeling studies. Harmful Algae 118:102296.

Murawski, J., J. She, C. Mohn, V. Frishfelds, and J. W. Nielsen. 2021. Ocean circulation model applications for the estuary-coastal-open sea continuum. Frontiers in Marine Science, 8, 657720.

Newton, J. A., and R. A. Horner. 2003. Use of phytoplankton species indicators to track the origin of phytoplankton blooms in Willapa Bay, Washington. Estuaries, 26, 1071-1078.

Novaczek, I., M. S. Madhyastha, R. F. Ablett, G. Johnson, M. S. Nijjar, and D. E. Sims. 1991. Uptake, disposition and depuration of domoic acid by blue mussels (Mytilus edulis). Aquatic toxicology 21(1-2):103-118.

Novaczek I., M. S. Madhyastha, R. F. Ablett, A. Donald, G. Johnson, M. S. Nijjar and D. E. Sims. 1992. Depuration of Domoic Acid from Live Blue Mussels (Mytilus-Edulis). Canadian Journal of Fisheries and Aquatic Sciences 49:312-318.

O'Connell, Gregory D. 2013. Who is chlorophyll a? Phytoplankton community structure in Humboldt Bay, California. Masters Dissertation. Humboldt State University.

Oksanen, J., Blanchet, F.G., Friendly, M., Kindt, R., Legendre, P., McGlin, D., Minchin, P.R., O'Hara, R.B., Simpson, G.L., Solymos, P., Stevens, M.H., Szoecs, E., and H. Wagner. 2020. vegan: Community Ecology Package. R package version 2.5-7.

Olson, R. J., and H. M. Sosik. 2007. A submersible imaging-in-flow instrument to analyze nano-and microplankton: Imaging FlowCytobot. Limnology and Oceanography: Methods, 5(6), 195-203.

Parsons, M. L., & Q. Dortch. 2002. Sedimentological evidence of an increase in Pseudo-nitzschia (Bacillariophyceae) abundance in response to coastal eutrophication. Limnology and Oceanography 47(2):551-558.

Peierls, B. L., N. S. Hall, & H. W. Paerl. 2012. Non-monotonic responses of phytoplankton biomass accumulation to hydrologic variability: a comparison of two coastal plain North Carolina estuaries. Estuaries and coasts, 35, 1376-1392.

Pequegnat, J. E., and J. H. Butler. 1981. The role of nutrients in supporting phytoplankton productivity in Humboldt Bay. Calif. Sea Grant Coll. Prog. Rep. R-CSGCP-004: 218-222.

Phlips, E.J., S. Badylak, M. Christman, J. Wolny, J. Brame, J. Garland, L. Hall, J. Hart, J. Landsberg, M. Lasi, and J. Lockwood. 2011. Scales of temporal and spatial variability in the distribution of harmful algae species in the Indian River Lagoon, Florida, USA. Harmful Algae, 10(3), pp.277-290.

Pitcher, G. C., F. G. Figueiras, B. M. Hickey and M. T. Moita. 2010. The physical oceanography of upwelling systems and the development of harmful algal blooms. Progress in oceanography 85(1-2):5-32.

Pitcher, G.C., A.B. Jiménez, R.M. Kudela, and B. Reguera. 2017. Harmful algal blooms in eastern boundary upwelling systems: A GEOHAB Core Research Project. Oceanography 30(1):22–35.

Qin, Q., and J. Shen. 2019. Physical transport processes affect the origins of harmful algal blooms in estuaries. Harmful algae 84:210-221.

Quilliam, M. A., P. G. Sim, A. W. McCulloch, and A. G. McInnes. 1989. High-performance liquid chromatography of domoic acid, a marine neurotoxin, with application to shellfish and plankton. International Journal of Environmental Analytical Chemistry, 36(3), 139-154.

Radan, R. L., and W. P. Cochlan. 2018. Differential toxin response of Pseudo-nitzschia multiseries as a function of nitrogen speciation in batch and continuous cultures, and during a natural assemblage experiment. Harmful algae 73:12-29.

Riisgård, H. U., C. Kittner, and D. F. Seerup. 2003. Regulation of opening state and filtration rate in filter-feeding bivalves (Cardium edule, Mytilus edulis, Mya arenaria) in response to low algal concentration. Journal of experimental marine biology and ecology 284, no. 1-2: 105-127.

Ritzman, J., A. Brodbeck, S. Brostrom, S. McGrew, S. Dreyer, T. Klinger, & S. K. Moore. 2018. Economic and sociocultural impacts of fisheries closures in two

fishing-dependent communities following the massive 2015 US West Coast harmful algal bloom. Harmful Algae, 80, 35-45.

Roegner, G. C. 1998. Hydrodynamic control of the supply of suspended chlorophyll a to infaunal estuarine bivalves. Estuarine, Coastal and Shelf Science 47:369-384.

Roegner, G. C., and A. L. Shanks. 2001. Import of coastally-derived chlorophyll a to South Slough, Oregon. Estuaries, 24, 244-256.

Roegner, G. C., J. A. Needoba, and A. M. Baptista. 2011. Coastal upwelling supplies oxygen-depleted water to the Columbia River estuary. PloS one, 6(4), e18672.

Rollwagen-Bollens, G., B. A. Bolam, S. M. Bollens, S. Henricksen, C. Sandison, and J. Zimmerman. 2021. Temperature-dependent functional response of the invasive Asian clam, Corbicula fluminea, feeding on natural phytoplankton. Inland Waters 11. no. 2: 250-256.

Rourke, W. A., A. Justason, J. L. Martin, and C. J. Murphy. 2021. Shellfish toxin uptake and depuration in multiple Atlantic Canadian molluscan species: Application to selection of sentinel species in monitoring programs. Toxins 13, no. 2: 168.

Rowland-Pilgrim, S., S.C. Swan, A. O'Neill, S. Johnson, L. Coates, P. Stubbs, K. Dean, R. Parks, K. Harrison, M. T. Alves, and A. Walton. 2019. Variability of Amnesic Shellfish Toxin and Pseudo-nitzschia occurrence in bivalve molluscs and water samples–Analysis of ten years of the official control monitoring programme. Harmful algae, 87:101623.

Rue, H., S. Martino, and N. Chopin. 2009. Approximate Bayesian inference for latent Gaussian models using integrated Laplace approximations (with discussion). Journal of the Royal Statistical Society, Series B. 71(2):319-392.

Ryan, J.P., M. A. McManus, R. M. Kudela, M. Lara Artigas, J. G. Bellingham, F. P. Chavez, G. Doucetter, D. Foley, M. Godin, J. B. J. Harvey, and R. Marin III. 2014. Boundary influences on HAB phytoplankton ecology in a stratification-enhanced upwelling shadow. Deep Sea Research Part II: Tropical Studies in Oceanography. 101:63-79.

Sandoval-Belmar, M., J. Smith, A. R. Moreno, C. Anderson, R. M. Kudela, M. Sutula, F. Kessouri, D. A. Caron, F. P. Chavez, and D. Bianchi. 2023. A cross-regional examination of patterns and environmental drivers of Pseudo-nitzschia harmful algae blooms along the California coast. Harmful Algae. 102435.

Saucedo, P. E., L.Ocampo, M. Monteforte, and H. Bervera. 2004. Effect of temperature on oxygen consumption and ammonia excretion in the Calafia mother-of-pearl oyster, Pinctada mazatlanica (Hanley, 1856). Aquaculture 229. no. 1-4: 377-387.

Sauvey, A., F. Denis, H. Hégaret, B. Le Roy, C. Lelong, O. Jolly, M. Pavie, and J. Fauchot. 2021. Interactions between Filter-Feeding Bivalves and Toxic Diatoms: Influence on the Feeding Behavior of Crassostrea gigas and Pecten maximus and on Toxin Production by Pseudo-nitzschia. Toxins 13(8):577.

Schnetzer, A., P. E. Miller, R. A. Schaffner, B. A. Stauffer, B. H. Jones, S. B. Weisberg, P. M. DiGiacomo, W. M. Berelson, and D. A. Caron. 2007. Blooms of Pseudo-nitzschia and domoic acid in the San Pedro Channel and Los Angeles harbor areas of the Southern California Bight, 2003–2004. Harmful algae 6, no. 3: 372-387.

Sekula-Wood, E., A. Schnetzer, C. R. Benitez-Nelson, C. Anderson, W. M. Berelson, M. A. Brzezinski, J. M. Burns, D. A. Caron, I. Cetinic, J. L. Ferry, E. Fitzpatrick, B. H. Jones, P. E. Miller, S. L. Morton, R. A. Schaffner, D. A. Siegel and R. Thunell. 2009. Rapid downward transport of the neurotoxin domoic acid in coastal waters. Nature Geoscience 2(4):272-275.

Sekula-Wood, E., C. Benitez-Nelson, S. Morton, C. Anderson, C. Burrell and R. Thunell. 2011. Pseudo-nitzschia and domoic acid fluxes in Santa Barbara Basin (CA) from 1993 to 2008. Harmful Algae 10(6):567-575.

Send, U., R. C. Beardsley, and C. D. Winant. 1987. Relaxation from upwelling in the coastal ocean dynamics experiment. Journal of Geophysical Research: Oceans 92.C2: 1683-1698.

Shanks, A. L., S. G. Morgan, J. MacMahan, A. JHM Reniers, M. Jarvis, J. Brown, A. Fujimura, and C. Griesemer. 2014. Onshore transport of plankton by internal tides and upwelling-relaxation events. Marine Ecology Progress Series 502: 39-51.

Silvert, W. and D. V. S. Rao. 1992. Dynamic Model Of The Flux Of Domoic Acid A Neurotoxin Through A Mytilus-Edulis Population. Canadian Journal of Fisheries and Aquatic Sciences 49:400-405.

Silvert, W. L. and A. D. Cembella. 1995. Dynamic modelling of phycotoxin kinetics in the blue mussel, Mytilus edulis, with implications for other marine invertebrates. Canadian Journal of Fisheries and Aquatic Sciences 52:521-531.

Smith, J., D. Shultz, M. D. Howard, G. Robertson, V. Phonsiri, V. Renick, D. A. Caron, R. M. Kudela, and K. McLaughlin. 2021. Persistent domoic acid in marine sediments and benthic infauna along the coast of Southern California. Harmful Algae, 108:102103.

Sosik, H. M., and R. J. Olson. 2007. Automated taxonomic classification of phytoplankton sampled with imaging-in-flow cytometry. Limnology and Oceanography: Methods, 5(6), 204-216.

Stewart J.E., L.J. Marks, M.W. Gilgan, E. Pfeiffer, and B.M. Zwicker. 1998. Microbial utilization of the neurotoxin domoic acid: blue mussels (Mytilus edulis) and soft shell clams (Mya arenaria) as sources of the microorganisms. Canadian journal of microbiology. 44.5:456-464.

Sun J., D. A. Hutchins, Y. Feng, E. L. Seubert, D. A. Cardon, & F. X. Fu. 2011. Effects of changing pCO2 and phosphate availability on domoic acid production and physiology of the marine harmful bloom diatom Pseudo-nitzschia multiseries. Limnology and Oceanography 56: 829–840.

Sutula, M., R. Kudela, J. D. Hagy III, L. W. Harding Jr, D. Senn, J. E. Cloern, S. Bricker, G. Mine Berg, and M. Beck. 2017. Novel analyses of long-term data provide a scientific basis for chlorophyll-a thresholds in San Francisco Bay. Estuarine, coastal and shelf science 197: 107-118.

Tas, S., & N. Lundholm. 2017. Temporal and spatial variability of the potentially toxic Pseudo-nitzschia spp. in a eutrophic estuary (Sea of Marmara) Journal of the Marine Biological Association of the United Kingdom 97(7):1483-1494.

Teegarden, G. J., A. D. Cembella, C. L. Capuano, S. H. Barron, and E. G. Durbin. 2003. Phycotoxin accumulation in zooplankton feeding on Alexandrium fundyense—vector or sink?. Journal of Plankton Research 25(4):429-443.

Thessen, A.E., H. A. Bowers and D. K. Stoecker. 2009. Intra- and interspecies differences in growth and toxicity of Pseudo-nitzschia while using different nitrogen sources. Harmful Algae 8:792–810.

Thessen, A. E., T. M. Soniat, Q. Dortch, and G. J. Doucette. 2010. Crassostrea virginica grazing on toxic and non-toxic diatoms. Toxicon 55(2-3):570-579.

Thompson, R., & B. L. Bayne. 1972. Active metabolism associated with feeding in the mussel Mytilus edulis L. Journal of Experimental Marine Biology and Ecology, 9(1), 111-124.

Thorel, M., P. Claquin, M. Schapira, R. Le Gendre, P. Riou, D. Goux, B. Le Roy, V. Raimbault, A. F. Deton-Cabanillas, P. Bazin and V. Kientz-Bouchart. 2017. Nutrient ratios influence variability in Pseudo-nitzschia species diversity and particulate domoic acid production in the Bay of Seine (France). Harmful Algae, 68:192-205.

Tominack, S. A., and M. S. Wetz. 2022. Variability in Phytoplankton Biomass and Community Composition in Corpus Christi Bay, Texas. Estuaries and Coasts, 1-22.

Townhill, B. L., J. Tinker, M. Jones, S. Pitois, V. Creach, S. D. Simpson, S. Dye, E. Bear and J. K. Pinnegar. 2018. Harmful algal blooms and climate change: exploring future distribution changes. ICES Journal of Marine Science 75(6):1882-1893.

Trainer, V. L., N. G. Adams, B. D. Bill, B. F. Anulacion, and J. C. Wekell. 1998. Concentration and dispersal of a Pseudo-nitzschia bloom in Penn Cove, Washington, USA. Natural Toxins 6(3-4):113-125.

Trainer, V. L., N. G. Adams, B. D. Bill, C. M. Stehr, J. C. Wekell, P. Moeller, M. Busman, and D. Woodruff. 2000. Domoic acid production near California coastal upwelling zones, June 1998. Limnology and oceanography 45, no. 8: 1818-1833.

Trainer, V. L., B. M. Hickey, & R. A. Horner. 2002. Biological and physical dynamics of domoic acid production off the Washington coast. Limnology and Oceanography, 47(5), 1438-1446.

Trainer, V. L., W. P. Cochlan, A. Erickson, B. D. Bill, F. H. Cox, J. A. Borchert, & K. A. Lefebvre. 2007. Recent domoic acid closures of shellfish harvest areas in Washington State inland waterways. Harmful Algae, 6(3), 449-459.

Trainer, V. L., B. M. Hickey, E. J. Lessard, W. P. Cochlan, C. G. Trick, M. L. Wells, A. MacFadyen and S. K. Moore. 2009. Variability of Pseudo-nitzschia and domoic acid in the Juan de Fuca eddy region and its adjacent shelves. Limnology and Oceanography 54(1):289-308.

Trainer, V. L., G. C. Pitcher, B. Reguera and T. J. Smayda. 2010. The distribution and impacts of harmful algal bloom species in eastern boundary upwelling systems. Progress in oceanography 85(1-2):33-52.

Trainer, V. L., S. S. Bates, N. Lundholm, A. E. Thessen, W. P. Cochlan, N. G. Adams, & C. G. Trick. 2012. Pseudo-nitzschia physiological ecology, phylogeny, toxicity, monitoring and impacts on ecosystem health. Harmful algae, 14, 271-300.

Trainer, V., R. M. Kudela, M. Hunter, N. G. Adams and R. M. McCabe. 2020. Climate extreme seeds a new domoic acid hotspot on the US west coast. Frontiers in Climate 2:23.

Trimborn S., N. Lundholm, S. Thoms, K. U. Richter, B. Krock, P. J. Hansen, & B. Rost. 2008. Inorganic carbon acquisition in potentially toxic and non-toxic diatoms: the

effect of pH-induced changes in seawater carbonate chemistry. Physiologia Plantarum 133: 92–105.

Wang, Z., K. L. King, J. S. Ramsdell and G. J. Doucette. 2007. Determination of domoic acid in seawater and phytoplankton by liquid chromatography–tandem mass spectrometry. Journal of Chromatography A 1163.1-2:169-176.

Wekell, J. C., E. J. Gauglitz Jr, H. J. Bamett, C. L. Hatfield, D. Simons and D. Ayres. 1994. Occurrence of domoic acid in Washington state razor clams (Siliqua patula) during 1991-1993. Natural Toxins 2(4):197-205.

Wells, B.K., I.D. Schroeder, S.J. Bograd, E.L. Hazen, M.G. Jacox, A. Leising, N. Mantua, J.A. Santora, J. Fisher, W.T. Peterson, E. Bjorkstedt, R.R. Robertson, F.P. Chavez, R. Goericke, R. Kudela, C. Anderson, B.E. Lavaniegos, J. Gomez-Valdes, R.D. Brodeur, E.A. Daly, C.A. Morgan, T.D. Auth, J.C. Field, K. Sakuma, S. McClatchie, A.R. Thompson, E.D. Weber, W. Watson, R.M. Suryan, J. Parrish, J. Dolliver, S. Loredo, J.M. Porquez, J.E. Zamon, S.R. Schneider, R.T. Golightly, P. Warzybok, R. Bradley, J. Jahncke, W. Sydeman, S.R. Melin, J. Hildebrand, A.J. Debich, B. Thayre. 2017. State of the California Current 2016–2017: Still anything but "normal" in the North. California Cooperative Oceanic Fisheries Investigations Reports, 58, pp.1-55.

Wells, M. L., C. G. Trick, W. P. Cochlan, M. P. Hughes, and V. L. Trainer. 2005. Domoic acid: the synergy of iron, copper, and the toxicity of diatoms. Limnology and Oceanography 50(6):1908-1917.

Wetz, M.S., P. A. Wheeler, and R. M. Letelier. 2004. Light-induced growth of phytoplankton collected during the winter from the benthic boundary layer off Oregon, USA. Marine Ecology Progress Series 280:95-104.

Wickham, H. 2016. Ggplot2: Elegant Graphics for Data Analysis. Springer-Verlag New York.

Wingert, C. J., and W. P. Cochlan. 2021. Effects of ocean acidification on the growth, photosynthetic performance, and domoic acid production of the diatom Pseudo-nitzschia australis from the California Current System. Harmful Algae 107:102030.

Winter, J. E. 1978. A review on the knowledge of suspension-feeding in lamellibranchiate bivalves, with special reference to artificial aquaculture systems. Aquaculture, 13(1), 1-33.

Wood, S. N. 2011. Fast stable restricted maximum likelihood and marginal likelihood estimation of semiparametric generalized linear models. Journal of the Royal Statistical Society: Series B (Statistical Methodology). 73(1), 3-36.

Yñiguez, A. T., J. Maister, C. L. Villanoy, J. D. Deauna, E. Peñaflor, A. Almo, L. T. David, G. A. Benico, E. Hibay, I. Mora, S. Arcamo, J. Relox and R. V. Azanza. 2018. Insights into the dynamics of harmful algal blooms in a tropical estuary through an integrated hydrodynamic-Pyrodinium-shellfish model. Harmful algae 80:1-14.

Zheng, G., H. Wu, H. Che, X. Li, Z. Zhang, J. Peng, M. Guo, and Z. Tan. 2022. Residue Analysis and Assessment of the Risk of Dietary Exposure to Domoic Acid in Shellfish from the Coastal Areas of China. Toxins 14, no. 12: 862.

Zuur, A. F., E. N. Ieno, N. J. Walker, A. A. Saveliev, and G. M. Smith. 2009. Mixed effects models and extensions in ecology with R. Vol. 574. New York: Springer.

Zuur, A. F., E. N. Ieno, & A. A. Saveliev. 2017. Spatial, temporal and spatial-temporal ecological data analysis with R-INLA. Highland Statistics Ltd, 1.

APPENDIX A

Appendix A Intra-annual variability in daily averages of water age for the years 2015, 2016, 2017, and 2018 for all North Bay sites (Figure A1) and South Bay sites (Figure A2). Black line (± SE in gray) represents the predictive line from a generalized additive mode fit to observations. Color and line type corresponds to observed year.

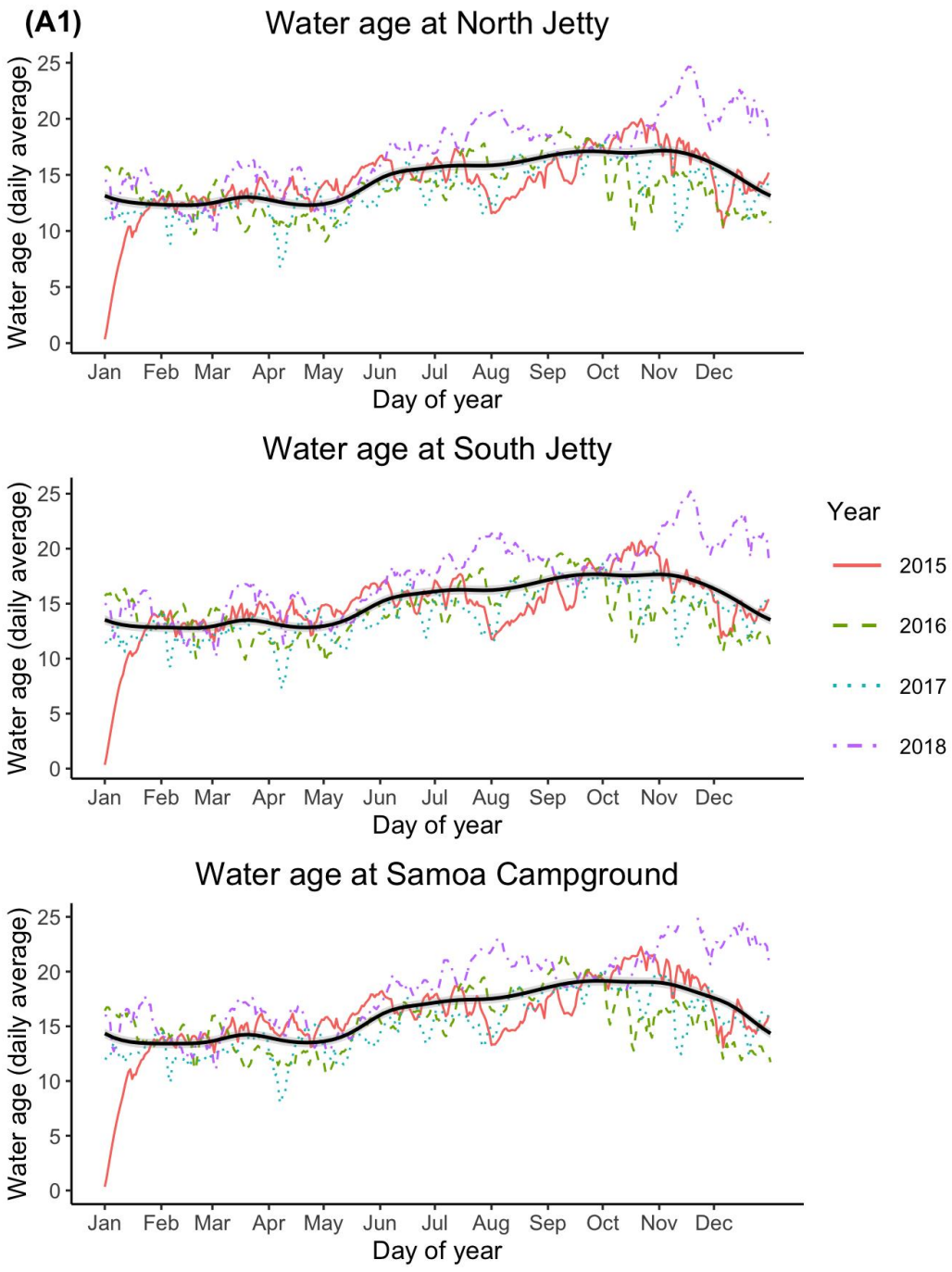
(A1)
Water age at North Jetty
Water age (daily average)
0
5
10
15
20
25
Jan Feb Mar Apr May Jun Jul Aug Sep Oct Nov Dec
Day of year
Water age at South Jetty
Water age (daily average)
Jan Feb Mar Apr May Jun Jul Aug Sep Oct Nov Dec
Day of year
Water age at Samoa Campground
Water age (daily average)
Jan Feb Mar Apr May Jun Jul Aug Sep Oct Nov Dec
Day of year
Year
2015
2016
2017
2018

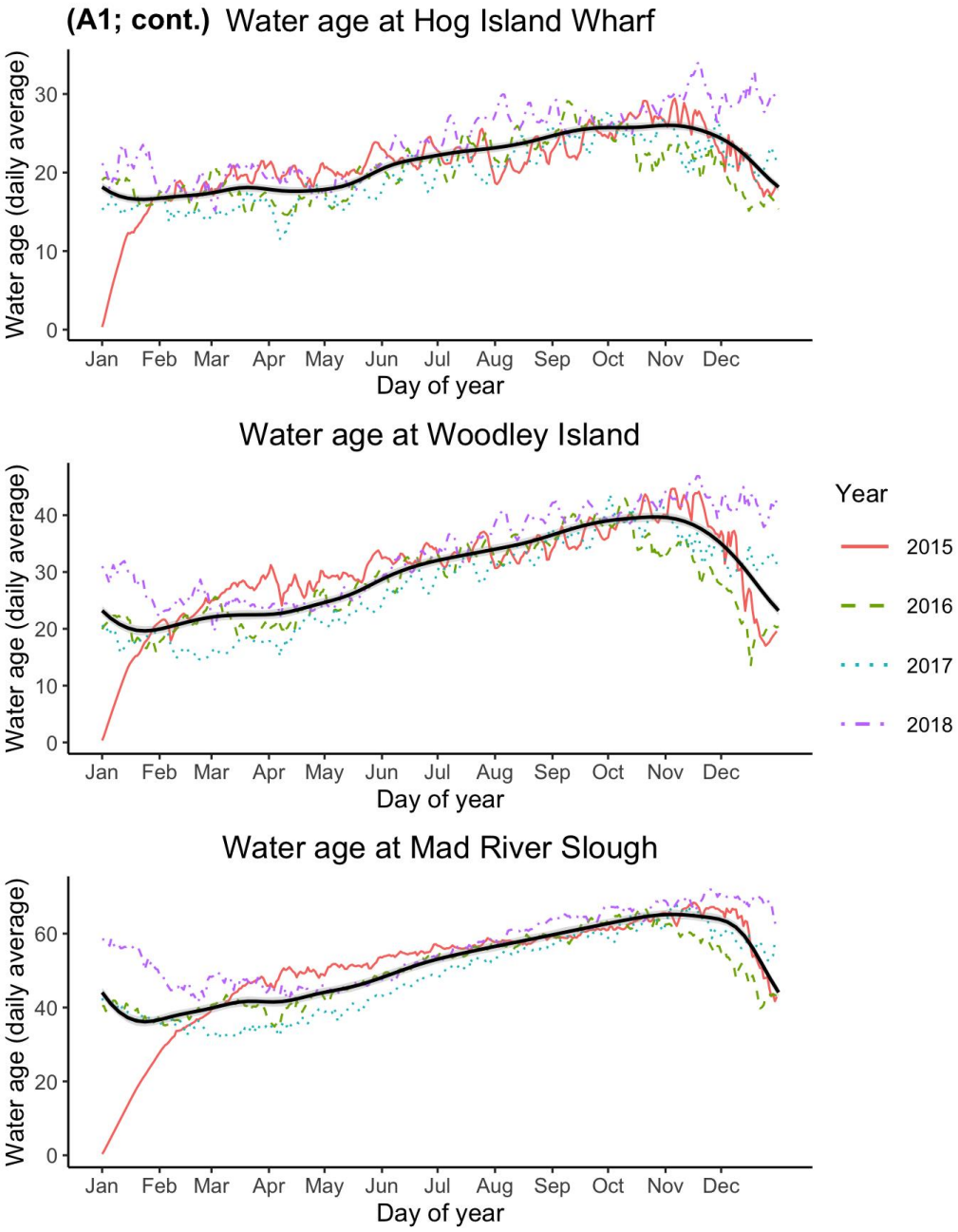
(A1; cont.) Water age at Hog Island Wharf
Water age (daily average)
0
10
20
30
Jan Feb Mar Apr May Jun Jul Aug Sep Oct Nov Dec
Day of year
Water age at Woodley Island
Water age (daily average)
0
10
20
30
40
Jan Feb Mar Apr May Jun Jul Aug Sep Oct Nov Dec
Day of year
Year
2015
2016
2017
2018
Water age at Mad River Slough
Water age (daily average)
0
20
40
60
Jan Feb Mar Apr May Jun Jul Aug Sep Oct Nov Dec
Day of year

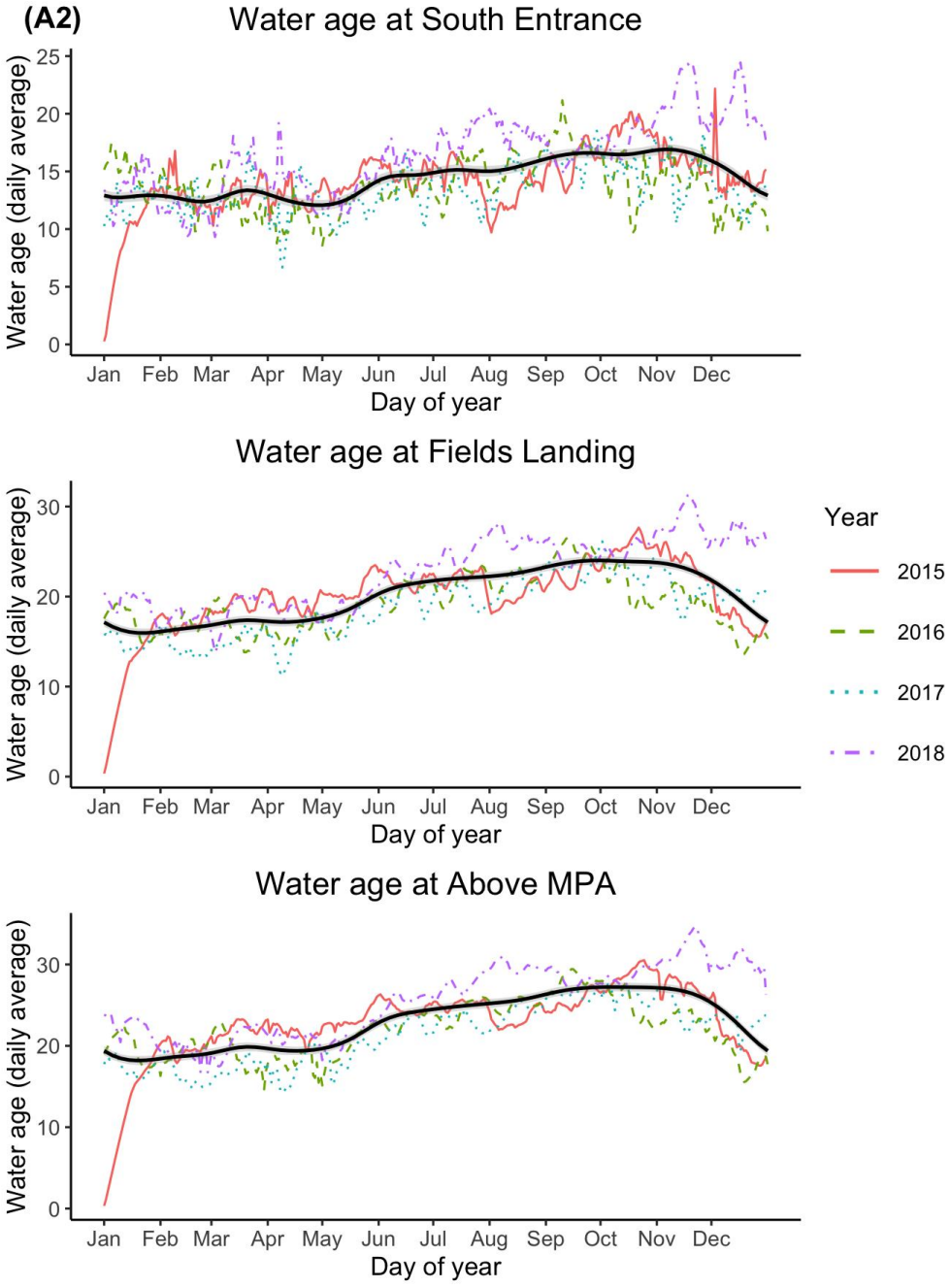
(A2)
Water age at South Entrance
Water age (daily average)
0
5
10
15
20
25
Jan Feb Mar Apr May Jun Jul Aug Sep Oct Nov Dec
Day of year
Water age at Fields Landing
Water age (daily average)
0
10
20
30
Jan Feb Mar Apr May Jun Jul Aug Sep Oct Nov Dec
Day of year
Year
2015
2016
2017
2018
Water age at Above MPA
Water age (daily average)
0
10
20
30
Jan Feb Mar Apr May Jun Jul Aug Sep Oct Nov Dec
Day of year

APPENDIX B

Appendix B: Methods describing predictive modeling of domoic acid.

Given the threat that *Pseudo-nitzschia* spp. HABs pose to vital aquaculture along the US West Coast, research has been conducted to develop predictive models with the goal to develop an early warning system that could be used by regional stakeholders and help mitigate the threat caused by these events (e.g., Moreno et al. 2022). The California Harmful Algae Risk Mapping (C-HARM) was developed to predict the probability of *Pseudo-nitzschia* HABs along the US West coast based on high resolution environmental variables (Anderson et al. 2016). Such models are useful in mitigating the effects that *Pseudo-nitzschia* spp. HABs have on vital aquaculture sources along the US West Coast.

For my project, I attempted to create a predictive model for my weekly pDA samples collected from Hog Island Wharf based on high resolution environmental data that may impact DA production (i.e., temperature (McCabe et al. 2016; McKibben et al. 2017), salinity (Doucette et al. 2008), upwelling and chlorophyll concentrations (Trainer et al. 2012)). These time series were obtained from a CeNCOOS observation site in Humboldt Bay (Humboldt Bay shore station at Chevron Dock; CeNCOOS, 2023). Since my pDA data had a higher-than-expected number of zero observations, I used a hurdle model (delta-GAM) to predict pDA concentrations during dates that were not sampled. First, this method models the presence and absence of pDA as a function of a set of candidate explanatory variables, and then models the relationship between pDA and model covariates only when pDA was present. The first model was fit using a generalized

additive model (GAM; R package “mgcv”; Wood 2011) with a binomial distribution and the second model was fit using a gaussian distribution on $\log_{10}$-transformed pDA values. Covariates to predict pDA in both steps of the hurdle model included temperature, salinity, chlorophyll and in index for upwelling (Coastal Upwelling Transport Index, CUTI and Biologically Effective Transport Index, BEUTI; Jacox et al. 2018). I tested these covariates to see if they were collinear by using the variance inflation factor (VIF; R package “car”; Fox et al. 2012). I found that CUTI and BEUTI were correlated, and based on AIC a model that included BEUTI was better. I then used the “dredge” function (R package “MuMin”; Barton & Barton 2015) on both models to obtain the best model based on AIC values. To obtain the final predicted pDA value, I multiplied the predicted pDA outputs from both models.

APPENDIX C

Appendix C: Relationship between log_{10}-transformed DA concentrations in mussels and log_{10}-transformed weight during the early September 2021 sampling occasion (Figure C1) and Histogram of the slopes obtained from models of the form log_{10}-transformed DA concentrations in mussels as a function of log_{10}-transformed weight (Figure C2). In Figure C1, the left panel depicts the relationship between log_{10}-transformed DA concentrations in mussels from early September 2021 sampling occasion and log_{10}-transformed weight (g). Points represent individual bivalves, the blue line is the global line of best fit, and the gray shaded error indicates the standard error. The right panel depicts log_{10}-transformed DA concentrations in mussels from the early September 2021 sampling occasion by log_{10}-transformed weight at each site. Individuals are grouped by sites (color and symbol) and the line of best fit is created for each site. In Figure C2, each model was based on mussels from a given site and sampling occasion.

Figure C1 establishes that an apparent positive relationship between log_{10}-transfromed DA concentration and individual log_{10}-transfromed mass was not reflected at the site level. Figure C2 corroborates these results, where the apparent relationship appears to be close to zero. Moreover, a vast majority of the weight by site models did not include weight as a significant covariate (30 out of 31 models fit). This observed global relationship contradicts patterns reported in the experimental literature (e.g., Mafra et al. 2010a).

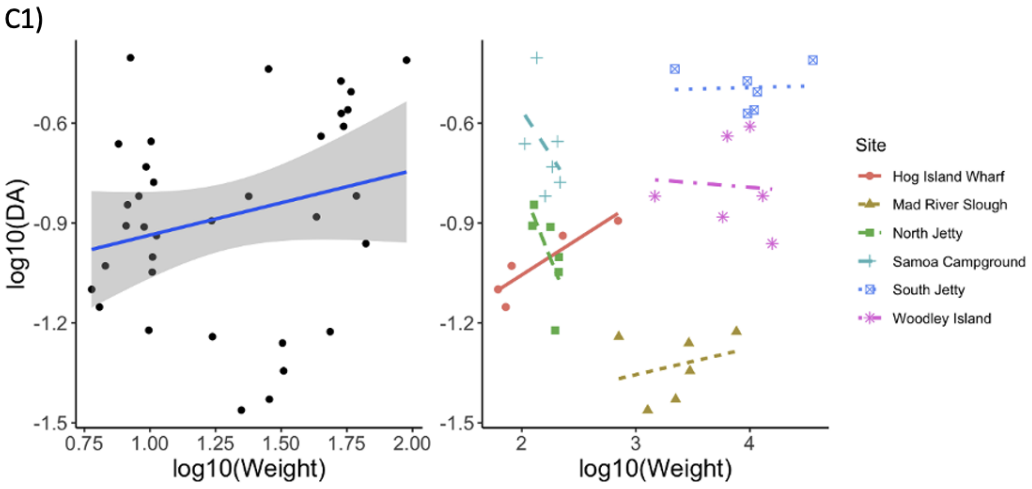

C2)

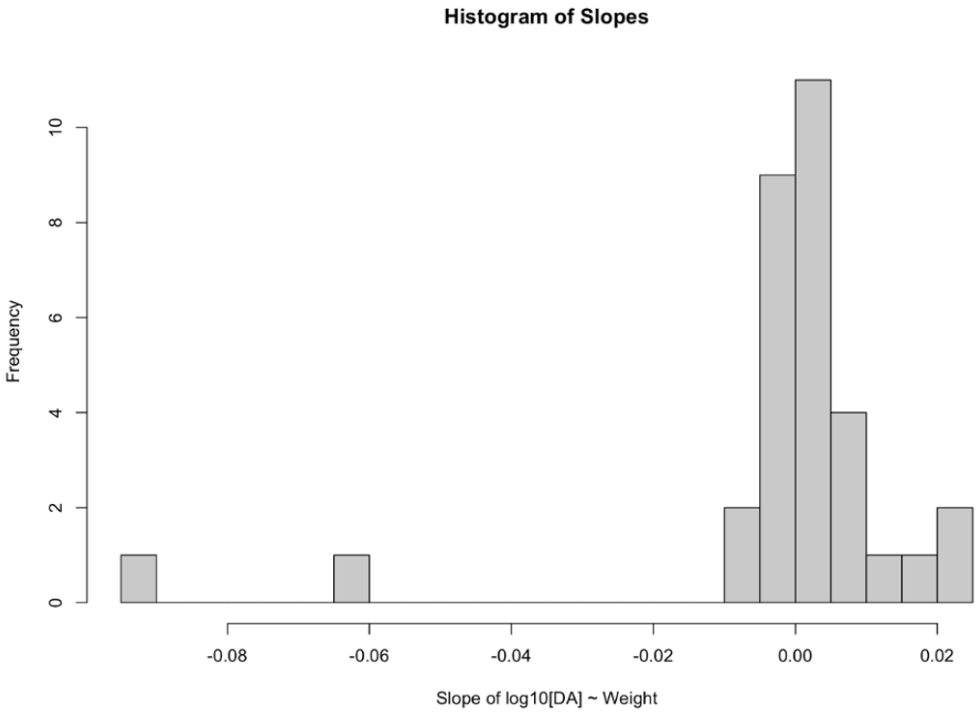
Histogram of Slopes
Frequency
0
2
4
6
8
10
-0.08
-0.06
-0.04
-0.02
0.00
0.02
Slope of log10[DA] ~ Weight

APPENDIX D

Appendix D: Model selection tables for mussel HAB index spatial generalized linear mixed effects models for linear distance (km) and age of water (days).

Table D1. Model selection tables for HAB index generalized linear mixed effect models relating log_{10}-transformed DA concentrations in mussels as a function of linear distance (Dist; km) and integrated pDA from Hog Island Wharf with a random intercept for date (sampling occasion). Models are listed in a ranking order based on AICc, delta AICc, and model weight.

Model	*Dist*	*pDA*	*Dist*pDA*	*AICc*	*Delta AICc*	*Model Weight*
1	+	+	-	-68.8	0	0.607
2	+	+	+	-67.1	1.63	0.268
3	+	-	-	-65.6	3.17	0.124
4	-	+	-	-50.0	18.8	0
5	-	-	-	-46.2	22.5	0

Table D2. Model selection tables for HAB index generalized linear mixed effect models relating log_{10}-transformed DA concentrations in mussels as a function of age of water (WA; days) and integrated pDA from Hog Island Wharf with a random intercept for date (sampling occasion). Models are listed in a ranking order based on AICc, delta AICc, and model weight.

Model	*WA*	*pDA*	*WA*pDA*	*AICc*	*Delta AICc*	*Model Weight*
1	+	+	-	-70.1	0	0.588
2	+	+	+	-68.7	1.37	0.296
3	+	-	-	-66.9	3.24	0.117
4	-	+	-	-50.0	20.1	0
5	-	-	-	-46.2	23.9	0

APPENDIX E

Appendix E: Model selection tables for butter clam HAB index spatial generalized linear mixed effects models for linear distance (km) and age of water (days).

Table E1. Model selection tables for HAB index generalized linear mixed effect models relating log_{10}-transformed DA concentrations in butter clams as a function of linear distance (Dist; km) and integrated pDA from Hog Island Wharf with a random intercept for date (sampling occasion). Models are listed in a ranking order based on AICc, delta AICc, and model weight.

Model	*Dist*	*pDA*	*Dist*pDA*	*AICc*	*Delta AICc*	*Model Weight*
1	+	+	+	-77.8	0	0.999
2	+	+	-	-63.5	14.3	0.001
3	+	-	-	-62.0	15.8	0
4	-	+	-	-26.3	51.6	0
5	-	-	-	-24.7	53.1	0

Table E2. Model selection tables for HAB index generalized linear mixed effect models relating log_{10}-transformed DA concentrations in butter clams as a function of age of water (WA; days) and integrated pDA from Hog Island Wharf with a random intercept for date (sampling occasion). Models are listed in a ranking order based on AICc, delta AICc, and model weight.

Model	*WA*	*pDA*	*WA*pDA*	*AICc*	*Delta AICc*	*Model Weight*
1	+	+	+	-81.6	0	1.0
2	+	+	-	-65.7	14.3	0
3	+	-	-	-63.6	15.8	0
4	-	+	-	-26.3	51.6	0
5	-	-	-	-24.7	53.1	0

APPENDIX F

Appendix F: Spatial model using integrated nested Laplace approximations (INLA) to model the spatial pattern of domoic acid (DA) loading in Humboldt Bay bivalves.

Introduction

DA, produced by some members of the harmful algae genus *Pseudo-nitzschia* spp. pose a major threat to bivalves located inside Humboldt Bay due to their proximity to a recently discovered *Pseudo-nitzschia* spp. harmful algal bloom "hot spot" (Trainer et al. 2020). During the summer months, Humboldt Bay experiences little freshwater input, and tidal exchange is the primary driver of circulation in the Bay (Barnhart et al. 1992). As a result, I expect that bivalves located closer to the mouth of the Bay will experience higher exposure to ocean-origin *Pseudo-nitzschia* spp. HABs than bivalves located farther away from the mouth. To examine this, I collect bivalves from multiple locations along the ocean to upper estuary transects and process them for DA concentrations.

Methods

To test Hypothesis 3, that DA concentrations in bivalves decrease with increased distance from the mouth of the Bay, I fit spatial models using INLA (Martins et al. 2013; Lindgren et al. 2011; Rue et al. 2009) to both mussels and butter clams using species as a covariate following methods outlined in Zuur et al. (2017). Since there is no overlap in species collected from each basin, the species covariate also represents a North and South Bay comparison. For simplicity, I assume that uptake and depuration dynamics are fast enough to be able to treat sampling occasions as independent observations, so sampling

occasion was included as a random intercept. DA concentrations in bivalves were $\log_{10}$-transformed to achieve a normal distribution and a better model fit. In developing the mesh for my model, due to the limited number of sites sampled, the resolution of the mesh needed to be scaled to reflect the resolution of the data and reveal the gradients in exposure. R-INLA uses a Matern Correlation function to estimate a spatial covariance matrix which is used to account for spatial autocorrelation in data (Zuur et al. 2017). Sampling locations that are closer to one another may share similar exposures, so this is accounted for in the model. Models were fit with and without a spatial dependence structure, and the model with the lowest (best) WAIC (Watanabe-Akaike Information Criteria) was used.

Results

The model with the spatial random field had a lower WAIC (-184.4) than the non-spatial model (-88.48), indicating a better model fit. For this model, a relatively coarse mesh with 16 vertices was found to adequately resolve patterns in the data. The fitted model included a statistically significant effect on species. The posterior mean of the spatial random field indicates that the probability of finding above average DA concentrations in bivalves near the mouth of the Bay is higher than at sites located farther away from the mouth of the Bay (Figure F1).

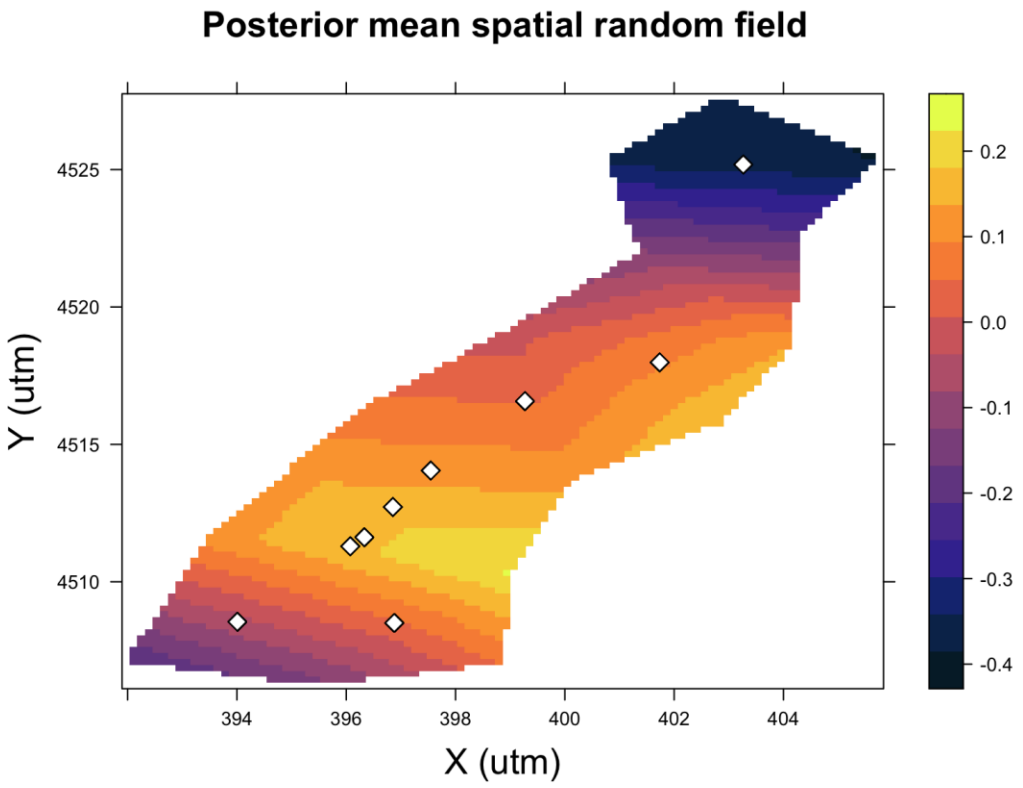

Figure F1. Posterior mean values of the spatial field of Humboldt Bay with all bivalve sites (diamond shapes) with areas within the Bay represented as above average (light yellow) and below average (dark blue) DA concentrations. Sites at the top of the plot represent North Bay (top diamond is the Mad River Slough site), and sites at the bottom of the plot represent the South Bay sites (bottom two diamonds from left to right are Above the MPA and Fields Landing site).